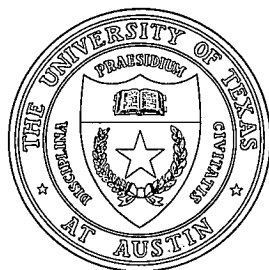# INSTITUTE FOR
FUSION STUDIES

Low Frequency Fluctuations of Plasma Magnetic Fields

SAMUEL BENJAMIN CABLE
Institute for Fusion Studies
The University of Texas at Austin
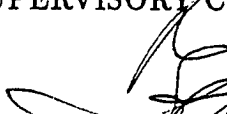Austin, Texas 78712
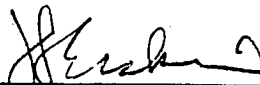
(THESIS)

September 1992

THE UNIVERSITY OF TEXAS

AUSTIN
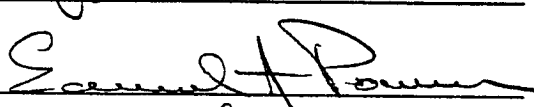
LOW FREQUENCY FLUCTATIONS OF PLASMA MAGNETIC FIELDS
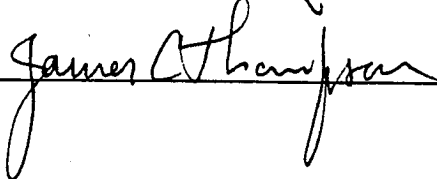
APPROVED BY

SUPERVISORY COMMITTEE:

_____

Wendell Horton

_____

_____

_____

James C Thompson

This dissertation is dedicated to my parents, Clyde Joseph and Ann Shaw Cable. This work would certainly not exist without all the support and encouragement they have shown me.

LOW FREQUENCY FLUCTUATIONS OF PLASMA MAGNETIC FIELDS

by

SAMUEL BENJAMIN CABLE, B.S.

DISSERTATION

Presented to the Faculty of the Graduate School of

The University of Texas at Austin

in Partial Fulfillment

of the Requirements

for the Degree of

DOCTOR OF PHILOSOPHY

THE UNIVERSITY OF TEXAS AT AUSTIN

May, 1992

Acknowledgments

Where do I begin? There are so many people who have helped me along the way for the past seven years. I suppose that if I were to write down everything everyone has done for me since I started graduate school, "the whole world could not contain all that would be written." Well, maybe that's a bit of an exaggeration, but the quote seemed appropriate. In any event I will do my best here as I finish up writing this dissertation. (It is rather sad that saying "thank you" is the thing we always leave for last, or at any rate, the thing that I always leave for last.)

First of all, I want to thank everyone who has made my five years of research and dissertation work a little less of a purgatory than it could have been. Thanks most of all to my parents who helped me through quite a few emotional and financial tight spots. They have continually stood by me, believing I could actually do all this, and wanting me to succeed. Thanks to the family of Casey and Linda Carter, whose unflagging hospitality helped me greatly in coming to feel at home in Austin. Thanks to Pat and Tracey Villareal and Dallas and Maria Hutton. They have been some of the best friends that I could hope to have. Thanks for all the encouragement and all the laughs (especially the laughs). I have to give a special thanks to Dorothy Parungao, whose heart is surely made of pure gold. She was my support through some of the toughest times I have had here. I sadly have to say that my capacity for friendship and loyalty has not equaled hers. If my heart can ever grow into something like hers, I will be a happy man. A few words need to be

said about my comrade in arms in the graduation war, Jim Koga. He has let me interrupt him countless times to ask questions about FORTRAN, NERSC, NCAR, UNIX, and almost every other word in the English language spelled with all capitols; he has been one of the few people with whom I could discuss both science and religion in depth; but more important than all this, he laughed at me when I got gastroenteritis at the 1990 APS conference so thanks for nothing you stupid pinhead, you still owe me big time. Everybody from George Bush to George Foreman wants to thank God these days, so I guess I might as well too. Thanks to Him for all the details that seemed to work themselves out over the past few years, details which were often completely out of my hands, and for all the patience with my whining and complaining, and most of all, for giving me a reason to do all this in the first place.

Plenty of people have helped me out academically too, of course. First and foremost among them is my advisor, Prof. Toshiki Tajima. I want to thank him for all my conference trips he paid for, and the uncountable job prospects he brought my way. And I want to thank him for one of the most well-rounded physics educations I could have received, and for the opportunity to do some very new and interesting research. Thanks to Profs. Wendell Horton, Jim Thompson, Jim Erskine, and Ed Powers for serving on my dissertation committee. Thanks to Dr. Richard Steinolfson for helping me understand the workings of his MHD fluid code, and, of course, for offering me a job. Thanks to Dr. Kikuo Umegaki for his help with my MHD particle problems. Thanks to Dr. Bill Rowan for an opportunity to do some experimental work on the Tokamak a few years back, and thanks for all those letters of reference. Thanks to David Lindberg for doing many of the numerical integrals in this dissertation.

Thanks to Eva Riley for professionally preparing many of the figures contained herein (not an easy job, given my convoluted instructions). Thanks to Suzy Crumley for her great amount of help in typing this thing.

I am sure that I am leaving out many people who deserve to be mentioned here but, if it's any consolation, I would put you in if I could remember. Anyway, to all of you guys - you're great, really. Give yourselves a hand.

SAMUEL BENJAMIN CABLE

The University of Texas at Austin

May, 1992

LOW FREQUENCY FLUCTUATIONS OF PLASMA MAGNETIC FIELDS

Samuel Benjamin Cable, Ph.D.
The University of Texas at Austin, 1992

Supervisor: Toshiki Tajima

The fluctuation-dissipation theorem is used to study fluctuation power spectra in various plasmas, particularly at low frequencies. Gaseous and degenerate plasmas are studied. Careful application of the theorem shows that a cold, non-magnetized plasma has a sharp zero-frequency peak in its magnetic field power spectrum. When a uniform magnetic field is applied to the plasma, the energy under the zero-frequency peak is shifted into the Alfvén and cyclotron modes. A simple relation between the fluctuation spectra and dispersion relations of electromagnetic waves is found in deriving this result. Using a kinetic theory treatment, a warm, isotropic plasma is shown to exhibit a zero-frequency peak in its magnetic power spectrum, with a different functional dependence on frequency. In a stationary degenerate plasma the magnetic power spectrum again has a zero-frequency peak. In a degenerate plasma with net drift velocity, a white noise spectrum in voltage fluctuation is found. This spectrum is similar to shot noise.

Effects of fluid expansion on the Rayleigh-Taylor instability are studied. Overall fluid expansion often has a retarding effect on the growth of Rayleigh-Taylor (RT) instabilities. Two new analytical examples of this phenomenon of reduced growth or stabilization are given. Confirmation of this phenomenon is also obtained from a new MHD code constructed specifically for modelling fluids undergoing nearly homogeneous expansion or contraction. In the code, expansion is treated by making each point of the computational grid co-moving with a predetermined overall expansion.

Short-range force effects on the Rayleigh-Taylor instability are also studied with the help of a new PIC MHD code. It is to be expected that short-range forces would effect the instability much like surface tension, slowing the growth of the instability. Comparisons of simulations with and without short-range forces do not give unambiguous confirmation of this expectation, however. Limitations to the accuracy of the code exist at short wavelengths, where the effects of the short-range forces would be expected to be most pronounced.

Table of Contents

List of Tables

List of Figures

Chapter 1

Fluctuation Power Spectra in Gaseous and Degenerate Plasmas

1.1 Introduction and Outline

In a plasma, quantities such as local electron density, ion density, electric field, and magnetic field are all smoothly varying and well-defined functions of space and time, on some practical or coarse-grained scale. This is part and parcel of the definition of a plasma. However, since the constituents of a plasma are discrete particles, these quantities are in a constant state of flux in the most quiescent of plasmas, always rising and falling about their well-defined mean values.

The fluctuations in electromagnetic field are the main concerns of this paper. These fluctuations may be aptly described as random fluctuations for the cases of weakly correlated plasmas such as gaseous plasmas and ideal degenerate plasmas. The statistics of these fluctuations — their root-mean-square amplitudes, for instance — are completely determined by the mean values of the plasma quantities in thermal equilibrium. In particular, the power spectrum of a given quantity's fluctuations is determined completely by: 1) the amount of energy needed to produce a fluctuation of a given size in a given mode, 2) the temperature of the plasma, and 3) the dissipation mechanisms at work in the plasma. This determination is expressed for weakly correlated (and nearly linear) plasmas not far from equilibrium by the fluctuation-dissipation

theorem [1,2,3]. In this report, we apply the fluctuation-dissipation theorem to plasmas in thermal equilibrium, and derive the power spectra of fluctuations in the plasma magnetic field. An alternative method for deriving the spectra, which we will not use here, would be to derive the kinetic theoretic equation applying the superposition principle [4,5].

We begin in Sec. 3 with a homogeneous, isotropic, non-magnetized cold plasma. (We will say a few words about Sec. 2 momentarily.) We see that the fluctuation spectra of the magnetic field is particularly interesting because it exhibits a strong zero-frequency component. This zero-frequency component is a Dirac δ function in a non-dissipative plasma, and is broadened into a Lorentzian curve in a dissipative plasma. This phenomenon may have implications for the physics of the early universe. Because of this, much of our calculations in this section are made for an electron-positron plasma whose temperature and density have been chosen so that it, presumably, describes the universe in the early radiation epoch.

Since we assume, in beginning, an isotropic, non-magnetized plasma, it is curious that our mathematics should tell us that we actually have a plasma with a magnetic field which is nearly stationary in time (even though it is far from uniform in space). Does a plasma in a presupposed stationary magnetic field exhibit a similar fluctuation spectrum? As a consistency check, then, we study in Sec. 4 the fluctuation spectra of a thermal equilibrium plasma in a uniform, constant magnetic field $\mathbf{B}_0$. On the way to deriving the spectra, a relationship between the dispersion relation of an electromagnetic wave and its fluctuations is found. We find a substantial amount of low-frequency fluctuations, but they are not concentrated in the Dirac δ-function we found for the isotropic plasma. Rather, it is seen that the imposed magnetic field transfers

energy out of $\omega = 0$ into a range of frequencies running from $\omega = 0$ up to the lower hybrid frequency. We find, however, that the limit $\mathbf{B}_0 \rightarrow 0$ is completely consistent with the results of Sec. 3.

We take another look at the isotropic plasma by way of kinetic theory in Sec. 5. We again find a zero-frequency peak in the magnetic field fluctuation power spectrum, though its frequency dependence differs from that of the peak found in Sec. 3.

In Sec. 6, we discuss magnetic field fluctuation spectra obtained from computer simulations of thermal equilibrium plasmas. In these particle simulations, the fluctuation spectrum of the magnetic field has been recorded. We discuss its size and shape in light of the predictions made in Sec. 3.

Throughout our calculations, we need to introduce a phenomenological cutoff in wavenumber k. The legitimacy of such a cutoff is established in Sec. 7 by way of quantum mechanical considerations.

In Sec. 8, we address the Bohr-van Leeuwen theorem, namely, that classical statistical mechanics does not allow the magnetization of a physical medium. This might seem to present a contradiction to our result of finite magnetic field energy at $\omega = 0$ in the non-magnetized plasma. This contradiction is shown to be only apparent.

In Sec. 9 we look at electrostatic and electromagnetic fluctuations in a degenerate electron gas. We find that electric field fluctuations and particle density fluctuations vanish at zero frequency. However, magnetic field fluctuations diverge at zero frequency. This divergence is proportional to ω^{-1} over a large frequency range.

In Sec. 10, we examine some possible cosmological consequences of our results. Low-frequency magnetic fields may have consequences for structure

formation in the radiation epoch of the early Universe. They might also be the seed fields for the presently observed galactic magnetic fields.

In Sec. 11, other possible consequences are considered. The low-frequency magnetic fields we discuss may effect particle transport in plasmas. They may also be responsible for anomalous spin relaxation in condensed matter.

Before we discuss these subjects for real plasmas, however, it may be instructive to begin with a model problem which involves the Brownian motion of a system described by a one dimensional wave equation. In such a system, the resultant fluctuations can be treated as random fluctuations without any correlations. This section should involve some familiar physics, but is intended to elucidate the theoretical foundation of the present paper in a simplified model problem. This is treated in Sec. 2.

1.2   One-Dimensional Waves with Brownian Motion

The point to this section is to provide the reader with some examples of low-frequency divergences in the power spectra of some simple wave motions, before we go on to study the phenomenon in electromagnetic plasma waves, where the mathematics may be opaque in comparison.

We consider a physical system described by a wave equation:

$$\frac{\partial^2 y}{\partial t^2} = c^2 \frac{\partial^2 y}{\partial x^2},$$

(1.1)

where $y(x,t)$ is the local displacement of some quantity from its equilibrium value and c is the phase velocity of waves in the system. We could be speaking here about sound waves in air or water, longitudinal waves in a compressional spring, transverse waves on a piano wire, *etc.* What we want to ask is: Given

that our physical system is in thermal equilibrium, what is the power spectrum of the motion it undergoes because of thermal fluctuations?

To this end, we make our wave equation a little more realistic, adding two terms to it:

$$\frac{\partial^2 y}{\partial t^2} = c^2 \frac{\partial^2 y}{\partial x^2} - \eta \frac{\partial y}{\partial t} + a(x,t). \tag{1.2}$$

The first new term is a damping term. It could have as its source some internal friction of the system, or it could be the dissipative effect of thermal fluctuations such as what we see in Brownian motion. $a(x,t)$ is a spatially and temporally random function, describing the fluctuating accelerations imparted to local elements of the system. If we were describing a piano wire here, $a(x,t)$ could represent local accelerations from internal thermal fluctuations in the molecules making up the wire, or it could describe the momentum transferred from air molecules constantly bombarding the wire. In the mathematics that follows, we make the reasonable assumption that $\langle a(x,t) \rangle$ (the ensemble average of $a(x,t)$) is equal to zero and that, therefore, $\langle y(x,t) \rangle$ is equal to zero.

First of all, we Fourier transform our new equation to get

$$(-\omega^2 + c^2 k^2 - i\eta\omega)y(k,\omega) = a(k,\omega). \tag{1.3}$$

Let $Y(k,\omega)$ be the ensemble averaged intensity of $y(k,\omega)$ and let $A(k,\omega)$ be the ensemble averaged intensity of $a(k,\omega)$. Then we see

$$Y(k,\omega) = \frac{A(k,\omega)}{(-\omega^2 + c^2 k^2)^2 + \eta^2 \omega^2}. \tag{1.4}$$

The simplest assumption is that $a(x,t)$ is a series of Dirac-δ functions randomly distributed in space and time. That is, we assume that the fluctuating accelerations take the form of momentum impulses delivered over very short

lengths of the system. The fluctuations are uncorrelated with one another, and have a white-noise power spectrum. This being given, $a(x,t)$ will have a correlation function given by

$$\langle a(x_0, t_0) a(x_0 + x, t_0 + t) \rangle = a^2 \delta(t) \delta(x), \qquad (1.5)$$

where a^2 is a number derived from the distribution of the strength of the random impulses and the space and time intervals between them. The dimension of a^2 is that of $(a(x,t))^2$ times length and time. From this it follows that

$$A(k, \omega) = \int dt\, dx\, e^{-ikx + i\omega t} \langle a(x_0, t_0) a(x_0 + x, t_0 + t) \rangle$$

$$= a^2. \qquad (1.6)$$

Eq. (1.4) then becomes

$$Y(k, \omega) = \frac{a^2}{(-\omega^2 + c^2 k^2)^2 + \eta^2 \omega^2}. \qquad (1.7)$$

Now we find $Y(k,t)$ by Fourier transforming $Y(k,\omega)$:

$$Y(k, t) = \frac{1}{2\pi} \int d\omega\, e^{-i\omega t} \frac{a^2}{(-\omega^2 + c^2 k^2)^2 + \eta^2 \omega^2}$$

$$= \frac{a^2 e^{-\eta|t|/2}}{2\eta c^2 k^2} [\cos(\omega_1 t) + \frac{\eta}{2\omega_1} \sin(\omega_1 t)] \qquad (1.8)$$

where

$$\omega_1 = (c^2 k^2 - \frac{\eta^2}{4})^{1/2}.$$

From this, it immediately follows that

$$Y(k, t = 0) = \langle y(k) y^*(k) \rangle = \frac{a^2}{2\eta c^2 k^2}. \qquad (1.9)$$

If we assume that the system is in classical thermal equilibrium with some heat bath at temperature T, we are constrained by the equipartition law to say

$$\mu \frac{c^2 k^2}{2} \langle y(k) y^*(k) \rangle = \frac{T}{2} \qquad (1.10)$$

where μ is a constant representing the inertia of the system. If our system is a wire, μ is the mass per unit length of the wire. It follows from Eq. (1.9) and Eq. (1.10) that

$$a^2 = \frac{2\eta T}{\mu}$$

and

$$Y(k,\omega) = \frac{2\eta T/\mu}{(\omega^2 - c^2 k^2)^2 + \eta^2 \omega^2}. \qquad (1.11)$$

To find the limit of $Y(k,\omega)$ in the limit $\eta \to 0$, we make use of a standard definition of the Dirac δ-function to obtain:

$$Y(k,\omega) = \frac{2T\pi}{\mu \omega^2} \delta \left(\frac{-\omega^2 + c^2 k^2}{\omega} \right). \qquad (1.12)$$

Note that each mode in k-space behaves exactly like a Brownian particle in a harmonic oscillator potential with a characteristic frequency $\omega_0 = ck$. This can be seen most clearly by comparing the current results with Kubo's results for the Brownian motion of a harmonic oscillator [6]. In a sense then, there is nothing new here. And yet, some interesting results appear. We can content ourselves with examining the simpler form of $Y(k,\omega)$ in Eq. (1.12). If we want the fluctuation strength as a function of wavenumber alone, then we integrate $Y(k,\omega)$ over $d\omega$ and divide by 2π. If we want the fluctuation spectrum of frequency alone, we integrate $Y(k,\omega)$ over dk and divide by 2π. We find

$$Y(k) = \frac{T}{\mu c^2 k^2} \qquad (1.13)$$

and

$$Y(\omega) = \frac{T}{\mu c \omega^2}. \qquad (1.14)$$

If we have a harmonic oscillator of mass m and frequency ω_0, vibrating with an amplitude A, the potential energy of the oscillation $W(\omega_0)$ is, on average, $mA^2\omega_0^2/2$. Each mode k of our oscillator is a harmonic oscillator of mass density μ and frequency ck, vibrating with an amplitude of $\sqrt{Y(k)}$. Therefore, the wavenumber power spectrum W(k) is given by

$$W(k) = \frac{\mu c^2 k^2}{2} Y(k) = \frac{T}{2}. \tag{1.15}$$

Also, since $W(k)dk = W(\omega)d\omega$,

$$W(\omega) = \frac{T}{2c}. \tag{1.16}$$

$W(k)$ and $W(\omega)$ both integrate to give the same total energy density E. The two spectra are consistent with each other and with Parceval's theorem. In this purely classical treatment, however, both spectra integrate to give $(1/2\pi)\int T/2 dk$, resulting in a one-dimensional ultraviolet divergence.

What happens if we add a "mass" to our system? We may get an equation like:

$$\frac{\partial^2 y}{\partial t^2} = c^2 \frac{\partial^2 y}{\partial x^2} - \omega_0^2 y - \eta \frac{\partial y}{\partial t} + a(x,t). \tag{1.17}$$

We now have an equation more nearly describing a plasma wave, or a massive Klein-Gordon field, or a taut piano wire sitting on top of a set of uncoupled springs. Now, to study this system, we run through all of our above mathematical analysis with the substitution $c^2 k^2 \rightarrow c^2 k^2 + \omega_0^2$. We find for $Y(k,\omega)$

$$Y(k,\omega) = \frac{2\eta T/\mu}{(\omega^2 - c^2 k^2 - \omega_0^2)^2 + \eta^2 \omega^2}. \tag{1.18}$$

If we take the limit $\eta \rightarrow 0$ again, we find

$$Y(k,\omega) = \frac{2\pi T}{\mu \omega^2} \delta\left(\frac{\omega^2 - c^2 k^2 - \omega_0^2}{\omega}\right), \tag{1.19}$$

$$Y(k) = \frac{T}{\mu(c^2 k^2 + \omega_0^2)}, \tag{1.20}$$

and

$$Y(\omega) = \begin{cases} \frac{T}{\mu c \omega (\omega^2 - \omega_0^2)^{1/2}} & |\omega| \geq \omega_0 \\ 0 & |\omega| < \omega_0 \end{cases} \qquad (1.21)$$

$Y(\omega)$ diverges as $(\omega^2 - \omega_0^2)^{-1/2}$ at $\omega = \omega_0$.

Since $\omega(k) = (c^2 k^2 + \omega_0^2)^{1/2}$, $W(k) = T/2$, again satisfying the equipartition law. However, since, once again, $W(k)dk = W(\omega)d\omega$, we find

$$W(\omega) = \frac{T}{2} \frac{\omega}{c(\omega^2 - \omega_0^2)^{1/2}}. \qquad (1.22)$$

Without the system "mass," $Y(\omega)$ diverged at $\omega = 0$ but $W(\omega)$ remained finite. Now $W(\omega)$ diverges as well. It would appear that this effect is real, despite the fact that the integral of $W(\omega)$ over all ω is infinite. The divergence in the integral is caused by contributions to the integral from $\omega \to \infty$, not from $\omega \approx \omega_0$. In other words, the divergence in the integral is an ultraviolet divergence. It corresponds to the ultraviolet divergence we get when we integrate $W(k) = T/2$ over all k. In fact, $\int W(\omega)d\omega = \int W(k)dk$. Therefore, once again, the two spectra are consistent with one another and with Parceval's theorem.

The ultraviolet divergence we see here is, as well as in Eqs. (1.15) and (1.16), in essence, the blackbody radiation problem Planck solved by introducing his quantum mechanical energy distribution. The general quantum mechanical fluctuation-dissipation theorem is presented in detail by Sitenko [3]. It might be worthwhile, however, to review it here, and present the quantum mechanical analogue to the work we have done thus far.

Suppose we have some kind of quantum mechanical, Hamiltonian system. It can be a hydrogen atom or a harmonic oscillator or anything describable by quantum mechanics. In this system, we will have a potential energy, $V(x, t)$. Let us assume that we can break this potential up into a fairly smoothly varying part and a random part. Let us also assume that the random part of the

potential couples to the expectation value of some current in the system so that

$$V(t) = - \int dx A(x,t) \langle j(x,t) \rangle. \tag{1.23}$$

For instance, $j(x,t)$ could be the electrostatic current in a dielectric and $A(x,t)$ could be the vector potential. We make two more assumptions: First, V(t) is the only explicitly time-dependent part of the Hamiltonian. Then

$$\frac{\partial V(t)}{\partial t} = - \int dx \dot{A}(x,t) \langle j(x,t) \rangle. \tag{1.24}$$

Lastly we assume $A(x,t)$ and $j(x,t)$ are related to one another by some linear operator so that

$$j_i(x,t) = \hat{\alpha}_{ij} A_j(x,t) \tag{1.25}$$

or, after Fourier transforming in x and t,

$$j_i(\mathrm{k},\omega) = \alpha_{ij}(\mathrm{k}\omega) A_j(\mathrm{k}\omega). \tag{1.26}$$

The spectral distribution of the space-time correlation function $\langle j_i j_j \rangle_{\mathrm{rt}}$ will be denoted by $\langle j_i j_j \rangle_{\mathrm{k},\omega}$. It is related to the expectation value of the product of the Fourier components of $\mathbf{j}$ by

$$\langle j_i^*(\mathrm{k}) j_j(\mathrm{k}') \rangle_\omega = (2\pi)^3 \delta(\mathrm{k} - \mathrm{k}') \langle j_i j_j \rangle_{\mathrm{k},\omega}. \tag{1.27}$$

A calculation of the transition probabilities arising from the action of $A(x,t)$ on the system shows that the energy absorbed per unit time by the system is

$$Q = \frac{\omega}{4\pi} \sum_{\mathrm{k},\mathrm{k}'} A_i(\mathrm{k}\omega) A_j^*(\mathrm{k}',\omega) \{ \langle j_i^*(\mathrm{k}) j_j(\mathrm{k}') \rangle_\omega^{\hbar\omega} - \langle j_i^*(\mathrm{k}) j_j(\mathrm{k}') \rangle_\omega \}, \tag{1.28}$$

where

$$\langle j_i^*(\mathrm{k}) j_j(\mathrm{k}') \rangle_\omega = 2\pi \sum_{m,n} f(E_n) j_i^*(\mathrm{k})_{nm} j_j(\mathrm{k}')_{mn} \delta(\omega - \omega_{nm}),$$

and

$$\langle j_i^*(\mathbf{k})j_j(\mathbf{k}')\rangle_\omega^{\hbar\omega} = 2\pi \sum_{m,n} f(E_n - \hbar\omega)j_i^*(\mathbf{k})_{nm}j_j(\mathbf{k}')_{mn}\delta(\omega - \omega_{nm}).$$

In the above expressions, $\omega_{nm} = (E_n - E_m)/\hbar$, and $f(E_n)$ is the statistical distribution of the states of the system.

However, averaging Eq. (1.24) over one period of oscillation shows that the energy absorbed per unit time is also equal to

$$Q = \frac{\omega}{4}\sum_{\mathbf{k}}(\alpha_{ij}^* - \alpha_{ji})A_i(\mathbf{k}\omega)A_j^*(\mathbf{k},\omega). \tag{1.29}$$

Comparing Eqs. (1.28) and (1.29), and making use of Eq. (1.27) shows

$$\langle j_ij_j\rangle_{\mathbf{k}\omega}^{\hbar\omega} - \langle j_ij_j\rangle_{\mathbf{k}\omega} = i\hbar\{\alpha_{ij}^*(\mathbf{k}\omega) - \alpha_{ji}(\mathbf{k}\omega)\}. \tag{1.30}$$

If the system is in thermodynamic equilibrium, immersed in a heat bath with temperature T, $f(E_n)$ is given by the Gibbs distribution

$$f(E_n) = e^{(F-E_n)/T},$$

where F is the free energy of the system and T is the system temperature. In this case

$$\langle j_ij_j\rangle_{\mathbf{k}\omega}^{\hbar\omega} = e^{\hbar\omega/T}\langle j_ij_j\rangle_{\mathbf{k}\omega}.$$

Therefore

$$\langle j_ij_j\rangle = \frac{\hbar}{e^{\hbar\omega/T} - 1}i(\alpha_{ij}^* - \alpha_{ji}). \tag{1.31}$$

Now, for our specific problem,

$$\frac{\partial V(x,t)}{\partial t} = \int dx\, \mu a(x,t)\dot{y}(x,t). \tag{1.32}$$

So then, comparing Eq. (1.23) with Eq. (1.32), we see that in our piano wire system, $-\dot{A}(x,t) = \mu a(x,t)$ and $j(x,t) = \dot{y}(x,t)$. From our equation of motion we can find the factor α:

$$\alpha(k,\omega) = \frac{\omega^2}{\mu(-\omega^2 + c^2 k^2 - i\eta\omega)}. \tag{1.33}$$

And a little bit of algebra will show that Eq. (1.31) gives

$$\langle |\dot{y}|^2 \rangle = \frac{\hbar}{e^{\hbar\omega/T} - 1} \frac{2\eta\omega^3}{\mu[(\omega^2 - c^2 k^2)^2 + \eta^2\omega^2]}. \tag{1.34}$$

Now, since $\dot{y} = -i\omega y$, $|\dot{y}|^2 = \omega^2 |y|^2$. So

$$\langle |y|^2 \rangle = \frac{\hbar}{e^{\hbar\omega/T} - 1} \frac{2\eta\omega}{\mu[(\omega^2 - c^2 k^2)^2 + \eta^2\omega^2]}. \tag{1.35}$$

Note that in the limit $\hbar \to 0$, Eq. (1.35) will give Eq. (1.11). The power spectrum is $\mu\omega^2\langle |y|^2 \rangle/2$; it equals

$$W(k,\omega) = \frac{\hbar}{e^{\hbar\omega/T} - 1} \frac{\eta\omega^3}{[(\omega^2 - c^2 k^2)^2 + \eta^2\omega^2]}. \tag{1.36}$$

As $\hbar \to 0$, this expression also gives the classical limit of Eq. (1.16). In the this quantum mechanical expression, however, the ultraviolet divergence ($\omega \to \infty$) is clearly removed by the Planck distribution factor. If we add a mass term to the system again, the result will be

$$W(k,\omega) = \frac{\hbar}{e^{\hbar\omega/T} - 1} \frac{\eta\omega^3}{[(\omega^2 - c^2 k^2 - \omega_0^2)^2 + \eta^2\omega^2]}. \tag{1.37}$$

Again, the Planck distribution cures the ultraviolet divergence, but the divergence at ω_0 remains. In the rest of this dissertation, our focus is on the lower frequency behavior of functions corresponding to $W(\omega)$ in a plasma. In many instances we shall see infrared divergences due to plasma effects.

1.3 A Gaseous Plasma with no External Field

Even at or near thermal equilibrium, a plasma has fluctuations. The various fields of a plasma (electromagnetic, electrostatic, density, etc.) fluctuate about their mean values. The strengths of these fluctuations are functions of two characteristics of the plasma: the dissipation mechanisms present in it, and its temperature T. The relation between these quantities can be found by means of the fluctuation-dissipation theorem [2]. In this section, we employ the fluctuation-dissipation theorem to derive the power spectra of magnetic field fluctuations in an isotropic, non-magnetized plasma which we describe with fluid equations of motion.

The following derivation closely parallels the work of Geary *et al.* [7]. We consider a homogeneous, isotropic plasma in thermal equilibrium. From the fluctuation-dissipation theorem, the strength of the electric field fluctuations as a function of frequency and wave vector is

$$\frac{1}{8\pi}\left(\langle E_i E_j\rangle_{\mathbf{k}\omega}^{\hbar\omega} - \langle E_i E_j\rangle_{\mathbf{k}\omega}\right) = i\hbar\{\Lambda_{ji}^{-1} - \Lambda_{ij}^{-1*}\}$$

where

$$\Lambda_{ij}(\omega,\mathbf{k}) = \frac{c^2 k^2}{\omega^2}\left(\frac{k_i k_j}{k^2} - \delta_{ij}\right) + \epsilon_{ij}(\omega,\mathbf{k}),$$

$\epsilon_{ij}(\omega,\mathbf{k})$ being the dielectric tensor of the plasma [3]. $\langle E_i E_j\rangle_{\mathbf{k}\omega}^{\hbar\omega}$ and $\langle E_i E_j\rangle_{\mathbf{k}\omega}$ are related to one another in the same way as $\langle j_i j_j\rangle_{\mathbf{k}\omega}^{\hbar\omega}$ and $\langle j_i j_j\rangle_{\mathbf{k}\omega}$ were in the previous section.

If the plasma is in thermal equilibrium, then

$$\langle E_i E_j\rangle_{\mathbf{k}\omega}^{\hbar\omega} = e^{\hbar\omega/T}\langle E_i E_j\rangle_{\mathbf{k}\omega},$$

as can be inferred from the results given in the previous section. Therefore,

$$\frac{1}{8\pi}\langle E_i E_j\rangle_{\mathbf{k}\omega} = \frac{i}{2}\frac{\hbar}{e^{\hbar\omega/T} - 1}\{\Lambda_{ji}^{-1} - \Lambda_{ij}^{-1*}\}.$$

Consider an electromagnetic wave in the plasma; call its wave vector $\mathbf{k} = k\hat{x}$. Invoking Faraday's law, we find

$$\frac{\langle B_2^2 \rangle_{\mathbf{k}\omega}}{8\pi} = \frac{i}{2} \frac{\hbar}{e^{\hbar\omega/T} - 1} \frac{c^2 k^2}{\omega^2} \{ \Lambda_{33}^{-1} - \Lambda_{33}^{-1*} \},$$

and

$$\frac{\langle B_3^2 \rangle_{\mathbf{k}\omega}}{8\pi} = \frac{i}{2} \frac{\hbar}{e^{\hbar\omega/T} - 1} \frac{c^2 k^2}{\omega^2} \{ \Lambda_{22}^{-1} - \Lambda_{22}^{-1*} \},$$

where the subscripts 1, 2, and 3 refer to the x, y, and z directions respectively. So the total magnetic field fluctuation strength is

$$\frac{\langle B_{tot}^2 \rangle_{\mathbf{k}\omega}}{8\pi} = \frac{i}{2} \frac{\hbar}{e^{\hbar\omega/T} - 1} \frac{c^2 k^2}{\omega^2} \{ \Lambda_{22}^{-1} + \Lambda_{33}^{-1} - \Lambda_{22}^{-1*} - \Lambda_{33}^{-1*} \}. \qquad (1.38)$$

We now find $\epsilon_{ij}(\omega, \mathbf{k})$, in order to determine $\Lambda_{ij}(\omega, \mathbf{k})$. First, we specify the equation of motion of the plasma. From the equation of motion, we find a relationship between the electric field and the current. The dielectric $\epsilon_{ij}(\omega, \mathbf{k})$ will follow from this relationship.

We introduce a simple model of a plasma based on a cold plasma fluid theory, neglecting kinetic effects necessary to adequately describe warm plasmas. (Perhaps the model is too simplistic; a discussion of this point will follow below.) If the velocities and electromagnetic fields are small enough that we can neglect the $\mathbf{v} \times \mathbf{B}$ forces, then

$$m_\alpha \frac{d\mathbf{v}_\alpha}{dt} = e_\alpha \mathbf{E} - \eta_\alpha m_\alpha \mathbf{v}_\alpha, \qquad (1.39)$$

where α is a particle species label and η_α is the effective collision frequency of species α. An equation of motion more accurate than Eq. (1.39) may lead to an expression for $\langle B^2 \rangle_{\mathbf{k}\omega}$ with more realistic mathematical properties. Be that as it may, the equation of motion we have yields

$$(-i\omega + \eta_\alpha)\mathbf{j}_\alpha = \frac{\omega_{p\alpha}^2}{4\pi} \mathbf{E}, \qquad (1.40)$$

where $\mathbf{j}_\alpha$ is the current density of species α. The dielectric tensor $\epsilon_{ij}(\omega, \mathbf{k})$ is given by

$$\epsilon_{ij}(\omega, \mathbf{k}) = \delta_{ij} + 4\pi \sum_\alpha \chi_{\alpha ij}(\omega, \mathbf{k}), \qquad (1.41)$$

where the susceptibility tensor $\chi_{\alpha ij}$ is defined by the relation

$$j_{\alpha i} = -i\omega \chi_{\alpha ij}(\omega, \mathbf{k}) E_j(\omega, \mathbf{k}).$$

So, from Eq. (1.40),

$$4\pi \chi_{\alpha ij}(\omega, \mathbf{k}) = \frac{\omega_{p\alpha}^2}{\omega(\omega + i\eta_\alpha)} \delta_{ij},$$

and

$$\epsilon_{ij}(\omega, \mathbf{k}) = \delta_{ij} - \sum_\alpha \frac{\omega_{p\alpha}^2}{\omega(\omega + i\eta_\alpha)} \delta_{ij}. \qquad (1.42)$$

It will be seen below that the results of these calculations have a particularly interesting impact on the physics of dense plasmas, such as the plasma of the early Universe radiation epoch. Just prior to cooling below 1 MeV, the universe was, apparently, an electron-positron plasma [8], and it is this type of plasma that we will discuss in the next several paragraphs. However, the derivations and results are valid, with minor modifications, for more ordinary plasmas as well.

In an electron-positron plasma, $\omega_{pe+}^2 = \omega_{pe-}^2$ and $\eta_{e+} = \eta_{e-} = \eta$. So Eq. (1.42) becomes

$$\epsilon_{ij}(\omega, \mathbf{k}) = \delta_{ij} - \frac{\omega_p^2}{\omega(\omega + i\eta)} \delta_{ij} \qquad (1.43)$$

where $\omega_p^2 = \omega_{pe+}^2 + \omega_{pe-}^2$. We now obtain

$$\Lambda_{ij} = \begin{pmatrix} 1 - \dfrac{\omega_p^2}{\omega(\omega + i\eta)} & & \\ & 1 - \dfrac{c^2 k^2}{\omega^2} - \dfrac{\omega_p^2}{\omega(\omega + i\eta)} & \\ & & 1 - \dfrac{c^2 k^2}{\omega^2} - \dfrac{\omega_p^2}{\omega(\omega + i\eta)} \end{pmatrix} \qquad (1.44)$$

We combine Eqs. (1.38) and (1.44) and obtain, after some algebra,

$$\frac{\langle B^2 \rangle_{\mathbf{k}\omega}}{8\pi} = \frac{2\hbar\omega}{e^{\hbar\omega/T} - 1}\eta\omega_p^2\frac{c^2k^2}{\omega^2}\frac{1}{[\omega^2 - c^2k^2 - \omega_p^2]^2 + \eta^2[\omega - c^2k^2/\omega]^2}, \quad (1.45)$$

or

$$\frac{\langle B^2 \rangle_{\mathbf{k}\omega}}{8\pi} = \frac{2\hbar\omega}{e^{\hbar\omega/T} - 1}\eta\omega_p^2 \times$$

$$\frac{c^2k^2}{(\omega^2 + \eta^2)c^4k^4 + 2\omega^2c^2k^2(\omega_p^2 - \omega^2 - \eta^2) + [(\omega^2 - \omega_p^2)^2 + \eta^2\omega^2]\omega^2}. \quad (1.46)$$

The first form of $\langle B^2 \rangle_{\mathbf{k}\omega}/8\pi$, with a pole being clearly offset from the electromagnetic plasma wave pole, might be more physically understandable, whereas the second form will make integration over d^3k a less difficult task. Note that if relativistic temperature effects are included, the above formulae are altered by the substitution $\omega_p \rightarrow \omega_p/\sqrt{\gamma}$. Fig. 1.1 shows a contour plot of the natural logarithm of Eq. (1.46) weighted with the geometrical factor k^2. The density ($n_e = 4.84 \times 10^{30}/\text{cm}^3$) and temperature ($T = 10^{10}\,^\circ\text{K} = 1\text{MeV}$) have been chosen to represent the early Universe plasma at 1 sec. after the Big Bang. The collision frequency η has been set at $0.1\omega_{pe}$, which is about 100 times larger than expected. This smooths out the contours of the graph and gives a better view of the qualitative behavior of the spectrum.

We now want to find the fluctuation power spectrum as a function of frequency, that is $\langle B^2 \rangle_{\omega}$. We find this spectrum by integrating $\langle B^2 \rangle_{\mathbf{k}\omega}$ over wavenumber d^3k and dividing the result by $(2\pi)^3$. We obtain:

$$\frac{\langle B^2 \rangle_{\omega}}{8\pi} = \frac{2\hbar\omega}{e^{\hbar\omega/T} - 1}\frac{2\eta}{2\pi^2\omega_{pe}^2}\left(\frac{\omega_{pe}}{c}\right)^3\int_0^\infty dx\frac{x^4}{(\omega'^2 + \eta'^2)x^4 + \ldots}, \quad (1.47)$$

where $x = ck/\omega_{pe}$ and the primed quantities are normalized by ω_{pe} (e.g. $\eta' = \eta/\omega_{pe}$). However, we are immediately faced with a problem. At large k, which corresponds directly to large x, the integrand of Eq. (1.47) becomes effectively constant, so the integral diverges.

The divergence occurs at high wavenumbers. However, this divergence at high k is different from the one we discussed in Sec. 2. As seen in Eq. (46), the Planck factor $(e^{\hbar\omega/T} - 1)^{-1}$ is already incorporated and thus no ultraviolet divergence arises as $\omega \rightarrow \infty$. Rather, the divergence resides in the more subtle interaction between matter and radiation. Up to this point, we have based our calculations on classical equations of motion with a model collision term. In these equations the photon fields appear as smooth electromagnetic fields. In this sense, these equations may be regarded as multicomponent fluid equations for electrons. At some small enough physical scale (or, equivalently, some large enough wavenumber) the granular nature of any fluid (photons or electrons) will become apparent and render the continuum fluid equations invalid. Where the fluid "picture" breaks down, we need new equations. We might obtain such equations from a kinetic theory which includes more exact collisional effects, wave-particle interactions, etc. In the interest of tractability, however, we want to continue with the simple model presently before us. How do we manage this?

Our reasoning is as follows: Consider electromagnetic waves propagating through a plasma. The dispersion relation for waves of long wavelength is strongly dependent on the collective effects of the plasma. Waves of shorter wavelength are affected less by the plasma. If a wave has a wavelength much shorter than the collisionless skin depth c/ω_p, it moves through the plasma almost as if it were moving through empty space. It stands to reason that, for wavelengths much smaller than c/ω_p and frequencies much greater than ω_p, the fluctuation spectrum of the magnetic field must be much the same as a blackbody radiation spectrum. In particular, collisionality of electrons should not matter. This being the case, a reliable high frequency, high wavenumber limit should be obtained if we let $\eta \rightarrow 0$. A more rigorous quantum mechanical

justification is presented in Section 7. We take the $\eta \to 0$ limit with the aid of a standard definition of the Dirac δ-function, and obtain

$$\frac{\langle B^2 \rangle_{\mathbf{k}\omega}}{8\pi} = \frac{2\hbar\omega}{e^{\hbar\omega/T} - 1}\omega_p^2 c^2 k^2 \pi \delta \left(\frac{\omega(\omega^2 - c^2 k^2 - \omega_p^2)}{\omega^2 - c^2 k^2} \right) \frac{1}{(\omega^2 - c^2 k^2)^2}. \quad (1.48)$$

Integrating Eq. (1.48) over $d^3 k$ and dividing by $(2\pi)^3$ gives

$$\frac{\langle B^2 \rangle_\omega}{8\pi} = \frac{T}{\pi}\delta(\omega)\int \frac{\omega_p^2 k^2}{\omega_p^2 + c^2 k^2}dk + \frac{1}{2\pi c^3}\frac{\hbar}{e^{\hbar\omega/T} - 1}(\omega^2 - \omega_p^2)^{3/2}. \quad (1.49)$$

Remembering that the magnetic field energy will make up roughly half of the total electromagnetic energy in high frequencies, and remembering that the magnetic energy density is found by integrating $\langle B^2 \rangle_\omega$ over $d\omega$ and then dividing by 2π, we can see that the second term in this expression closely resembles the black-body radiation spectrum at frequencies much greater than ω_p. In fact, if $\omega_p \to 0$ the entire expression reduces exactly to the black-body spectrum.

This suggests a possible procedure: We break up the integral in Eq. (1.47) into two intervals. One interval runs from $|\mathbf{k}| = 0$ to $|\mathbf{k}| = k_{cut}$. The other interval runs from $|\mathbf{k}| = k_{cut}$ to $|\mathbf{k}| = \infty$. (The choice of k_{cut} will be clarified below.) In the first interval, we keep η finite and treat the integrand exactly. In the second interval, we let $\eta \to 0$ and drop the zero-frequency part of the spectrum. The result, thus approximated, is

$$\frac{\langle B^2 \rangle_\omega}{8\pi} = \frac{1}{\pi^2}\frac{\hbar\omega'}{e^{(\hbar\omega_{pe}/T)\omega'} - 1}2\eta'\left(\frac{\omega_{pe}}{c}\right)^3 \int_0^{x_{cut}} dx \frac{x^4}{(\omega'^2 + \eta'^2)x^4 + \ldots}$$

$$+ \frac{\hbar(\omega'^2 - \omega_p'^2)^{3/2}}{2\pi(e^{(\hbar\omega_{pe}/T)\omega'} - 1)}\left(\frac{\omega_{pe}}{c}\right)^3 \Theta(\omega' - \sqrt{x_{cut}^2 + \omega_p'^2}), \quad (1.50)$$

where Θ is the Heaviside-step function. The integration can be done analytically, as shown in Appendix A. The second term is the high frequency and high wavenumber expression we obtained in Eq. (1.49). Elsewhere, we have referred to these two types of photons as soft and hard photons [9], and have dealt with

the matter of the plasticity of photons [10]. The cut-off in integration removes the divergence. At $\omega = 0$, we get

$$\lim_{\omega \to 0} \frac{\langle B^2 \rangle_\omega}{8\pi} = \frac{2T}{\pi^2 \eta} \left(\frac{\omega_{pe}}{c} \right)^3 x_{\text{cut}}. \tag{1.51}$$

At relativistic temperatures, this result is altered by a single factor of $1/\gamma$.

In reality, η should vanish smoothly as $k \to \infty$. However, as long as our results do not critically depend on the manner in which η approaches zero, the abrupt cutoff we suggest here should be acceptable as a crude model. We are interested in the contribution to the zero-frequency peak from collective plasma fluctuations, so we will choose $x_{\text{cut}} = 1$. This corresponds to $k_{\text{cut}} = \omega_p/c$, which, as can be inferred from the first term of Eq. (1.49), is the spatial correlation length of the zero-frequency fluctuations.

Three plots of the spectrum shown in Eq. (1.50) are shown in Figs. 1.2, 1.3, and 1.4. These plots show the fluctuation spectrum in plasmas with parameters approximating the early universe during the plasma epoch. They represent the early universe at about 1 second, 10^8 seconds, and 10^{12} seconds after the big bang, respectively. Note that the rise in the zero-frequency peak is so sharp in each graph that it is difficult to distinguish the peak from the vertical axis. (A break at the top of the graph indicates the height of the peak.) Note also that the (b) frames of Figs. 1.2-1.4 are log-log plots of Eq. (1.50) and clearly show the ω^{-2} behavior at the low-frequency end of the spectrum. This is characteristic of the Lorentzian tail found in Appendix A.

An alternative method exits for ensuring the convergence of the integral in Eq. (1.47). It will prove to be unsatisfactory, but we mention it here for completeness. We go back to our original equation of motion and include

viscosity:

$$\frac{d\mathbf{v}_\alpha}{dt} = e_\alpha \mathbf{E} - \eta_\alpha \mathbf{v}_\alpha + \mu_\alpha \nabla^2 \mathbf{v}_\alpha. \tag{1.52}$$

We can now make the substitution $\eta \to \eta + \mu k^2$ in Eqs. (1.39)–(1.47). Doing this, we find:

$$\frac{\langle B^2 \rangle_\omega}{8\pi} = \frac{\hbar}{\pi^2} \frac{\omega'}{e^{(\hbar\omega_{pe}/T)\omega'} - 1} \left(\frac{\omega_{pe}}{c}\right)^3 \frac{\omega_p'^2}{\omega_{pe}} \times$$

$$\int_0^\infty \frac{(\eta' + \mu' x^2) x^4}{\omega'^2(\omega'^2 - x^2 - \omega_p'^2)^2 + (\eta' + \mu' x^2)^2(\omega'^2 - x^2)^2} dx. \tag{1.53}$$

We now have an integrand which varies as $1/x^2$ as $x \to \infty$. We therefore have a convergent integral. We also have a modified value of the magnetic fluctuation strength at $\omega = 0$:

$$\frac{\langle B^2 \rangle_\omega}{8\pi} = T^2 \frac{\omega_p'^2}{\omega_{pe}} \left(\frac{\omega_{pe}}{c}\right)^3 \sqrt{\frac{1}{\mu'\eta'}} \; (\mu' = \mu \frac{\omega_{pe}}{c^2}). \tag{1.54}$$

If we take $\mu = 0.73 T/\eta m$ [11], we find

$$\frac{\langle B^2 \rangle_\omega}{8\pi} = \frac{0.85}{\pi} \frac{1}{\eta'} \frac{T}{\omega_{pe}} \left(\frac{\omega_{pe}}{c}\right)^3 \left(\frac{T}{m_e c^2}\right)^{1/2}. \tag{1.55}$$

We see that $\frac{\langle B^2 \rangle_\omega}{8\pi}$ still has a $1/\eta$ dependence, but its dependence on temperature has changed: it is now proportional to $T^{3/2}$.

As has been stated, however, this reliance on viscosity to produce a convergent integral is unacceptable. What is needed is a means of modifying the integrand of Eq. (1.47) which does not alter the blackbody spectrum at high frequencies and wavenumbers, where the plasma should have less and less effect on the electromagnetic spectrum. Viscosity does not do the job: including viscosity in the above manner puts terms in $\langle B^2 \rangle_{k\omega}/8\pi$ which *increase* in importance as wave vector increases, thus modifying the blackbody spectrum.

Perhaps, at low frequencies and wavenumbers, viscosity should be included for higher accuracy. However, it does not solve any basic problems of the theory outlined thus far, nor does it lead to a qualitatively different shape of $\frac{\langle B^2 \rangle_\omega}{8\pi}$ at low frequencies, so we will dispense with it from here on.

We have, so far, concentrated our efforts on electron-positron plasmas. We say a few words about plasmas with one major ion species. An analysis similar to what we have done in Eqs. (1.39)–(1.43) shows that the dielectric tensor of such a plasma may be given as

$$\epsilon_{ij}(\omega, \mathbf{k}) = \delta_{ij} - \frac{\omega_{pe}^2}{\omega(\omega + i\eta_e)}\delta_{ij} - \frac{\omega_{pi}^2}{\omega(\omega + i\eta_i)}\delta_{ij}. \qquad (1.56)$$

From this we find that, when $\omega \to 0$,

$$\frac{\langle B^2 \rangle_\omega}{8\pi} = \frac{T}{\pi^2 c^2} \left(\frac{\omega_{pe}^2}{\eta_e} + \frac{\omega_{pi}^2}{\eta_i} \right) k_{cut}. \qquad (1.57)$$

In an equilibrium hydrogen plasma, $\omega_{pe}^2 \approx 2000 \times \omega_{pi}^2$. Also,

$$\eta_e = 2.91 \times 10^{-6} n_e ln(\Lambda) T^{-3/2} \sec^{-1}$$

and

$$\eta_i = 4.78 \times 10^{-18} n_e ln(\Lambda) T^{-3/2} \sec^{-1}. [12]$$

The ratio between the first and second terms in Eq. (1.57) is approximately 16.4. Therefore, ion motion raises the value of the $\omega = 0$ peak by about 6 per cent of the value it would have if the ions were frozen.

We now turn our attention to the wavenumber spectrum of magnetic fluctuations, i.e. $\langle B^2 \rangle_{\mathbf{k}}/8\pi$. This spectrum is found by integrating Eq. (1.46) over frequency. The Planck factor $(e^{\hbar\omega} - 1)^{-1}$ makes the integral difficult. However, we can find an exact result in the limit $\eta \to 0$:

$$\frac{\langle B^2 \rangle_{\mathbf{k}}}{8\pi} = \int_{-\infty}^{\infty} \frac{d\omega}{2\pi} \frac{2\hbar\omega}{e^{\hbar\omega/T} - 1} \omega_p^2 c^2 k^2 \pi \delta \left(\frac{\omega(\omega^2 - c^2 k^2 - \omega_p^2)}{\omega^2 - c^2 k^2} \right) \frac{1}{(\omega^2 - c^2 k^2)^2}$$

$$= \int_0^\infty \frac{d\omega}{2} \frac{2\hbar\omega}{e^{\hbar\omega/T}-1} \omega_p^2 c^2 k^2 [\delta(\omega) + \delta(\omega \pm \sqrt{c^2 k^2 + \omega_p^2})] \times$$

$$\frac{1}{|(\omega^2 - c^2 k^2)(3\omega^2 - c^2 k^2 - \omega_p^2) - 2\omega^2(\omega^2 - c^2 k^2 - \omega_p^2)|}. \qquad (1.58)$$

After integration we obtain

$$\frac{\langle B^2 \rangle_{\mathrm{k}}}{8\pi} = \frac{\hbar c^2 k^2}{\left(e^{\hbar(\omega_p^2 + c^2 k^2)^{1/2}/T} - 1\right)(\omega_p^2 + c^2 k^2)^{1/2}} + T\frac{\omega_p^2}{\omega_p^2 + c^2 k^2}. \qquad (1.59)$$

The second term of this expression has the same physical source as the first term of the right-hand side of Eq. (1.49), namely, the zero-frequency fluctuations. The magnetic field energy contained in these fluctuations can be found by integrating the second term of the present expression over $d^3 k$ (in the range $k < k_{cut}$) and dividing by $(2\pi)^3$, or by integrating over the first term of Eq. (1.49) over $d\omega$ and dividing by 2π. The result given by the two methods will be identical regardless of the value of k_{cut}. (Note that, once again, the limit $\omega_p \to 0$ gives the standard black-body radiation spectrum.) The first term in this expression is clearly the black-body spectrum modified by the plasma. The second term was obtained by Geary *et al.* [7]. They obtained this term via the Darwin approximation, *i.e.* by neglecting radiation. Therefore, our result satisfies both radiative and non-radiative limits.

Notice that, in the classical limit $\hbar(\omega_p^2 + c^2 k^2)^{1/2} \ll T$, the two terms of Eq. (1.59) add together to yield

$$\frac{\langle B^2 \rangle_{\mathrm{k}}}{8\pi} \to T. \qquad (1.60)$$

Remembering that we have obtained this expression by summing over both polarizations of the magnetic field, we see that we have satisfied the equipartition

law of classical statistical mechanics. This raises an interesting point. The first term in Eq. (1.59) is the contribution to the magnetic fluctuation spectrum from the standard, cold-plasma, electromagnetic waves. The second term, as has been stated above, is a contribution from some kind of non-radiative fluctuation in the electromagnetic field. The standard cold-plasma waves do not satisfy the classical equipartition law. The cold-plasma equations do not allow any other plasma wave. Therefore, it would seem that, if the equipartition law is to be satisfied, the energy needed to make up the difference must be contained in $\omega = 0$ fluctuations qualitatively similar to those discussed here.

We end this section with one further observation. The energy under the $\omega = 0$ peak shows itself in the wavenumber spectrum by way of the second term in Eq. (1.59). The total energy under this peak is on the order of $T(\omega_p/c)^3 1/6\pi^2$. The energy lost to the black-body spectrum because of the plasma can be approximated by the Rayleigh-Jeans formula:

$$\int_0^{\omega_p} \frac{d\omega}{2\pi} \frac{\omega^2}{c^3} = \frac{1}{6\pi^2} T \left(\frac{\omega_p}{c} \right)^3 . \tag{1.61}$$

The energy under the $\omega = 0$ is approximately equal to the energy cut off from the black-body spectrum. Figuratively, we can say the plasma squeezes the fluctuation energy of modes with frequencies less than ω_p into modes with frequencies very close to zero.

1.4   Fluctuations with an Imposed Magnetic Field

We began our study of magnetic field fluctuations in an electron-positron plasma by assuming a cold plasma equation of motion Eq. (1.39). In adopting this equation we assumed that the effects of magnetic fields *on* plasma motion were small. Yet, when the fluctuation spectrum of the magnetic field

is calculated, a zero-frequency magnetic "fluctuation" is found. This "fluctuation" can be quite large, depending on the parameters of the plasma. We begin with an equation of motion which takes no account of magnetic fields, and we end with a plasma which has a temporally fairly constant (though far from spatially uniform) magnetic field which the plasma has "imposed on itself." This may be looked upon as an example of spontaneous breakdown of symmetry. Should this (nearly) constant (but tangled) magnetic field have been included in the original equation of motion? If it had been included, would the fluctuation spectra turn out to be much the same, or do we have a contradiction here? Toward resolving this quandary, we now attempt a calculation of interest in its own right. Namely, we find the magnetic fluctuation spectrum of a plasma with an imposed, temporally constant, spatially uniform magnetic field.

We take the equation of motion of our plasma to be

$$m_\alpha \frac{d\mathbf{v}_\alpha}{dt} = e_\alpha \mathbf{E} + e_\alpha \frac{\mathbf{v}_\alpha}{c} \times \mathbf{B}_0 - \eta_\alpha m_\alpha \mathbf{v}_\alpha, \tag{1.62}$$

where $\mathbf{B}_0 = B_0 \hat{z}$. Admittedly, this constant magnetic field will not capture the complexity of the spontaneous zero-frequency field that was calculated in the last section. So it is best to regard the following analysis as a qualitative, rather than thoroughly quantitative, consistency check of the calculations which we have already completed. We continue on with this proviso in mind.

The simultaneous presence of collisions and magnetic field in the equation of motion will complicate our algebra. For the time being, we drop the collisional term from the equation of motion. As long as we are dealing with plasma waves in which $\mathbf{v}_j$ is largely perpendicular to $\mathbf{B}_0$, this approximation amounts to ignoring η in favor of $\Omega_\alpha = |e_\alpha B_0 / m_\alpha c|$. However, when we deal with modes in which $\mathbf{v}_\alpha$ is purely parallel to $\mathbf{B}_0$, collisionality must be re-

introduced. We will not worry about crossing this bridge, however, until we see it burning.

Our first step in calculating the magnetic field fluctuation spectrum is to set $\mathbf{k} = k_y \hat{y} + k_z \hat{z}$. We then find the dielectric permittivity tensor to be

$$
\Lambda = \begin{pmatrix}
K_\perp - \dfrac{c^2 k^2}{\omega^2} & -iK_\times & 0 \\[2em]
iK_\times & K_\perp - \dfrac{c^2 k^2}{\omega^2}\cos^2\theta & \dfrac{c^2 k^2}{\omega^2}\sin\theta\cos\theta \\[2em]
0 & \dfrac{c^2 k^2}{\omega^2}\sin\theta\cos\theta & K_\| - \dfrac{c^2 k^2}{\omega^2}\sin^2\theta
\end{pmatrix},
$$

(1.63)

where θ is the angle between $\mathbf{k}$ and $\mathbf{B_0}$, and:

$$
K_\perp = 1 - \frac{\omega_{pi}^2}{\omega^2 - \Omega_i^2} - \frac{\omega_{pe}^2}{\omega^2 - \Omega_e^2},
$$

$$
K_\times = -\frac{\omega_{pi}^2}{\omega^2 - \Omega_i^2}\frac{\Omega_i}{\omega} + \frac{\omega_{pe}^2}{\omega^2 - \Omega_e^2}\frac{\Omega_e}{\omega},
$$

$$
K_\| = 1 - \frac{\omega_{pi}^2}{\omega^2} - \frac{\omega_{pe}^2}{\omega^2}.
$$

(Here, Ω_α has been taken equal to $|\Omega_\alpha|$.) The results of the damped equation of motion can be recovered by making the substitutions [13]

$$
\omega_{p\alpha} \to \omega_{p\alpha}\frac{\omega}{\omega + i\eta},
$$

$$
\Omega_\alpha \to \Omega\frac{\omega}{\omega + i\eta}.
$$

As in the previous sections, we use the inverse of the dielectric permittivity tensor, i.e. Λ^{-1}, to calculate the fluctuation spectra of the magnetic

field:

$$\frac{\langle B_x^2 \rangle_{\mathbf{k}\omega}}{8\pi} = \frac{i}{2} \frac{\hbar}{e^{\hbar\omega/T} - 1} \times \qquad (1.64)$$

$$\frac{c^2}{\omega^2} \{ k_y^2 \Lambda_{33}^{-1} + k_z^2 \Lambda_{22}^{-1} - k_y k_z (\Lambda_{23}^{-1} + \Lambda_{32}^{-1}) - \text{c.c} \},$$

$$\frac{\langle B_y^2 \rangle_{\mathbf{k}\omega}}{8\pi} = \frac{i}{2} \frac{\hbar}{e^{\hbar\omega/T} - 1} \cdot \frac{c^2}{\omega^2} \{ k_z^2 \Lambda_{11}^{-1} - \text{c.c.} \}, \qquad (1.65)$$

$$\frac{\langle B_z^2 \rangle_{\mathbf{k}\omega}}{8\pi} = \frac{i}{2} \frac{\hbar}{e^{\hbar\omega/T} - 1} \cdot \frac{c^2}{\omega^2} \{ k_y^2 \Lambda_{11}^{-1} - \text{c.c.} \}. \qquad (1.66)$$

Before we calculate the spectra, we will make several observations which will make the calculations much simpler. First, we note that the sum of all of the magnetic field energy can be written

$$\frac{\langle B^2 \rangle_{\mathbf{k}\omega}}{8\pi} = \frac{i}{2} \frac{\hbar}{e^{\hbar\omega/T} - 1} \cdot \frac{c^2}{\omega^2} \epsilon_{inp} \epsilon_{ilm} k_n k_l \{ \Lambda_{pm}^{-1} - \Lambda_{mp}^{-1*} \}$$

$$= \frac{i}{2} \frac{\hbar}{e^{\hbar\omega/T} - 1} \cdot \frac{c^2}{\omega^2} (k^2 \delta_{pm} - k_p k_m) \{ \Lambda_{pm}^{-1} - \Lambda_{mp}^{-1*} \}, \qquad (1.67)$$

where ϵ_{ilm} is the fully antisymmetric tensor. Next, let us define the tensor λ_{ij} by the relationship

$$\lambda_{ij} = \det(\Lambda) \Lambda_{ij}^{-1}. \qquad (1.68)$$

Then:

$$\frac{\langle B^2 \rangle_{\mathbf{k}\omega}}{8\pi} = \frac{i}{2} \frac{\hbar}{e^{\hbar\omega/T} - 1} \cdot \frac{c^2}{\omega^2} (k^2 \delta_{pm} - k_p k_m) \left[\left(\frac{\lambda_{pm}}{\det(\Lambda)} \right) - \left(\frac{\lambda_{mp}}{\det(\Lambda)} \right)^* \right]$$

$$= \frac{\pi\hbar}{e^{\hbar\omega/T} - 1} \cdot \frac{c^2}{\omega^2} (k^2 \delta_{pm} - k_p k_m) \lambda_{pm} \delta(\det(\Lambda))$$

$$= \frac{\pi\hbar}{e^{\hbar\omega/T} - 1} \cdot \frac{c^2}{\omega^2} (k^2 \delta_{pm} - k_p k_m) \lambda_{pm} \frac{\sum_i \delta(\omega - \omega_i(\mathbf{k}))}{|\frac{\partial}{\partial \omega} \det(\Lambda)|}, (1.69)$$

where $\{\omega_i(\mathbf{k})\}$ is the set of roots of the equation $\det(\Lambda(\mathbf{k}, \omega)) = 0$.

The cold plasma model dielectric tensor is independent of $\mathbf{k}$: $\epsilon_{ij} = \epsilon_{ij}(\omega)$. Therefore

$$\Lambda_{ij} = \left(1 - \frac{c^2}{\omega^2}\right)\delta_{ij} + \frac{c^2}{\omega^2}k_i k_j + \epsilon_{ij}(\omega). \tag{1.70}$$

It follows that

$$\frac{\partial \Lambda_{ij}}{\partial k} = -2\frac{c^2}{\omega^2}k\delta_{ij} + 2\frac{c^2}{\omega^2}\frac{k_i k_j}{k}, \tag{1.71}$$

where $k = |\mathbf{k}|$. When we substitute this result into Eq. (1.69), we find

$$\frac{\langle B^2\rangle_{\mathbf{k}\omega}}{8\pi} = \frac{\pi\hbar}{e^{\hbar\omega/T} - 1} \cdot \left(-\frac{k}{2}\right) \frac{\partial_k(\Lambda_{ij})\lambda_{ij}}{|\frac{\partial}{\partial\omega}\det(\Lambda)|} \sum_i \delta(\omega - \omega_i(\mathbf{k})). \tag{1.72}$$

A straightforward calculation shows: given any 3×3 matrix A, whose elements depend on some set of parameters $x, y, ...$, the derivative of the determinant of A with respect to any one of these parameters is:

$$\partial_x(\det(A(x, y, ...))) = \partial_x A_{ij}(x, y, ...)a_{ij}(x, y, ...), \tag{1.73}$$

where $a_{ij}(x, ...)$ is the matrix whose elements are made up of the co-factors of $A_{ij}(x, ...)$ and repeated indices represent summation. This result holds true for $\Lambda_{ij}(\omega, \mathbf{k})$. Since Λ_{ij} and λ_{ij} are symmetric matrices, we can now rewrite Eq. (1.72) as:

$$\frac{\langle B^2\rangle_{\mathbf{k}\omega}}{8\pi} = \frac{\pi\hbar}{e^{\hbar\omega/T} - 1} \cdot \left(-\frac{k}{2}\right) \frac{\partial_k(\det(\Lambda))}{|\frac{\partial}{\partial\omega}\det(\Lambda)|} \sum_i \delta(\omega - \omega_i(\mathbf{k})). \tag{1.74}$$

What we have here is a sum of the magnetic fluctuation intensities of all modes. We wish to investigate the fluctuation intensities in given particular modes. The magnetic fluctuations are characterized by the dispersion relation:

$$\det(\Lambda(\mathbf{k}, \omega)) = 0.$$

The function $\det(\Lambda(\mathbf{k},\omega))$ will be equal to zero on several different surfaces in $\mathbf{k} - \omega$ space, one surface for each mode. If we infinitesimally vary $\mathbf{k}$ and ω so as to remain on a given $\mathbf{k} - \omega$ surface where $\det(\Lambda) = 0$, we must vary $\mathbf{k}$ and ω such that

$$0 = \triangle\det(\Lambda(\mathbf{k},\omega)) = \triangle\mathbf{k} \cdot \partial_{\mathbf{k}}(\det(\Lambda)) + \triangle\omega\partial_{\omega}(\det(\Lambda)),$$

which implies

$$\frac{\partial\omega}{\partial\mathbf{k}} = -\frac{\partial_{\mathbf{k}}(\det(\Lambda))|_{\omega=\omega(\mathbf{k})}}{\partial_{\omega}(\det(\Lambda))|_{\omega=\omega(\mathbf{k})}}. \tag{1.75}$$

This implies, further, that

$$\frac{\partial\omega}{\partial k} = -\frac{\partial_k(\det(\Lambda))|_{\omega=\omega(\mathbf{k})}}{\partial_{\omega}(\det(\Lambda))|_{\omega=\omega(\mathbf{k})}}. \tag{1.76}$$

This result will be independently true for each $\mathbf{k}-\omega$ surface on which $\det(\Lambda(\mathbf{k},\omega))$ equals zero. This means it will be true independently for each propagating mode.

We can substitute this result into Eq. (1.74), finding that the total magnetic fluctuation strength for a given mode is

$$\frac{\langle B^2\rangle_{\mathbf{k}\omega}}{8\pi}\bigg|_{\text{mode }i} = \delta(\omega - \omega_i(\mathbf{k}))\frac{\pi\hbar}{e^{\hbar\omega_i/T} - 1} \cdot (\frac{k}{2})\left(\frac{\partial\omega_i(\mathbf{k})}{\partial k}\right). \tag{1.77}$$

$\langle B^2\rangle_{\mathbf{k}}/8\pi$ is found by integrating $\langle B^2\rangle_{\mathbf{k}\omega}/8\pi$ over $d\omega$ and dividing by 2π. For a given mode, it is

$$\frac{\langle B^2\rangle_{\mathbf{k}}}{8\pi}\bigg|_{\text{mode }i} = \frac{\hbar}{e^{\hbar\omega_i/T} - 1} \cdot (\frac{k}{2})\left(\frac{\partial\omega_i(\mathbf{k})}{\partial k}\right). \tag{1.78}$$

(In deriving this expression, one must remember that, wherever ω enters $\det(\Lambda)$, it enters in an even power. This means $\det(\Lambda)$ is even in ω and, for a given mode

i, the contribution to the sum from frequency ω_i is matched by the contribution from $-\omega_i$.) In the limit $\hbar \to 0$, this becomes:

$$\frac{\langle B^2 \rangle_{\mathbf{k}}}{8\pi}\bigg|_{\text{mode } i} = \frac{T}{2}\frac{k}{\omega_i(\mathbf{k})}\left(\frac{\partial \omega_i}{\partial k}\right).$$

(1.79)

We can write this as

$$\frac{\langle B^2 \rangle_{\mathbf{k}}}{8\pi}\bigg|_{\text{mode } i} = \frac{T}{2}\frac{\mathbf{v}_{ph\,i}(\mathbf{k}) \cdot \mathbf{v}_{g\,i}(\mathbf{k})}{v_{ph\,i}^2(\mathbf{k})},$$

(1.80)

where $\mathbf{v}_{ph\,i}(\mathbf{k})$ is the phase velocity of a wave of mode i with wave vector $\mathbf{k}$, and $\mathbf{v}_{g\,i}(\mathbf{k})$ is the group velocity of the wave.

Because of Faraday's law it must also be true that the fluctuation spectrum of transverse electric fields is given for each mode by

$$\frac{\langle E_\perp^2 \rangle_{\mathbf{k}}}{8\pi}\bigg|_{\text{mode } i} = \frac{1}{2}\frac{\hbar}{e^{\hbar\omega_i/T} - 1} \cdot \frac{(\omega_i(\mathbf{k}))^2}{c^2 k}\left(\frac{\partial \omega_i}{\partial k}\right).$$

(1.81)

In the limit $\hbar \to 0$, this gives

$$\frac{\langle E_\perp^2 \rangle_{\mathbf{k}}}{8\pi}\bigg|_{\text{mode } i} = \frac{T}{2}\frac{\omega_i(\mathbf{k})/k}{c^2}\left(\frac{\partial \omega_i}{\partial k}\right)$$

$$= \frac{T}{2}\frac{\mathbf{v}_{ph\,i}(\mathbf{k}) \cdot \mathbf{v}_{g\,i}(\mathbf{k})}{c^2}.$$

(1.82)

We should note that these results are not valid without limit. Specifically, if there is a zero-frequency mode in the plasma, $\partial\omega/\partial k$ will be exactly zero, while k/ω will be infinite. In this case, we cannot use Eq. (1.79) to calculate the magnetic fluctuation spectrum of this mode, unless we can make use of some sort of limiting procedure to take care of the product of zero with infinity. However, on the other hand, Eq. (1.82) tells us unequivocally that the transverse electric field intensity of a zero-frequency mode will be zero.

We have, in general, made the task of calculating the magnetic fluctuation spectrum much simpler: if we have the functional form of the dispersion

relation of a given mode, we can easily calculate the magnetic and transverse electric fluctuation spectra.

We proceed to calculate the magnetic fluctuation spectrum for an electron-positron plasma. Since the masses of the particles are equal and the charges are exactly opposite,

$$\Omega_{e+} = \Omega_{e-} = \Omega, \quad \omega_{pe-} = \omega_{pe+} = \omega_p/\sqrt{2}$$

and

$$K_\perp = 1 - \frac{\omega_p^2}{\omega^2 - \Omega^2}, \quad K_\parallel = 1 - \frac{\omega_p^2}{\omega^2}, \quad K_\times = 0.$$

This all means

$$\Lambda = \begin{pmatrix} K_\perp - \dfrac{c^2 k^2}{\omega^2} & 0 & 0 \\ 0 & K_\perp - \dfrac{c^2 k^2}{\omega^2}\cos^2\theta & \dfrac{c^2 k^2}{\omega^2}\sin\theta\cos\theta \\ 0 & \dfrac{c^2 k^2}{\omega^2}\sin\theta\cos\theta & K_\parallel - \dfrac{c^2 k^2}{\omega^2}\sin^2\theta \end{pmatrix}. \qquad (1.83)$$

There are five distinct modes in the plasma. Two of them solve the dispersion relation

$$K_\perp - \frac{c^2 k^2}{\omega^2} = 0. \qquad (1.84)$$

The other three solve

$$\left(K_\perp - \frac{c^2 k^2}{\omega^2}\cos^2\theta\right)\left(K_\parallel - \frac{c^2 k^2}{\omega^2}\sin^2\theta\right) - \left(\frac{c^2 k^2}{\omega^2}\right)^2\sin^2\theta\cos^2\theta = 0. \qquad (1.85)$$

The first two modes have their electric fields polarized purely in the x-direction (that is, perpendicular to both $\mathbf{B}_0$ and the direction of propagation). This is evident from the requirement that $\Lambda_{ij}E_j = 0$. The magnetic fields of these modes lie in the plane common to $\mathbf{B}_0$ and the wave vector. Note that the

dispersion relations of these waves are dependent on the magnitude of $\mathbf{B}_0$ but are not dependent on the direction of propagation. The dispersion relations of these modes are plotted in Fig. 1.5(a). $\langle B^2 \rangle_\mathbf{k}/8\pi$ is plotted for each mode in Fig. 1.5(b).

The other three modes have their electric fields polarized in the plane common to $\mathbf{B}_0$ and the wave vector. Their magnetic fields lie in the x-direction, that is, perpendicular to both $\mathbf{B}_0$ and the wave vector. The dispersion relations and fluctuation spectra of these modes are plotted in Figs. 1.6(a1)–1.6(d2). for various directions of propagation relative to $\mathbf{B}_0$.

Are there any zero-frequency modes which we may have overlooked because of our neglect of damping in the equation of motion? Also, even if these modes do not exist, is there a finite amount of fluctuation energy in the magnetic field when ω is very small or even equal to zero?

A glance at Fig. 1.5(b) will show that the total energy density per k-space volume deposited in the first two modes we mentioned is $T/2$. We thus conclude that, if there is a "hidden" zero-frequency mode, it must be among the second set of modes we have mentioned. That is, it must be polarized so that its magnetic field lies perpendicular to both $\mathbf{B}_0$ and $\mathbf{k}$. We look at the remaining three modes, all thus polarized. We can see from Fig. 1.6 that, for almost all angles, $\langle B_x^2 \rangle_\mathbf{k}/8\pi$ added over all three modes gives $T/2$, regardless of $\mathbf{k}$. We conclude again, that, in general, there are no hidden $\omega = 0$ modes.

There is one exception to this rule: it occurs when $\theta = \pi/2$, that is, when the wave is propagating perpendicularly to $\mathbf{B}_0$. In this case, we find

$$\Lambda = \begin{pmatrix} 1 - \dfrac{c^2 k^2}{\omega^2} - \dfrac{\omega_p^2}{\omega^2 - \Omega^2} & & \\ & 1 - \dfrac{\omega_p^2}{\omega^2 - \Omega^2} & \\ & & 1 - \dfrac{c^2 k^2}{\omega^2} - \dfrac{\omega_p^2}{\omega^2} \end{pmatrix}.$$

(1.86)

$\langle B_x^2 \rangle_{k\omega}/8\pi$ is calculated from Λ_{33}^{-1}:

$$\frac{\langle B^2 \rangle_{k\omega}}{8\pi} = \frac{i}{2} \frac{\hbar}{e^{\hbar\omega/T} - 1} \cdot \frac{c^2 k^2}{\omega^2} \{\Lambda_{33}^{-1} - \text{c.c.}\} =$$

$$= \frac{\hbar}{e^{\hbar\omega/T} - 1} \cdot \frac{c^2 k^2}{\omega^2} \pi \delta(1 - \frac{c^2 k^2}{\omega^2} - \omega_p^2 \omega^2)$$

$$= \frac{\pi\hbar}{e^{\hbar\omega/T} - 1} \cdot \frac{c^2 k^2 |\omega|}{2(c^2 k^2 + \omega_p^2)} \times$$

$$\{\delta(\omega - \sqrt{c^2 k^2 + \omega_p^2}) + \delta(\omega + \sqrt{c^2 k^2 + \omega_p^2})\}.$$

(1.87)

$\langle B_x^2 \rangle_k/8\pi$ is found by integrating this expression over $d\omega$ and dividing by 2π:

$$\frac{\langle B_x^2 \rangle_k}{8\pi} = \frac{\hbar}{e^{(\hbar\omega_p^2 + c^2 k^2)^{1/2}/T} - 1} \cdot \frac{1}{2} \frac{c^2 k^2}{(c^2 k^2 + \omega_p^2)^{1/2}}.$$

(1.88)

In the limit $\hbar \to 0$, this becomes

$$\frac{\langle B_x^2 \rangle_k}{8\pi} = \frac{T}{2} \frac{c^2 k^2}{c^2 k^2 + \omega_p^2}$$

(1.89)

which is less energy than required by the equipartition law. We then look for a mode at $\omega = 0$ which can be derived when damping is considered.

If we revive damping in the equation of motion, we find that

$$\Lambda_{33} = 1 - \frac{c^2 k^2}{\omega^2} - \frac{\omega_p^2}{\omega(\omega + i\eta)}.$$

(1.90)

This implies

$$\frac{\langle B_x^2 \rangle_{\mathbf{k}}}{8\pi} = \frac{T}{2} \frac{\omega_p^2}{c^2 k^2 + \omega_p^2} + \frac{\hbar}{e^{(\hbar \omega_p^2 + c^2 k^2)^{1/2}/T} - 1} \cdot \frac{1}{2} \frac{c^2 k^2}{(c^2 k^2 + \omega_p^2)^{1/2}}. \quad (1.91)$$

The $\hbar \to 0$ limit is now

$$\frac{\langle B_x^2 \rangle_{\mathbf{k}}}{8\pi} = \frac{T}{2} \left(\frac{\omega_p^2}{c^2 k^2 + \omega_p^2} + \frac{c^2 k^2}{c^2 k^2 + \omega_p^2} \right), \quad (1.92)$$

which satisfies the equipartition law.

Notice that the propagating mode represented in the second term is the ordinary mode. Its electric field is polarized in the direction of $\mathbf{B}_0$. This implies that the motion of the plasma itself is, in the linear regime, purely parallel to $\mathbf{B}_0$. This is the exceptional case which we noted at the beginning of this section. Using satisfaction of the equipartition law as our criterion, we have decided that this is the one case in need of special consideration of damping effects. Note also, as we can see from Fig. 1.6(d2), the zero-frequency mode represented in the first term is the shear Alfvén mode. We can see this by following the changes in the shear Alfvén wave dispersion relation and magnetic field spectrum as the angle of propagation changes from $\theta = 0$ to $\theta \to \pi/2$. The frequency of the Alfvén mode goes to zero for all k when $\theta = \pi/2$, even though the wave's energy density per k-space volume remains finite. This is why it is necessary to consider the dissipative effect in this case. Similar effects have been found by Chu, Chu and Ohkawa [14] and recently by Agim and Prager [15]. Suppose that in a plasma in a uniform magnetic field, we turn the magnetic field strength down. The dispersion relations of the various modes change. Some modes merge into each other and the shear and compressional Alfvén waves become lower and lower in frequency. We examine the compressional Alfvén wave first. The dispersion relation for this wave is contained in the

equation

$$K_\perp - \frac{c^2 k^2}{\omega^2} = 0,$$

which can be written

$$\omega^4 + \omega^2(-\Omega^2 - \omega_p^2 - c^2 k^2) + \Omega^2 c^2 k^2 = 0. \tag{1.93}$$

To obtain the low k dispersion relation, we assume ck and ω are small compared to Ω and ω_p. We find

$$\omega^2 = \frac{\Omega^2}{\omega_p{}^2 + \Omega^2} c^2 k^2. \tag{1.94}$$

To obtain the high k dispersion relation, we assume ck and ω_p are much larger than ω and Ω. We then find

$$\omega^2 = \frac{\Omega^2 c^2 k^2}{\omega_p{}^2 + c^2 k^2}. \tag{1.95}$$

The energy density per k-volume contained in the magnetic field is, from Eq. (1.79),

$$\frac{\langle B^2 \rangle_{\mathbf{k}}}{8\pi} = \frac{T}{2} \tag{1.96}$$

for small k, and

$$\frac{\langle B^2 \rangle_{\mathbf{k}}}{8\pi} = \frac{T}{2} \cdot \frac{\omega_p{}^2}{\omega_p{}^2 + c^2 k^2} \tag{1.97}$$

for large k. Notice that $\langle B^2 \rangle_{\mathbf{k}}/8\pi$ is independent of Ω. In the limit $\Omega \to 0$, $\langle B^2 \rangle_{\mathbf{k}}/8\pi$ remains finite. Notice also that the spectrum is equal to exactly half that of the zero-frequency mode of the previous section, where we included both polarizations of $\mathbf{B}$.

Now we examine the shear Alfvén wave. At low k, the dispersion relation is

$$\omega^2 = \frac{\Omega^2 c^2 k^2 \cos^2 \theta}{\Omega^2 + \omega_p^2}. \tag{1.98}$$

At high k, it is

$$\omega^2 = \frac{\Omega^2 c^2 k^2 \cos^2 \theta}{\omega_p^2 + c^2 k^2}.$$

(1.99)

The magnetic energy spectrum at low k is obtained from Eq. (1.79) as

$$\frac{\langle B^2 \rangle_{\mathbf{k}}}{8\pi} = \frac{T}{2}$$

(1.100)

and, at high k, as

$$\frac{\langle B^2 \rangle_{\mathbf{k}}}{8\pi} = \frac{T}{2} \cdot \frac{\omega_p{}^2}{\omega_p{}^2 + c^2 k^2}.$$

(1.101)

The shear Alfvén wave vector spectrum has exactly the same behavior as that of the compressional Alfvén wave. In particular, the spectrum is independent of Ω and, therefore, finite even if $\Omega = 0$. Further, notice that the wave vector spectra of both Alfvén modes are equal to half that of the zero-frequency mode at high k.

Therefore, it may be possible to interpret the zero-frequency mode as a composite of the two Alfvén modes, which are static in the absence of an imposed magnetic field. The zero-frequency mode is a virtual Alfvén wave excitation that is spontaneously generated as the virtual excitation itself creates a magnetic field over a short period of lifetime. In quantum mechanical terminology, this is usually called virtual particle creation. That is, the virtual Alfvén wave quantum (or magnon) is created in the absence of an external magnetic field, while in the presence of an external magnetic field, the (real) Alfvén wave quanta are excited.

Now we have to answer our second question: is the fluctuation energy of the magnetic field finite when ω is small or even zero? We answer this question by calculating $\langle B^2 \rangle_\omega / 8\pi$ for the two Alfvén modes. We could do this

by going back to $\langle B^2 \rangle_{\mathbf{k}\omega}/8\pi$ and integrating over d^3k. However, we have another method at our disposal. Since there is no damping, $\langle B^2 \rangle_{\mathbf{k}\omega}/8\pi$ is made up of functions of ω and $\mathbf{k}$ multiplying a sum of Dirac δ-functions, the arguments of which are also functions of ω and $\mathbf{k}$. This means that the energy density in a particular frequency interval $d\omega$ is distributed over a few well-defined, distinct surfaces in k-space. This implies the following: We measure the energy of a given mode in a particular frequency band $d\omega$, centered on frequency ω_0. It has some value $\langle B^2 \rangle_\omega/8\pi \times d\omega/2\pi$. This mode will have a single surface in k-space for which $\omega(\mathbf{k}) = \omega_0$. We study a differential volume surrounding this surface, a volume contained within the two surfaces defined by $\omega(\mathbf{k}) = \omega_0 - d\omega/2$ and $\omega(\mathbf{k}) = \omega_0 + d\omega/2$. The energy density contained in this differential volume must be equal to the energy density contained in the interval $d\omega$. Mathematically,

$$\frac{\langle B^2 \rangle_{\omega=\omega_0}}{8\pi} \frac{d\omega}{2\pi} = d\omega \int \frac{dS}{(2\pi)^3} \frac{1}{|\nabla_{\mathbf{k}}\omega|} \frac{\langle B^2 \rangle_{\mathbf{k}}}{8\pi} \tag{1.102}$$

where the integral is performed over the k-surface given by $\omega(\mathbf{k}) = \omega_0$.

In this cylindrically symmetric system we obtain, by Fig. 1.7 and the accompanying caption,

$$\frac{dS}{|\nabla_{\mathbf{k}}\omega|} = 2\pi \frac{k^2 \sin\theta\, d\theta}{|\partial_k\omega|}. \tag{1.103}$$

Substituting this into Eq. (1.102) and dividing common factors out of both sides of the equation gives

$$\left. \frac{\langle B^2 \rangle_\omega}{8\pi} \right|_{\text{mode } i} = \frac{1}{2\pi} \int d\theta \sin\theta \frac{k^2}{|\partial_k\omega|} \left. \frac{\langle B^2 \rangle_{k(\theta,\omega)}}{8\pi} \right|_{\text{mode } i}. \tag{1.104}$$

Combining this with Eq. (1.79), we see

$$\left. \frac{\langle B^2 \rangle_\omega}{8\pi} \right|_{\text{mode } i} = \frac{1}{2\pi} \int d\theta \sin\theta \frac{T}{2} \cdot \left. \frac{k^3(\omega,\theta)}{\omega} \right|_{\text{mode } i}$$

$$= \frac{T}{4\pi\omega} \int d\theta \sin\theta \quad k^3_{\text{mode } i}(\omega,\theta). \tag{1.105}$$

In a similar way, the perpendicular electric field power spectrum can be shown to be

$$\frac{\langle E_\perp^2 \rangle_\omega}{8\pi}\bigg|_{\text{mode i}} = \frac{T\omega}{4\pi c^2} \int d\theta \sin\theta \ k_{\text{mode i}}(\omega, \theta). \qquad (1.106)$$

(The integral is not necessarily performed over the full range $0 \le \theta \le \pi$. For instance, it might turn out that waves propagating at angles greater than some angle θ_0 always have frequencies smaller than some frequency ω_0. In this case, if we wanted the fluctuation spectrum for $\omega = \omega_0$, we would integrate only from $\theta = 0$ to $\theta = \theta_0$.)

We write down $\langle B^2 \rangle_\omega / 8\pi$ for the compressional Alfvén mode by making use of its dispersion relations, Eqs. (1.94) and (1.95), and Eq. (1.105). In the range of frequencies corresponding to small k,

$$\frac{\langle B^2 \rangle_\omega}{8\pi} = \frac{T}{2\pi}\omega^2 \left(\frac{\sqrt{\omega_p{}^2 + \Omega^2}}{c\Omega}\right)^3. \qquad (1.107)$$

In the range of frequencies corresponding to high k,

$$\frac{\langle B^2 \rangle_\omega}{8\pi} = \frac{T}{2\pi}\left(\frac{\omega_p}{c}\right)^3 \frac{\omega^2}{(\Omega^2 - \omega^2)^{3/2}}, \qquad (1.108)$$

for the electron-positron case.

For ω identically zero, the magnetic fluctuation energy is zero. However, there is a finite amount of energy density per frequency in low frequencies and, if we are justified in considering Ω a low frequency, then we have an infinite amount of low frequency energy. Once again we have run into a divergence problem. $\langle B^2 \rangle_\omega / 8\pi$ will diverge at $\omega = \Omega$. This is similar to the divergence in Eq. (1.22), though the degree of divergence in Eq. (1.108) is stronger. We will naively handle this problem by, again, introducing a cutoff in k. To estimate the total energy contained in shear Alfvén waves, Agim and Prager [15] used a

cutoff of $k_{\text{cut}} = \Omega_i/v_A = \omega_{pi}/c$ in an electron-ion plasma, where ω_{pi} is the ion plasma frequency.

We consider $\langle B^2 \rangle_\omega/8\pi$ of the shear Alfvén mode. The directional dependence of the dispersion relation makes the calculation of $\langle B^2 \rangle_\omega/8\pi$ a bit more difficult. In particular, we cannot divide up the frequency range into low k and high k ranges. For instance, looking at Eqs. (1.98) and (1.99), we can see that ω can become zero, no matter how large or small k is. However, in the case where $\Omega^2 \ll \omega_p^2$, the dispersion relation Eq. (1.99) can take the place of Eq. (1.98) at low k without too great a loss of accuracy. We find $\langle B^2 \rangle_\omega/8\pi$ by substituting $k(\omega, \theta)$ from Eq. (1.99) into Eq. (1.105). The result is

$$\frac{\langle B^2 \rangle_\omega}{8\pi} = \frac{T}{2\pi} \left(\frac{\omega_p}{c} \right)^3 \frac{1}{\Omega} \cdot \left. \frac{-u}{(u^2 - \omega^2/\Omega^2)^{1/2}} \right|_{\omega/\Omega}^{1}, \qquad (1.109)$$

where u is a dummy variable which represents $\cos\theta$ in the $d\theta$ integral of Eq. (1.105). There is actually an infinite amount of energy at low frequencies. $\langle B^2 \rangle_\omega/8\pi$ diverges at all frequencies less than Ω.

Let us compare $\langle B^2 \rangle_\omega/8\pi$ of the two Alfvén waves and the zero-frequency mode. First of all, they all have the same divergence problem, in differing degrees of severity. Secondly, they all scale by the factor $(\omega_p/c)^3$. It may be said that the imposed magnetic field creates Alfvén waves by taking energy out of a small frequency range enclosing $\omega = 0$ and spreading it over a frequency range extending from $\omega = 0$ to $\omega = \Omega$.

The effects of imposing a cut-off magnitude in wave vector k_{cut} are considered. We begin with the compressional Alfvén mode. From the dispersion relation, Eq. (1.95), we see that a cut-off in wave vector magnitude implies a cut-off in frequency:

$$\omega^2 < \omega_{\text{cut}}^2 = \frac{\Omega^2 c^2 k_{\text{cut}}^2}{\omega_p^2 + c^2 k_{\text{cut}}^2}. \qquad (1.110)$$

As long as ω is slightly less than $\Omega \cos \theta$ for the shear Alfvén wave, and lower than the lower hybrid frequency for the compressional wave, this divergence does not arise. In this sense, the choice of k_{cut} is not sensitive to the divergence. The choice of k_{cut} may be made on various considerations which have not been mentioned in this simple treatment. These considerations may include finite Larmor radius effects, kinetic effects, the discreteness of plasma particles, and quantum effects.

As for the shear Alfvén wave, its directional dependence makes calculations more complicated once again, but it is still tractable. The dispersion relation, Eq. (1.99) indicates that, given a value of ω, a cut-off in k implies a cut-off in θ:

$$\cos^2 \theta > \cos^2 \theta_0 = \omega^2 \frac{\omega_p^2 + c^2 k^2}{\Omega^2 c^2 k^2}. \qquad (1.111)$$

This means we need to change the lower limit of integration in Eq. (1.109) to $\cos \theta_0$. We then find:

$$\frac{\langle B^2 \rangle_\omega}{8\pi} = \frac{T}{4\pi} \frac{\omega_p^3}{\Omega c^3} \left\{ \frac{\sqrt{\omega_p^2 + c^2 k_{cut}^2}}{\omega_p} - \frac{1}{\sqrt{1 - \omega^2/\Omega^2}} \right\}. \qquad (1.112)$$

The maximum value of ω occurs at $k = k_{cut}$ and $\theta = 0$; it is the same as the cut-off frequency of the compressional Alfvén wave. Therefore, once again, we have headed off the divergence.

We now ask how much energy density is contained in the Alfvén modes. We answer by taking the expressions for $\langle B^2 \rangle_k / 8\pi$ of each mode, adding them together, integrating the sum over $d^3 k$, and dividing by $(2\pi)^3$. The result is

$$\frac{\langle B^2 \rangle^0}{8\pi} = T \int_0^{k_{cut}} \frac{d^3 k}{(2\pi)^3} 4\pi k^2 \frac{\omega_p^2}{\omega_p^2 + c^2 k^2}. \qquad (1.113)$$

We stress that the introduction of a cutoff in k in a magnetized plasma needs further investigation.

In this section, we have found, first of all, that the zero-frequency mode, derived from an equation of motion for a non-magnetized plasma, is consistent with the limit $B_0 \rightarrow 0$ for a plasma with an imposed uniform magnetic field. We have found that the zero-frequency mode is a composite of compressional and shear Alfvén waves, along with cyclotron waves at higher frequencies. When an external magnetic field is imposed on the plasma, however, the energy which was stored in $\omega = 0$ in the non-magnetized plasma is spread out in a range of frequency up to the cyclotron frequency. But in a progressively weak enough magnetic field this spread will be correspondingly small compared to the other relevant frequencies.

The fluctuations associated with the cyclotron waves are reminiscent of the Bernstein wave paradox: In a plasma with an imposed magnetic field, the Bernstein wave is not damped. This is true no matter how small B_0 may be. But then where does Landau damping come from in the limit $B_0 \rightarrow 0$? The resolution of this problem is that, as $B_0 \rightarrow 0$ in a thermal plasma, more cyclotron resonances become important. The effects of these resonances are added to the particle orbit; the net effect is a damping of the particle motion. This damping reduces to Landau damping when $B_0 \rightarrow 0$ [16,17]. Dealing with frequencies near the cyclotron resonance, then, may require accounting for subtle effects which we have not taken into account.

We briefly consider the magnetic energy spectra of an electron-ion plasma. From Eq. (1.79) we can obtain numerical results for the spectra, and make some valid qualitative comparisons to the electron-positron plasma.

The cold electron-ion plasma has five propagating electromagnetic

modes. The dispersion relations of these modes, propagating at various angles with respect to $\mathbf{B}_0$, are shown in Fig. 1.8. These plots were obtained by making contour plots of the determinant of the dielectric permittivity tensor, which we last saw explicitly in Eq. (1.63), and removing the contours of all values of $\det(\Lambda) \neq 0$.

In Fig. 1.8 are also plotted the wave vector fluctuation spectra of the magnetic field, $\langle B^2 \rangle_k / 8\pi$, for each of the five modes of the electron-ion plasma. The spectrum of each mode has been calculated by numerically approximating Eq. (1.79). Note that for all values of k, the total magnetic fluctuation energy summed over all modes is equal to T. Since both independent polarizations of the magnetic field are included in this sum, this is consistent with the equipartition law.

Note that the two branches of the dispersion relation associated with the Alfvén waves have spectra qualitatively similar to those of the Alfvén branches of the electron-positron plasma. In the low k limit, it is easy to show that the spectra are independent of the magnetic field strength. The low-k dispersion relation for the compressional Alfvén wave is

$$\omega^2 = \frac{1}{1 + \dfrac{4\pi n_0 c^2}{B_0}} c^2 k^2, \tag{1.114}$$

where n_0 is the plasma mass density. Eq. (1.79) tells us that

$$\frac{\langle B^2 \rangle_k}{8\pi} = \frac{T}{2}. \tag{1.115}$$

The proof is the same for the shear Alfvén mode, for which the dispersion relation is

$$\omega^2 = \frac{1}{1 + \dfrac{4\pi n_0 c^2}{B_0}} c^2 k^2 \cos^2 \theta, \tag{1.116}$$

and, once again,

$$\frac{\langle B^2 \rangle_{\mathbf{k}}}{8\pi} = \frac{T}{2}.$$ (1.117)

We see, then, that both Alfvén waves in the electron-ion plasma carry energy, even if the strength of the imposed magnetic field is brought down to zero. We can see from Eqs. (1.114) and (1.116) that, if $B_0 = 0$, the frequency of these modes is zero for all k. An isotropic electron-ion plasma will have a finite amount of magnetic field energy in a narrow frequency band surrounding $\omega = 0$.

Phenomenological wavenumber cutoffs can be given for the Alfvén modes in a weakly magnetized plasma. As stated above, Agim and Prager [15] used a cutoff of $k = w_{pi}/c$ when calculating the energy contained in shear Alfvén waves. The compressional Alfvén waves, on the other hand, exist in the frequency range of $\omega = 0$ to $\omega \leq \omega_{LH}$ where ω_{LH} is the lower hybrid frequency given by

$$\frac{1}{\omega_{LH}^2} = \frac{1}{\omega_{ci}^2 + \omega_{pi}^2} + \frac{1}{\omega_{ci}\omega_{ce}},$$

and ω_{ci} and ω_{ce} are the ion and electron cyclotron frequencies, respectively [13]. In a weakly magnetized plasma, $\omega_{LH} \approx \sqrt{\omega_{ci}\omega_{ce}}$. We choose k_{cut} to include all of the compressional Alfvén waves. The dispersion relation of these waves is $\omega = v_A k$. Therefore we choose k_{cut} to be

$$k_{cut} = \frac{\sqrt{\omega_{ci}\omega_{ce}}}{v_A} = \frac{\omega_{pe}}{c} \approx \frac{\omega_p}{c}.$$

Our cutoff value for the non-magnetized plasma seems to be a good choice for the compressional waves of the weakly magnetized plasma.

1.5 Kinetic Theoretic Analysis

Up to this point, we have derived all our results on fluctuations from a simple model with equations of motion describing a cold fluid plasma with a constant collision frequency. This model is good for studying, for example, propagating waves whose electromagnetic fields are largely transverse. Such waves have phase velocities usually exceeding the speed of light, therefore such thermal effects as Landau damping have no effect on them. But, when we deal with low frequencies, that is, when we study frequency and wave-vector regimes where ω/k is less than or close to the thermal speed of the plasma constituents, we ignore kinetic effects at our peril. It is incumbent on us to attempt a kinetic theory treatment of low-frequency magnetic field fluctuations. We will find that a kinetic theory treatment of the problem returns results which agree qualitatively with what we found in the Sec. 3.

We assume a homogeneous, isotropic, non-magnetized hydrogen plasma. We take the electrons and ions to be in equilibrium with one another, having Maxwellian velocity distributions with a temperature T. In this case, the transverse part of the dielectric permittivity is given by

$$\Lambda(\omega, \mathrm{k}) = 1 - \frac{c^2 k^2}{\omega^2} + \left(\frac{m}{2\pi T}\right)^{1/2} \frac{\omega_{pe}^2}{\omega} \int_L \frac{e^{-mv^2/2T}}{-\omega + kv} dv +$$

$$+ \left(\frac{M}{2\pi T}\right)^{1/2} \frac{\omega_{pi}^2}{\omega} \int_L \frac{e^{-Mv^2/2T}}{-\omega + kv} dv, \qquad (1.118)$$

where m is the electron mass and M is the hydrogen ion mass. The subscript "L" attached to each integral sign is meant to specify the contour taken in each integral; namely, each integral is performed over the Landau contour [16]. A problem with this treatment should be mentioned here. We are using

straight-line particle orbits to calculate the dielectric function. However, we will be applying our results to frequencies below typical collision frequencies of a plasma, where the straight-line approximation no longer holds. A thoroughly rigorous treatment here would include some consideration of particle collisions. This topic is deferred to future investigation.

As indicated above, we are interested in fluctuations at frequencies and wave vectors in the regime

$$\frac{\omega}{k} \leq v_e, v_i,$$

where $v_e = \sqrt{T/m}$ and $v_i = \sqrt{T/M}$. In this regime, we can approximate Λ by

$$\Lambda(\omega, \mathbf{k}) = 1 - \frac{c^2 k^2}{\omega^2} - \frac{\omega_{pe}^2}{v_e^2 k^2} - \frac{\omega_{pi}^2}{v_i^2 k^2} + i\sqrt{\frac{\pi}{2}} \frac{\omega_{pe}^2}{v_e \omega k} + i\sqrt{\frac{\pi}{2}} \frac{\omega_{pi}^2}{v_i \omega k}. \qquad (1.119)$$

Since $v_i^2/v_e^2 = \omega_{pi}^2/\omega_{pe}^2 = m/M$, we can write this as

$$\Lambda(\omega, \mathbf{k}) = 1 - \frac{c^2 k^2}{\omega^2} - \frac{2\omega_{pe}^2}{v_e^2 k^2} + i\sqrt{\frac{\pi}{2}} \alpha \frac{\omega_{pe}^2}{v_e \omega k}, \qquad (1.120)$$

where $\alpha = 1 + \sqrt{m/M}$.

It is still true that, in the limit $\hbar \to 0$,

$$\frac{\langle B^2 \rangle_{\mathbf{k}\omega}}{8\pi} = -\frac{2T}{\omega} \frac{c^2 k^2}{\omega^2} \cdot \text{Im}[\Lambda^{-1}]. \qquad (1.121)$$

(The factor of 2 is included to account for both B-field polarizations.) From Eq. (1.119), $\text{Im}[\Lambda^{-1}]$ is readily found to be

$$\text{Im}[\Lambda^{-1}] = \frac{-\sqrt{\frac{\pi}{2}} \alpha \omega_{pe}^2 \omega^3 k^3/v_e}{(\omega^2 k^2 - c^2 k^4 - 2\omega_{pe}^2 \omega^2/v_e^2)^2 + \frac{\pi}{2}\alpha^2 \omega_{pe}^4 \omega^2 k^2/v_e^2}. \qquad (1.122)$$

Therefore, from Eqs. (1.121) and (1.122),

$$\frac{\langle B^2 \rangle_{\mathbf{k}\omega}}{8\pi} = T \frac{2\sqrt{\frac{\pi}{2}} \alpha \omega_{pe}^2 c^2 k^5/v_e}{(\omega^2 k^2 - c^2 k^4 - 2\omega_{pe}^2 \omega^2/v_e^2)^2 + \frac{\pi}{2}\alpha^2 \omega_{pe}^4 \omega^2 k^2/v_e^2}. \qquad (1.123)$$

Here we see qualitative confirmation of our earlier results: $\langle B^2 \rangle_{k\omega}/8\pi$ has a maximum at $\omega = 0$ as long as $k^2 < 2\omega_{pe}^2/v_e^2$. True enough, in Sec. 3, $\langle B^2 \rangle_{k\omega}/8\pi$ had a maximum at $\omega = 0$ in the cold plasma, *regardless* of the size of k. However, this restriction on k is a very loose restriction: the value of k at which $\langle B^2 \rangle_{k\omega}/8\pi$ no longer has a zero-frequency maximum is several times larger than the wavenumber cutoff we chose in Sec. 3. The kinetic plasma effect smears out, but does not destroy, the zero-frequency fluctuations we found in the cold plasma theory. There is another similarity between the spectrum we have found here and that which we found for the cold plasma: namely, the problem that, if we integrate $\langle B^2 \rangle_{k\omega}/8\pi$ over d^3k to get $\langle B^2 \rangle_{\omega}/8\pi$, the integral diverges at high k. (The situation has improved a bit. The divergence here is logarithmic, whereas the divergence we faced with the cold plasma was linear.)

We examine the low frequency behavior of $\langle B^2 \rangle_{\omega}/8\pi$. If we ignore terms in the denominator of $\langle B^2 \rangle_{k\omega}/8\pi$ which are of order ω^4, we can approximate $\langle B^2 \rangle_{k\omega}/8\pi$ as

$$\frac{\langle B^2 \rangle_{k\omega}}{8\pi} = T \frac{2\sqrt{\frac{\pi}{2}}\alpha\omega_{pe}^2 c^2 k^3/v_e}{c^4 k^6 + 4\omega_{pe}^2\omega^2 c^2 k^2/v_e^2 - 2c^2\omega^2 k^4 + \frac{\pi}{2}\alpha^2\omega_{pe}^4\omega^2/v_e^2}. \tag{1.124}$$

Normalizing frequencies by ω_{pe} and wavenumbers by ω_{pe}/c, we rewrite this as

$$\frac{\langle B^2 \rangle_{k\omega}}{8\pi} = \frac{T}{\omega_{pe}} \frac{2\sqrt{\frac{\pi}{2}}\alpha x^3/\beta_e}{x^6 + 4\omega'^2 x^2/\beta_e^2 - 2\omega'^2 x^4 + \frac{\pi}{2}\alpha^2\omega'^2/\beta_e^2}, \tag{1.125}$$

where x and ω' have the same meanings as in Sec. 3, and $\beta_e = v_e/c$. Note that $\langle B^2 \rangle_{k\omega}/8\pi$ scales as T/ω_{pe}. To find $\langle B^2 \rangle_{\omega}/8\pi$, we integrate this expression over d^3k and divide by $(2\pi)^3$. This integral can be carried out exactly, as shown in Appendix B. As stated above, we must impose a wavenumber cutoff on the integral. As in Sec. 3, the cutoff will come sooner or later through plasma

discreteness or quantum mechanical effects, which will be discussed in more detail in Sec. 7. We will use the same cutoff as in the previous sections, namely ω_p/c. This does not cause any inconsistency as long as $\omega/\omega_p < v_i/c$.

$\langle B^2 \rangle_\omega/8\pi/(T\omega_{pe}^2/c^3)$ of plasmas at temperatures of $10^{5\circ}$K, $10^{6\circ}$K, and $10^{7\circ}$K are shown in Fig. 1.9. $\langle B^2 \rangle_\omega/8\pi$ scales as ω_p^2/c^3, so the Fig. 1.9 results are independent of plasma density. Also, for $\omega > .01 \times \omega_{pe}$, $\langle B^2 \rangle_\omega/8\pi$ exhibits an ω^{-2} behavior, whereas for very small frequencies, it diverges more slowly, growing approximately as $\omega^{-1/3}$.

We can obtain an expression for $\langle B^2 \rangle_k/8\pi$ by integrating $\langle B^2 \rangle_{k\omega}/8\pi$ over $d\omega$ and dividing by 2π. Considering that the contribution to the integral from high ω is ignorable, we integrate over all ω. When $k \leq \omega_{pe}/c$, the result is

$$\frac{\langle B^2 \rangle_k}{8\pi} = T\sqrt{\frac{\pi}{2}}\alpha\frac{\omega_{pe}}{\left(4c^2k^2 + \frac{\pi}{2}\alpha^2\omega_{pe}^2\right)^{1/2}}. \tag{1.126}$$

The cold plasma approximation should still hold rather well for the electromagnetic plasma wave. As we go through our standard calculations, we find that its magnetic field energy density per wave vector volume closely approximates what we found in Sec. 3. Specifically, $\langle B^2 \rangle_k/8\pi$ of the propagating electromagnetic plasma wave is very close to

$$\frac{\langle B^2 \rangle_k}{8\pi} = T \cdot \frac{c^2k^2}{c^2k^2 + \omega_p^2}. \tag{1.127}$$

We obtain the total $\langle B^2 \rangle_k/8\pi$ by adding this to the zero-frequency spectrum given in Eq. (1.126). We find that $\langle B^2 \rangle_k/8\pi$ is generally greater than T.

Two points should be considered here. First, at $k = 0$, $\langle B^2 \rangle_k/8\pi$, as given by Eq. (1.126) is exactly equal to T. Second, the deviation from T is

very small for small k. At small k, Eq. (1.126) is approximately

$$\frac{\langle B^2 \rangle_k}{8\pi} = T \left(1 - \frac{4c^2 k^2}{\pi \alpha^2 \omega_{pe}^2} \right).$$

(1.128)

The spectrum we might have expected to find in place of that given by Eq. (1.126) is $\langle B^2 \rangle_k / 8\pi = T \omega_p^2 / (c^2 k^2 + \omega_p^2)$. At small k, this is approximately

$$\frac{\langle B^2 \rangle_k}{8\pi} = T \left(1 - \frac{c^2 k^2}{\omega_p^2} \right).$$

(1.129)

The leading terms in these two expansions are certainly of the same order of magnitude. They differ by a ratio of essentially $4/\pi$ in a hydrogen plasma, and by a ratio of $2/\pi$ in an electron-positron plasma. This small deviation may arise from the expansion of the plasma dispersion function in Eq. (1.119). However, it would seem that there is no problem with the fundamental physics here. The zero-frequency peak does exist. The problem is that, in regimes where ω is larger than the thermal velocity times k, the value of the peak falls off faster than predicted by the hot plasma approximation which we used to obtain Eq. (1.119). When we integrated over ω to obtain Eq. (1.126), the high ω contribution was not quite "ignorable enough."

In any event, $\langle B^2 \rangle_k / 8\pi$ in the zero-frequency peak is on the order of T for small enough k. A rough approximation of the total energy density contained in this peak is then T times the k-space volume contained within $k = \omega_p / c$, divided by $(2\pi)^3$, yielding, once again,

$$\frac{\langle B^2 \rangle^0}{8\pi} = T \frac{1}{6\pi^2} \left(\frac{\omega_p}{c} \right)^3.$$

(1.130)

1.6 Particle Simulation

We have looked for zero-frequency magnetic field fluctuations in kinetic computer simulations of plasmas. We discuss the results of these simulations in this section.

Earlier, Geary *et al.* [7] discussed the low-frequency magnetic field fluctuations in numerical plasma simulations. The authors of [7] developed a magnetoinductive code to examine low frequency behavior in magnetized plasmas. They took as their starting point the Darwin approximation to Maxwell's equations, *i.e.* they dropped the displacement current from the $\nabla \times \mathbf{B}$ equation. They then made use of the fluctuation-dissipation theorem to derive the magnetic field fluctuation spectrum $\langle B^2 \rangle_\mathbf{k}/8\pi$. The fluctuation spectrum $\langle B^2 \rangle_\mathbf{k}/8\pi$ which they found for electromagnetic waves propagating perpendicularly to their imposed magnetic field $\mathbf{B}_0$ are exactly the same as our low-frequency result in our Eq. (1.59). A comparison of fluctuation spectra for waves in other directions is not useful because the present plasma is non-magnetized, while that in Geary *et al.* was magnetized, and the electron motion was treated by the guiding center approximation.

We have carried out particle simulations of thermal equilibrium plasmas employing both 1D and 2D fully electromagnetic, fully relativistic particle simulation codes (see, for example, [18]). We have recorded the magnetic field frequency spectra arising from these simulations. The particles were given initial uniform distributions in space, and Maxwellian velocity distributions. In all cases the computational space boundary conditions were periodic. We ran the simulations for several thousand time steps; at each time step we stored the series of spatial Fourier components of the z-component of the magnetic field, *i.e.* $B_z(\mathbf{k}, t)$ (the z-direction being perpendicular to the simulation space in each case). At the end of the simulation run, the B_z Fourier components were input into an autocorrelation function, whose frequency spectrum yields the spectral intensity $B_z^2(\mathbf{k}, \omega)$. Lastly, the $B_z^2(\mathbf{k}, \omega)$ were summed over $\mathbf{k}$ to give $B_z^2(\omega)$.

In the 1-D simulations, the parameters used were: the number of cells L_x 256, 10 electrons and 10 positrons per cell, $\Delta t = 0.1/\omega_{pe}$, number of time steps N_t 2048, and speed of light $c = 5\Delta\omega_{pe}$, where Δ is the grid spacing. Simulation runs were made with three different temperatures: $\gamma_{\mathrm{therm}} = 1.05$, 1.22, and 34.7 (corresponding to $T \sim 3 \times 10^{8}{}^\circ\mathrm{K}$, $1.3 \times 10^{9}{}^\circ\mathrm{K}$, and $2 \times 10^{11}{}^\circ\mathrm{K}$), where γ_{therm} is the relativistic factor corresponding to the thermal velocity of the plasma. To test the performance of these codes, we examined the dispersion relation produced for B_z for electromagnetic waves in a plasma and compared it with the standard result

$$\omega^2 = c^2 k^2 + \frac{\omega_{p0}^2}{\gamma_{\mathrm{therm}}}$$

where $\omega_{p0}^2 = \dfrac{4\pi n e^2}{m_e} + \dfrac{4\pi n e^2}{m_i}$. The dispersion relation comparisons were excellent. We also examined B_z fluctuation strengths as functions of wavevector, $i.e.$ $B_z^2(\mathbf{k})$. The fluctuation strengths compared fairly well with theory (Eq. (1.59).

The results of the $B_z^2(\omega)$ measurements are shown in Figs. 1.10 and 1.11. In each of these cases, a strong B_z fluctuation peak is seen at $\omega = 0$. In Fig. 1.10 the $2 \times 10^{11}{}^\circ\mathrm{K}$ result is shown, while Fig. 1.11 shows the $10^{9}{}^\circ\mathrm{K}$ result.

We made an additional test on the 1-D code by running the nonrelativistic ($\gamma_{\mathrm{therm}} = 1.05$) simulation for twice as long, $i.e.$ 4096 time steps. Again, the $\omega = 0$ peak appeared in the $B_z^2(\omega)$ spectrum. Its width did not change from the width it had in the $N_t = 2048$ time steps simulation. Fig. 1.12 shows these results. This indicates that the presence of the peak is not due to the restriction on the finite window width in the correlation function imposed by the length of the run ($i.e.$ not the Nyquist frequency width $\Delta\omega = 1/(N_t \Delta t)$), but is rather due to the intrinsic physics. In fact, traditionally, such a zero-frequency peak has been observed routinely in particle simulation but has not been well understood in its origin.

In the 2-D simulation, parameters were: computational area$= 32 \times 32$ cells, $9e^- + 9e^+$ per cell, $\Delta t = 0.1/\omega_{pe}$, $N_t = 2048$, and $\gamma_{\text{therm}} = 1.05$. Again, a strong B_z fluctuation peak is seen at $\omega = 0$. The 2D results, together with the results of the 1D run of the same temperature are shown in Fig. 1.13.

Our simulation results for the magnetic field wavenumber spectral intensity $S(\text{k})$ follow $1/(\omega_p^2 + c^2 k^2)$ (the second term in Eq. (1.59)) more closely than our low-wavenumber expansion (Eq. (1.60)). See the frames (b) of Figs. 1.10, 1.11, and 1.12. This is explained by the conditions of the simulation. First of all, the grid nature of the simulation puts a cap on the maximum k at π/Δ. Second, as can be seen from our derivation of $S(\text{k})$, the first term in Eq. (42) comes from the energy contained in the radiation. The results shown were obtained by summing $S(\text{k}, \omega)$ over frequencies ranging from 0 to $+5\omega_p \sim 1/\Delta t$, the Nyquist frequency. When the wave frequency of a given mode is higher than this range, the high-frequency energy of the radiation mode will not enter into the sum. These reduction factors of the radiation branch, plus sharing of energy between nonradiative modes, account for the closer agreement with the expression with only the second term in Eq. (1.59) rather than Eq. (1.60) in our simulation. After we take these factors into consideration, the agreement between our kinetic simulation and the theory is good.

1.7 Interaction between Plasma Particles and Electromagnetic Waves with High Momenta

We have deferred until now definitive resolution of the treatment of high wavenumbers in the integral in Eq. (1.47). In Secs. 3, 4, and 5, we phenomenologically introduced a cutoff wavenumber in k-space. Without this cut-

off, we obtain an infinity of energy in the magnetic field power spectrum at $\omega = 0$. Such high-k divergences are a common problem with fluid theories which take no account of the granularity of a fluid at some scale. In this section, we offer quantum mechanical justification for the introduction of a cutoff by showing qualitative handling of this problem.

The longitudinal dielectric function of a plasma, calculated from kinetic theory based on classical mechanics is

$$\epsilon_{\parallel}(\mathbf{k}, \omega) = 1 + \sum_j \frac{\omega_{pj}^2}{\omega^2} \int d^3 v \frac{\mathbf{k} \cdot \partial_{\mathbf{v}} f_{0j}(\mathbf{v})}{\omega - \mathbf{k} \cdot \mathbf{v} + i\eta}, \tag{1.131}$$

where the index j indicates species of the plasma constituents and $f_{0j}(\mathbf{v})$ is the unperturbed velocity distribution function of species j. (The end results we obtain in this section will be applicable to the transverse dielectric function as well.) If $f_{0j}(\mathbf{v})$ is a Maxwellian, the result is

$$\epsilon_{\parallel}(\mathbf{k}, \omega) = 1 + \sum_j \frac{k_{Dj}^2}{k^2} W \left(\frac{\omega}{k v_{thj}} \right), \tag{1.132}$$

where k_{Dj} is the Debye wave number of the species j and v_{thj} is the thermal velocity of species j. $W(z)$ is the plasma dispersion function.

Eq. (1.131) is , however, a classical approximation to a quantum mechanical expression, accurate when the momentum transfer between photons and matter, $\hbar \mathbf{k}$, is small. When we treat the plasma quantum mechanically, the derivative term $\mathbf{k} \cdot \partial_{\mathbf{v}} f_0(\mathbf{v})$ is replaced by a difference in f_0, and the $\mathbf{k} \cdot \mathbf{v}$ term in the denominator is replaced by a difference in energies of momentum states:

$$\mathbf{k} \cdot \partial_{\mathbf{v}} f_0(\mathbf{v}) \rightarrow \frac{m}{\hbar} \{ f_0(\mathbf{p} + \hbar \mathbf{k}/2) - f_0(\mathbf{p} - \hbar \mathbf{k}/2) \}, \tag{1.133}$$

$$\mathbf{k} \cdot \mathbf{v} \rightarrow \frac{1}{\hbar} [\epsilon(\mathbf{p} + \hbar \mathbf{k}/2) - \epsilon(\mathbf{p} - \hbar \mathbf{k}/2)]. \tag{1.134}$$

We then have

$$\epsilon_{\|}(\mathbf{k}, \omega) = 1 + \tag{1.135}$$

$$+ \sum_j \frac{\omega_{pj}^2}{\omega^2} \int \frac{d^3p}{m^2} \frac{f_0(\mathbf{p} + \hbar\mathbf{k}/2) - f_0(\mathbf{p} - \hbar\mathbf{k}/2)}{\hbar(\omega + i\eta) - [\epsilon(\mathbf{p} + \hbar\mathbf{k}/2) - \epsilon(\mathbf{p} - \hbar\mathbf{k}/2)]}.$$

If the plasma particles are free-particle Fermions, the distribution function is

$$f_0(\mathbf{p}) = [e^{\beta(p^2/2m - \mu)} + 1]^{-1}, \tag{1.136}$$

where β is $1/T$ and μ is the chemical potential. This means

$$\epsilon_{\|}(\mathbf{k}, \omega) = 1 + \sum_j \frac{\omega_{pj}^2}{\omega^2} \times$$

$$\int \frac{d^3p}{m^2} \frac{[e^{\beta(\mathbf{p} + \hbar\mathbf{k}/2)^2/2m - \mu} + 1]^{-1} - [e^{\beta(\mathbf{p} - \hbar\mathbf{k}/2)^2/2m - \mu} + 1]^{-1}}{\hbar(\omega + i\eta) - [\epsilon(\mathbf{p} + \hbar\mathbf{k}/2) - \epsilon(\mathbf{p} - \hbar\mathbf{k}/2)]}. \tag{1.137}$$

If $(\hbar k)^2/2m \gg k_B T$ and μ, we can approximate this expression by

$$\epsilon_{\|}(\mathbf{k}, \omega) = 1 + \sum_j \frac{\omega_{pj}^2}{\omega^2} e^{-\beta(\hbar k)^2/8m} \times$$

$$\int \frac{d^3p}{m^2} \frac{e^{-\beta[\mathbf{p} \cdot (\mathbf{p} + \hbar\mathbf{k})/2m - \mu]} - e^{-\beta[\mathbf{p} \cdot (\mathbf{p} - \hbar\mathbf{k})/2m - \mu]}}{\hbar(\omega + i\eta) - [\epsilon(\mathbf{p} + \hbar\mathbf{k}/2) - \epsilon(\mathbf{p} - \hbar\mathbf{k}/2)]}. \tag{1.138}$$

For very large k, therefore, the imaginary part of $\epsilon_{\|}(\mathbf{k}, \omega)$, obtained from the Landau contour integral of the second term in the above expression, falls off as $e^{-\beta\hbar^2 k^2/8m}$. It is this part of the dielectric which determines the strength of the fluctuations. Therefore, fluctuations are indeed negligible at high enough k.

1.8 The Bohr - van Leeuwen Theorem

Those readers familiar with the Bohr-van Leeuwen theorem might object that, when a permanent magnetic moment exists, it is always a quantum

mechanical effect. In 1911, Niels Bohr [19] demonstrated that a strict, rigorous application of classical statistical mechanics ruled out the possibility of macroscopic magnetization in classical physical systems. This result, among others, was independently discovered by H.-J. van Leeuwen and presented in her dissertation in 1919 [20]. We consider here the apparent contradiction between the Bohr-van Leeuwen theorem and the present theory after giving a short review of the theorem. We give a proof of this which closely follows one given by van Vleck [21]. His proof, in turn, is based on that given by van Leeuwen.

We wish to calculate the magnetization of a macroscopic body. Suppose that it is made up of molecules, perhaps possessing permanent or induced magnetic dipole moments. From a classical view point, the magnetic moment of one of the molecules is $e/2m_e c$ times the total angular momentum of the electrons orbiting the molecule. The z-component of the magnetic moment is

$$m_z = \frac{e}{2c} \sum_i (x_i \dot{y}_i - y_i \dot{x}_i). \tag{1.139}$$

We can write this more generally, thereby economizing notation and showing the power of the theorem more fully:

$$m_z = \sum_k a_k \dot{q}_k, \tag{1.140}$$

where the q_k's can be a set of generalized coordinates describing the system (in this case, the positions of a molecule's electrons), the $\dot{q}_k$'s are the corresponding generalized velocities, and the a_k's are functions of the q_k's but not of the $\dot{q}_k$'s.

Magnetization is found by taking an ensemble average of this magnetic moment

$$M_z = N \frac{\int \sum_k a_k \dot{q}_k e^{-H/kT} dq_1 \ldots dp_1 \ldots}{\int e^{-H/kT} dq_1 \ldots dp_1 \ldots}, \tag{1.141}$$

where N is the average molecular density, T is the temperature, and $H = H(\{q\}, \{p\})$ is the Hamiltonian of the system.

We note that $\dot{q}_k = \partial H/\partial p_k$, and obtain

$$M_z = -NkT \frac{\int \sum_k a_k \frac{\partial}{\partial p_k} e^{-H/kT} \prod_i dq_i \prod_i dp_i}{\int e^{-H/kT} \prod_i dq_i \prod_i dp_i} \qquad (1.142)$$

$$= -NkT \frac{\int \sum_k [a_k e^{-H/kT}]_{p_k=-\infty}^{p_k=+\infty} \prod_i dq_i \prod_{i \neq k} dp_i}{\int e^{-H/kT} \prod_i dq_i \prod_i dp_i}. \qquad (1.143)$$

We make the reasonable assumption that if any one of the p_k approaches $\pm\infty$, then $H(\{q\}, \{p\})$ becomes infinite. This being the case, we find

$$[a_k e^{-H/kT}]_{p_k=-\infty}^{p_k=+\infty} = 0. \qquad (1.144)$$

The magnetization is therefore identically zero.

The result is the same for a plasma. We pick some point which is stationary with respect to the center of mass of the plasma. We find the magnetic moment about this point

$$\mathbf{m} = \sum_i \frac{e_i}{2cm_i} (\mathbf{x}_i \times \mathbf{p}_i) \qquad (1.145)$$

where the sum extends over all charges in the plasma. We find magnetization by taking an ensemble average of this sum. The argument proceeds exactly as above and we find that the magnetization is, again, zero.

The question we address is whether this result contradict the zero-frequency (*i.e.* permanent) magnetic fields we have found in plasmas or not. The answer is that it does not. The contradiction is only apparent. van Leeuwen's proof deals with the *ensemble average* of the magnetic moment $\mathbf{m}$.

This average is zero. However, the theorem says nothing about *fluctuations about* this average. We take an ensemble of macroscopically identical plasmas. We measure the magnetic field at some particular point in each plasma, and average the measurements. We will, indeed, get a value of zero. However, in each plasma, the magnetic field at the particular point we have chosen will deviate from this zero average. What we have found is that this deviation in each element of the ensemble has, generally speaking, a *time average* different from zero. This result is surprising, but is not in contradiction with any well-established results of electromagnetism or statistical mechanics.

1.9 Fluctuations in Degenerate Electron Plasmas

1.9.1 Completely Degenerate Stationary Electron Plasmas

Our aim in this section is to obtain expressions for the frequency spectra of electrical current and magnetic field fluctuations in completely degenerate electron plasmas. We take a simple model of the degenerate plasma: a completely degenerate gas of Fermionic electrons in a uniform background of neutralizing positive charge. When the degeneracy is nearly complete, the Fermi distribution can be taken at its $T = 0$ form for the purpose of computing the dielectric function. This does not imply that the actual temperature or its associated fluctuations vanish. In this model, the wave functions of the electrons are simple plane waves, rather than the more complicated (and more realistic) Bloch functions associated with a periodic lattice. We can at least expect that our results hold for metallic crystals with a small number of conduction electrons filling the lowest portion of a single conduction band, where the electron Hamiltonian approximates that of a free particle.

Given this model of the degenerate electron gas, the longitudinal di-

electric function is [22]:

$$\epsilon'_l(\omega, \mathbf{k}) = 1 + \frac{3}{8} \frac{\omega_{pe}^2}{E_F^2} \frac{1}{q^2} \left\{ 1 + \frac{1}{2q} \left[1 - \frac{1}{4} \left(q - \frac{u}{q} \right)^2 \right] \ln \frac{|q(q+2) - u|}{|q(q-2) - u|} \right.$$

$$\left. + \frac{1}{2q} \left[1 - \frac{1}{4} \left(q + \frac{u}{q} \right)^2 \right] \ln \frac{|q(q+2) + u|}{|q(q-2) + u|} \right\},$$

$$\epsilon''_l(\omega, \mathbf{k}) = \frac{3\pi}{16} \frac{\omega_{pe}^2}{E_F^2} \frac{1}{q^3} \begin{cases} u, & 0 < u < q(2-q), \\ 1 - \frac{1}{4} \left(q - \frac{u}{q} \right)^2, & q|q-2| < u < q(q+2), \\ 0, & 0 < u < q(q-2), u > q(q+2) \end{cases} \qquad (1.146)$$

where $\epsilon'_l = \mathrm{Re}\{\epsilon_l\}$ and $\epsilon''_l = \mathrm{Im}\{\epsilon_l\}$, q is k/p_F, u is $|\omega|/E_F$, p_F is the Fermi momentum, E_F is the Fermi energy. In this section, we set $\hbar = 1$. The $\mathbf{k} - \omega$ regions in which ϵ''_l is non-zero are shown in Fig. 1.14(a).

$\langle \delta n^2 \rangle_{\mathbf{k}\omega}$ is given by

$$\langle \delta n^2 \rangle_{\mathbf{k}\omega} = \frac{k^2}{2\pi e^2} \frac{1}{e^{\omega/T} - 1} \frac{\epsilon''_l}{|\epsilon_l|^2}. \qquad (1.147)$$

As we remarked above, the temperature T appears in the Bose-Einstein distribution, while it does not appear in $\epsilon_l(\omega, \mathbf{k})$. When $T \to 0$, the factor $(e^{\omega/T} - 1)^{-1}$ approaches $-\Theta(-\omega)$, $\Theta(x)$ being the Heaviside step function. The last factor in the expression for $\langle \delta n^2 \rangle_{\mathbf{k}\omega}$ is $-\mathrm{Im}\{1/\epsilon\}$. It should be noted that this takes on non-zero values when: 1) $\mathbf{k}$ and ω lie within the regions specified by Eq. (1.146), and 2) $\mathbf{k}$ and ω satisfy the dispersion relation for the electrostatic plasma wave propagating through the degenerate plasma. The dispersion relation for the electrostatic plasma wave in the completely degenerate electron gas is [3]

$$\omega^2 = \omega_{pe}^2 + \frac{3}{5} k^2 v_F^2 + \frac{k^4}{4m^2}, \qquad (1.148)$$

where v_F is the Fermi velocity of the degenerate gas.

The equation of charge continuity, together with Eq. (1.147), tells us that the longitudinal current fluctuations are given by

$$\langle \delta j_{\parallel}^2 \rangle_{\mathbf{k}\omega} = \frac{\omega^2}{2\pi} \frac{1}{e^{\omega/T} - 1} \frac{\epsilon_l''}{|\epsilon_l|^2}. \tag{1.149}$$

Fig. 1.14(b) shows a contour plot of this function weighted by the geometrical factor $4\pi k^2$. We find the frequency spectrum of longitudinal current fluctuations $\langle \delta j_{\parallel}^2 \rangle_{\omega}$ by integrating this expression over d^3k and dividing by $(2\pi)^3$. We have performed this numerically. Fig. 1.15 shows the result obtained when the plasmon energy divided by the Fermi energy is 1.49. For very low frequencies, $\langle \delta j_{\parallel}^2 \rangle_{\omega}$ varies as ω^3. There is a kink in the spectrum at $\hbar\omega = 1.49 E_F$. This corresponds to the appearance of the electrostatic plasma wave, which exists in the frequency range of $u = 1.49$ to $u \approx 2.3$. Above $u \approx 2.3$, $\langle \delta j_{\parallel}^2 \rangle_{\omega}$ rises approximately as $\omega^{1.45}$.

The transverse current fluctuation spectrum in a completely degenerate electron plasma is derived from the transverse part of the dielectric function [3]

$$\epsilon_t(\omega, \mathbf{k}) = 1 - \frac{\omega_{pe}^2}{\omega^2} - \frac{4\pi e^2}{\omega^2 m^2} \cdot \frac{1}{V} \sum_{\mathbf{p}} n_{\mathbf{p}} \left(p^2 - \frac{(\mathbf{k} \cdot \mathbf{p})^2}{k^2} \right) \times$$

$$\left\{ \frac{1}{\omega - E_{\mathbf{p-k}} + E_{\mathbf{p}} + io} - \frac{1}{\omega - E_{\mathbf{p}} + E_{\mathbf{p-k}} + io} \right\}, \tag{1.150}$$

where V is the volume of the gas and $n_{\mathbf{p}}$ is the Fermionic occupation number of the state $\mathbf{p}$:

$$n_{\mathbf{p}} = \left(e^{\beta(E_{\mathbf{p}} - \mu)} + 1 \right)^{-1}. \tag{1.151}$$

Since we take the electron wave functions to be plane waves, $E_{\mathbf{p}}$, the energy of state $\mathbf{p}$, is $p^2/2m_e$. Assuming a large number of electrons, with two electrons per p-state, as allowed by the Pauli exclusion principle, we can approximate

the summation here by an integration. If the boundary conditions on the gas are periodic, we find

$$\epsilon_t'(\omega, \mathbf{k}) = 1 - \frac{3}{8}\frac{\omega_{pe}^2}{E_F^2}\frac{1}{u^2}\left[1 + \frac{q^2}{4} + \frac{3}{4}\frac{u^2}{q^2} - \right.$$

$$\frac{1}{2q}\left(1 - \frac{1}{4}\left(q + \frac{u}{q}\right)^2\right)^2 \ln\left|\frac{q(q+2)+u}{q(q-2)+u}\right|$$

$$\left. -\frac{1}{2q}\left(1 - \frac{1}{4}\left(q - \frac{u}{q}\right)^2\right)^2 \ln\left|\frac{q(q+2)-u}{q(q-2)-u}\right|\right]$$

$$\epsilon_t'' = \begin{cases} -\frac{3\pi}{16}\frac{\omega_{pe}^2}{E_F^2}\frac{1}{uq}(2 - \frac{1}{4q^2}a^2 - \frac{1}{4q^2}b^2, & 0 < u < q(2-q), \\ -\frac{3\pi}{16}\frac{\omega_{pe}^2}{E_F^2}\frac{1}{u^2q}\left(1 - \frac{1}{4q^2}b^2\right)^2, & q|q-2| < u < q(q+2) \\ 0, & 0 < u < q(q-2), u > q(q+2), \end{cases} \tag{1.152}$$

where $a = u + q^2$ and $b = -u + q^2$. The transverse current fluctuation spectrum is given by

$$\langle \delta j_\perp^2 \rangle_{\mathbf{k}\omega} = \frac{1}{2\pi}\frac{\omega^2}{e^{\omega/T}-1}\left(1 - \frac{c^2k^2}{\omega^2}\right)^2 \frac{\epsilon_t''}{\left|\epsilon_t - \frac{c^2k^2}{\omega^2}\right|^2}. \tag{1.153}$$

This function, weighted with $4\pi k^2$, is plotted in contour form in Fig. 1.14(c).In analogy with the longitudinal case, $\text{Im}(1/(\epsilon_t - c^2k^2/\omega^2))$ is a non-zero δ-function along the dispersion relation curve of the propagating electromagnetic wave. The dispersion relation is given, approximately, by [3]

$$\omega^2 = \omega_{pe}^2 + c^2k^2 + \tfrac{1}{5}v_F^2 k^2, \quad c^2k^2 << \omega_{pe}^2,$$
$$\omega^2 = c^2k^2 + \omega_{pe}^2\left(1 + \tfrac{1}{5}\frac{v_F^2}{c^2}\right), c^2k^2 >> \omega_{pe}^2. \tag{1.154}$$

We find the frequency spectrum of the transverse current fluctuations $\langle \delta j_\perp^2 \rangle_\omega$ by integrating over d^3k and dividing by $(2\pi)^3$. Our numerical result is shown in Fig. 1.16. The plasmon energy divided by the Fermi energy is, again, 1.49.

$\langle \delta j_\perp^2 \rangle_\omega$ does not exhibit a power law behavior at low frequencies. There is a kink in the spectrum at $\omega = E_F/\hbar$. This is due to the difference in behavior of ϵ_t'' below and above the curve $u = q(2-q)$. Above the kink, the spectrum rises approximately as $\omega^{0.45}$. The contribution to the current fluctuation spectrum given by the propagating electromagnetic wave is about 10^{-5} times that of the spectrum contributed by the dissipated plasma waves. Therefore it is not distinguishable in our figure.

One very curious aspect of all these spectra is that they increase in magnitude without limit as frequency increases. This follows mathematically from setting $E_p = p^2/2m_e$. E_p of a physical degenerate electron plasma, such as the conduction electrons in a metal, would be better described by the energy states of, for example, fermions in a finite square well potential. This being the case, the spectra presented here will be inaccurate above some substantial fraction of the frequency $\omega = w_0/\hbar$, where w_0 is the work function of the metal in question. w_0 will generally be of the same order of magnitude as E_F[23].

The magnetic field fluctuation spectrum is also studied. Maxwell's equations yield

$$\frac{\langle B^2 \rangle_{k\omega}}{8\pi} = \frac{2\pi}{c^2} \frac{k^2}{\left(\frac{\omega^2}{c^2} - k^2\right)^2} \langle \delta j_\perp^2 \rangle_{k\omega}. \tag{1.155}$$

This function is shown in contour form, with geometrical weighting of $4\pi k^2$, in Fig. 1.14(d). We obtain the frequency spectrum of the magnetic field fluctuations $\langle B^2 \rangle_{k\omega}/8\pi$ by integrating over k. Our numerical result is shown in Fig. 1.17. Here we have a quantity whose spectrum clearly diverges at low frequencies. Note that for $\omega < (E_F/\hbar) \times 10^{-2}$, $\langle B^2 \rangle_\omega/8\pi$ falls off as $\omega^{-1/3}$, whereas for $\omega > (E_F/\hbar) \times 10^{-2}$, it falls off as ω^{-1}.

1.9.2   Completely Degenerate Electron Plasmas with Net Drift Velocity

We now examine voltage fluctuations in a degenerate electron plasma with a finite drift velocity. Such a plasma is a simple model for conduction electrons carrying current in a metal. For the moment, we ignore the effects of the ion lattice potential, and continue to treat the electrons as free particles. In this approximation, if the gas has a drift velocity $\mathbf{v}_D$, the longitudinal dielectric function changes by way of a simple Galilean transformation:

$$\epsilon_l(\omega, \mathbf{k}) = \epsilon_{lS}(\omega - \mathbf{v}_D \cdot \mathbf{k}, \mathbf{k}), \tag{1.156}$$

where $\epsilon_{lS}(\omega, \mathbf{k})$ is the dielectric of the stationary plasma, namely that given by Eq. (1.146).

The charge density fluctuation spectrum also changes by a Galilean transformation:

$$\langle \delta\rho^2 \rangle_{\mathbf{k}\omega} = \frac{k^2}{2\pi} \frac{1}{e^{(\omega - \mathbf{v}_D \cdot \mathbf{k})/T} - 1} \frac{\epsilon_l''}{|\epsilon_l|^2}, \tag{1.157}$$

where ϵ_l is now defined by Eq. (1.156). Voltage is related to charge density by $V(\omega, \mathbf{k}) = 4\pi\rho(\omega, \mathbf{k})/k^2$. Therefore the voltage fluctuation spectrum is given by

$$\langle V^2 \rangle_{\mathbf{k}\omega} = \frac{16\pi^2}{k^2} \frac{1}{e^{(\omega - \mathbf{v}_D \cdot \mathbf{k})/T} - 1} \frac{\epsilon_l''}{|\epsilon_l|^2}. \tag{1.158}$$

If the plasma is completely degenerate, the voltage spectrum is

$$\langle V^2 \rangle_{\mathbf{k}\omega} = \frac{16\pi^2}{k^2} \Theta(\omega - \mathbf{v}_D \cdot \mathbf{k}) \left(\frac{-\epsilon_l''}{|\epsilon_l|^2} \right), \tag{1.159}$$

where $\Theta(x)$ is the Heaviside step function. The regions in $\mathbf{k}, \omega$-space where the fluctuation spectrum is finite can be inferred from the previous subsection,

where we discussed electron number density fluctuations: the boundaries given there are altered by the Galilean transformation $\omega \to \omega - \mathbf{v}_D \cdot \mathbf{k}$.

To obtain $\langle V^2 \rangle_\omega$, we integrate $\langle V^2 \rangle_{\mathbf{k}\omega}$ over d^3k and divide by $(2\pi)^3$. Fig. 1.22 displays $\langle V^2 \rangle_\omega$ for a degenerate electron plasma with a drift velocity of $2.82 \times 10^{-6} v_F$ and a plasmon energy to Fermi energy ratio of 1.52. (Here, v_F represents the Fermi velocity of the degenerate plasma.) These parameters correspond to a sample of copper with a current density of 1.92×10^{16} esu cm^{-2} sec^{-1}. The drift velocity has been chosen to be representative of the voltage noise measurement experiments of Eberhard and Horn [24].

Of particular interest to us in this section is the behavior of the voltage fluctuation spectrum $\langle V^2 \rangle_\omega$ at low frequencies, typically in the range of 1000 Hz and less. For a plasma with the above listed parameters, it was found that $\langle V^2 \rangle_\omega$ exhibited a white noise spectrum in this frequency range. The magnitude of the spectrum was $1.22 \times 10^{-6} p_F$, or, specific to copper, 1.57×10^{-21} Volt^2-sec. This white noise extends over several decades of frequency. The frequency range runs as high as $10^{-8} E_F/\hbar$, where the spectrum begins to increase in magnitude, and at least as low as $10^{-15} E_F/\hbar$ (1.7×10^7 Hz and 1.7 Hz respectively, specific to copper). Similar behavior is expected for other metals.

The results of Eberhard and Horn show marked contrast to what we have derived here. In the frequency range just mentioned, they found $1/f$ voltage fluctuation spectra for copper, silver, gold, and other conductors. In light of these results, the simple damped plasma oscillations studied here can be ruled out as the source of $1/f$ noise. It should be noted that the results of Eberhard and Horn are not strictly in contradiction with the results presented here. They report typical noise magnitudes of 10^{-14}–10^{-13} Volt^2-sec. The white noise mentioned here could have been present but greatly overshadowed by the

$1/f$ noise.

Calculating the magnitude of the white noise as a function of drift velocity shows that the white noise magnitude is directly proportional to the drift velocity. For copper, the constant of proportionality is $0.410 m_e$, or $3.36 \times 10^{-21} (\text{Volt-sec})^2 \text{m}^{-1}$. This linear dependence on the drift velocity extends over a large range of drift velocities, running as high as $0.05 v_f$ and at least as low as $5 \times 10^{-9} v_F$ (7.9×10^6 cm/sec and 0.79 cm/sec respectively, specific to copper). At $v_D \approx 0.05 v_F$, the magnitude of the white noise begins to increase faster than power law behavior but slower than exponential behavior. Up to $v \approx v_F$, it can be approximated fairly well by a power law of $\langle V^2 \rangle_\omega \sim v_D^{1.1}$. $\langle V^2 \rangle_\omega$ vs. v_D is shown in Fig. 1.23 for $v_D < 0.1 v_F$.

Calculations of the voltage spectrum have also been attempted with a dielectric computed from an expansion of Eq. (1.146) to first order in T/E_F, with T approximately at room temperature. The resulting spectrum is quite different. With finite current, a white noise spectrum is found at low frequencies. At low currents, specifically $v_D \approx .005 v_f$, the white noise is of the same order of magnitude as just described above. However, above this velocity, the white noise magnitude drops rapidly. A very limited amount of data is available in this regard because of limitations to the numerical integrator used to obtain these results. The reader is cautioned, then, that the following results are calculated at $T = 0$, and could change appreciably at finite temperatures, even when $T/E_F \ll 1$.

We denote the constant of proportionality between the white noise magnitude and the drift velocity by α. It is a function of one free parameter: the ratio of the plasmon energy to the Fermi energy, which we shall call r_E. This can be seen from the form of the dielectric in Eq. (1.146). Fig. 1.24 shows

a plot of α as a function of r_E. At small r_E (which corresponds to high electron density), $\alpha(r_E)$ behaves approximately linearly:

$$\alpha \approx (0.62 m_e) \times r_E \text{ or } \alpha \approx (5.08 \times 10^{-21} (\text{Volt-sec})^2 m^{-1}) \times r_E. \quad (1.160)$$

At large r_E (small electron density), α falls off as $r_E^{-1.94}$:

$$\alpha \approx (5.65 m_e) \times r_E^{-1.94} \text{ or}$$

$$\alpha \approx (4.63 \times 10^{-20} (\text{Volt-sec})^2 m^{-1}) \times r_E^{-1.94}. \quad (1.161)$$

Attempts to describe $\alpha(r_E)$ with a single analytic function have not met with success. In the range of $1.3 > r_E > 1.7$, where most metals are to be found, $\alpha(r_E)$ can be fit to a cubic polynomial

$$\alpha(r_E) \approx 0.043 + 0.571 r_E - 0.281 r_E^2 + 0.042 r_E^3 \quad (1.162)$$

with a maximum error of about 0.2%. $\alpha(r_e)$ is given here in units of electron mass.

The noise discussed here has strong qualitative similarities with shot noise. Namely, it is flat over a wide range of frequencies, and its magnitude is directly proportional to the current flowing in the system. There are differences, however. First, the flat spectrum ends in a slow rise, whereas shot noise falls off as $1/f^2$ at high frequencies [25]. Second, shot noise found in semiconductors and electronic devices where the discreteness of electron current can be important is describable by classical physics while the noise described here would seem to be a purely quantum mechanical effect [26]. It would seem that experimental searches for shot noise in conductors has always turned up $1/f$ noise instead, probably because of the relative sizes of the two spectra [27].

Consideration of the ion lattice in a metal will alter the above results in at least two ways. First, the electron energy, $E_\mathbf{k}$, will lose its simple parabolic

dependence on momentum. The allowed energy levels will be broken up into bands of states. Within each of these bands, the relative energy $E_\mathbf{k} - E_b$, E_b being the energy at the bottom of the band, will deviate from $\hbar^2 k^2 / 2m_e$.

It is expected that only the anisotropy of the electron energy $E_\mathbf{k}$ will possibly give qualitative change to the results obtained above for low frequencies. In this subsection, we have concerned ourselves with frequencies of 10^7 Hz and less. (And, in fact, our main concern has been with frequencies of 1000 Hz and less, in keeping with the experiments of Eberhard and Horn [234].) This corresponds to transitions between electron energy levels separated by about 10^{-9}eV. This is far less than the 0.1 to 1.0 eV involved in inter-band transitions or transitions between states with radically different effective electron masses [28]. We may obtain more accurate results by using the effective electron mass to calculate the plasmon energy to Fermi energy ratio r_E, and the Fermi energy E_F. However, this will change nothing substantially. The anisotropy of the electron energy may have a more noticeable effect, particularly in metals with especially complicated Fermi surfaces, such as aluminum [29].

The second effect an ion lattice may have will come through the motions of the ions themselves. We consider ion motion here. We take a simple model for the ion motion: ions interacting *via* electrostatic forces and simple spring forces. At low k, the dielectric is now altered:

$$\epsilon(\omega, \mathbf{k}) = 1 + 4\pi\chi_e(\omega, \mathbf{k}) + \frac{\omega_{pi}^2}{\omega^2 - v_S^2 k^2}, \qquad (1.163)$$

where $1 + 4\pi\chi_e(\omega, \mathbf{k})$ is the dielectric of the electron gas, given by Eq. (1.146), or by Eq. (1.156) if the electrons have a net drift velocity, v_S is the average sound speed of the lattice, and ω_{pi}^2 is the ion plasma frequency squared: $4\pi n_i(Ze)^2/M_i$. We find the new voltage fluctuation spectrum $\langle V^2 \rangle_\omega$ in the

Metal	$\langle V^2 \rangle_\omega / v_D$ in units of ...		velocity range in units of ...		frequency range in units of ...	
	m_e	(Volt-sec)^{2}m^{-1}	v_F	cm/sec	$E_F/\hbar$	Hz
Cu	.289	2.36×10^{-21}	10^{-3}	1.57×10^5	10^{-8}	1.69×10^7
Ag	.328	2.68×10^{-21}	10^{-3}	1.39×10^5	10^{-8}	1.32×10^7
Au	.328	2.68×10^{-21}	10^{-3}	1.39×10^5	10^{-8}	1.33×10^7
Al	.333	2.72×10^{-21}	10^{-3}	2.02×10^5	10^{-8}	2.81×10^7
Zn	.317	2.59×10^{-21}	10^{-3}	1.82×10^5	10^{-8}	2.27×10^7

Table 1.1: White noise voltage spectrum as predicted by simple model for several metals: ratio of white noise magnitude to drift velocity, drift velocity range in which white noise is proportional to drift velocity, and frequency range in which spectrum is very flat.

same way as above, only using the new dielectric in Eq. (1.157). We find low-frequency white noise again, with a decreased magnitude. For copper, with $v_D = 2.82 \times 10^{-6} v_F$ again, the magnitude is now $8.61 \times 10^{-7} p_F$, or 1.11×10^{-21}Volt^2-sec. The white noise spectrum runs up to $10^{-8} E_F/\hbar$ as before. The relationship between the drift velocity and the white noise magnitude is still linear, with a constant of proportionality of $2.89 \times 10^{-1} m_e$ or 2.36×10^{-21}(Volt-sec)^2/m. Table 1.1 gives $\langle V^2 \rangle_\omega / v_D$ and high frequency ranges of the white noise spectrum for several metals.

It is recognized that the model of ion motion used here is simplistic. A minimum correction to the model would account for the anisotropy of v_S. It is expected, however, that such a refinement will not qualitatively alter the results derived here. It should be noted that the ion addition to the dielectric is hopelessly inaccurate at high k (i.e. near the inverse of the lattice constant, or Brillouin zone boundary), where the dispersion relation of the sound wave departs significantly from a linear relationship. However, the phenomenon discussed here is a low-k, low-ω feature of the fluctuation spectrum.
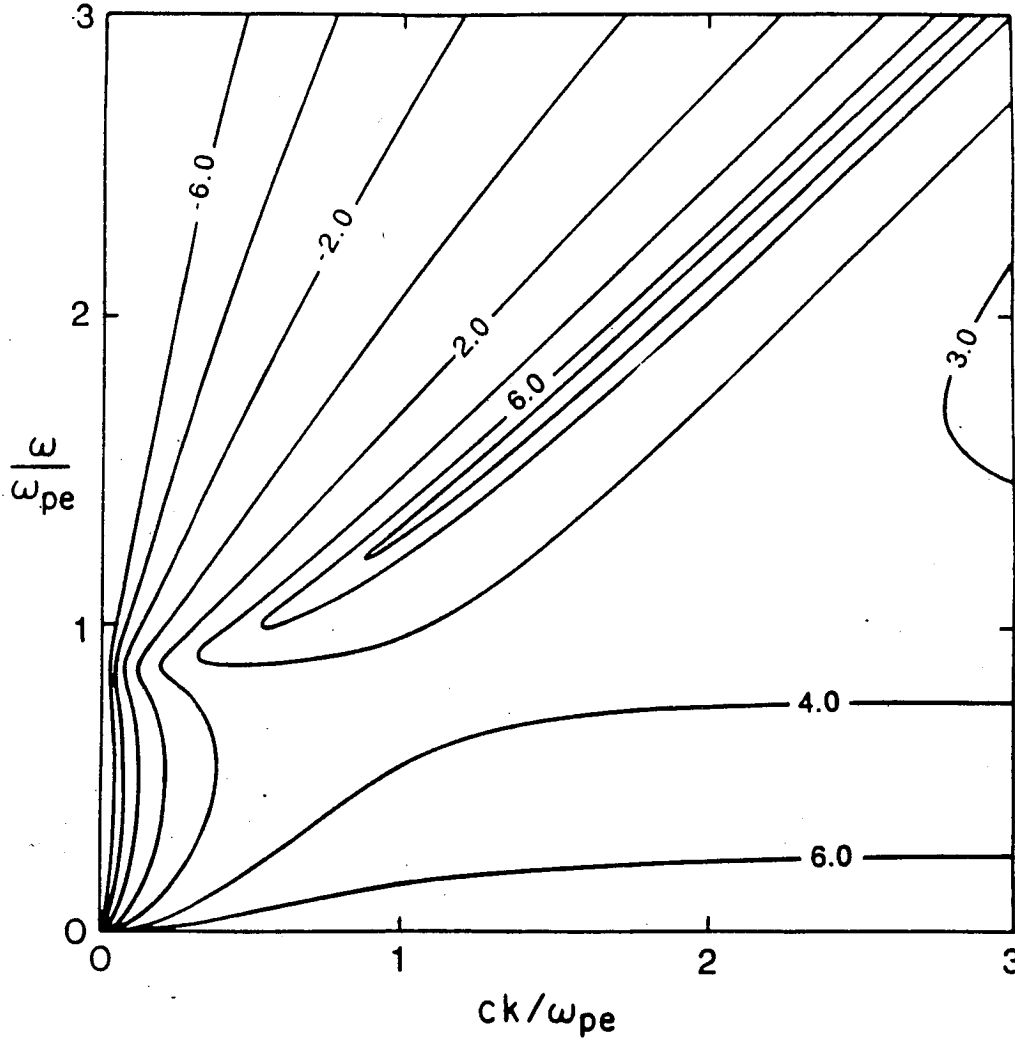
Figure 1.1: The natural logarithm of $\frac{\langle B^2 \rangle_{k\omega}}{8\pi} \times (k^2 c^2 / 2\pi^2 \omega_{pe}^2 \hbar)$. This plot corresponds to an electron positron plasma.
Electron density is $n_e = 4.84 \times 10^3 / \text{cm}^3$. Temperature is $T = 10^{10\circ}\text{K}$. Collision frequency is $2.2 \times 10^{19} \text{sec}^{-1}$. The collision frequency has been set at 100 times the expected value. This smoothes out the contour ridges without their locations drastically, thus giving a better view of the qualitative behavior of the spectrum. The difference in height between adjacent contours is 2.0, except for the solitary contour on the right edge, with a value of 3.0.
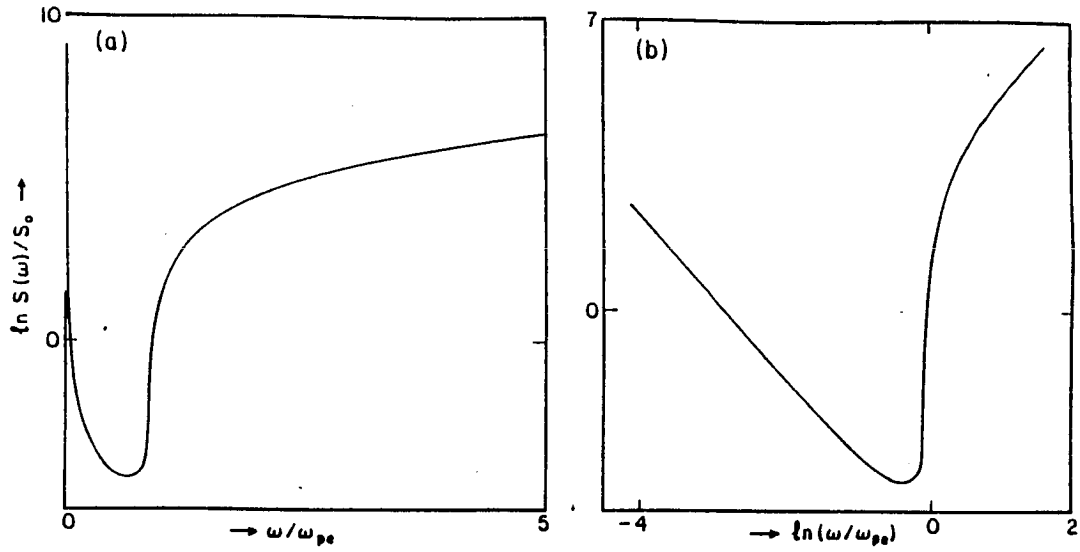
Figure 1.2: The spectral intensity of magnetic fields $S(\omega) = \langle B^2 \rangle_\omega / 8\pi$ in thermal equilibrium, non-magnetized plasmas corresponding to the plasma of 1 sec after big bang. $T = 10^{10\circ}K$; $n_e = 4.8 \times 10^{30}/\text{cc}$.)

a) $\ell n(S(\omega)/S_0)$ plotted linearly in ω. Zero-frequency peak is at the top of the graph, where S_0 is the normalization.

b) $\ell n(S(\omega)/S_0)$ plotted logarithmically in ω. Low-frequency line has slope around -2. Rises to peak at $\omega = 0$.

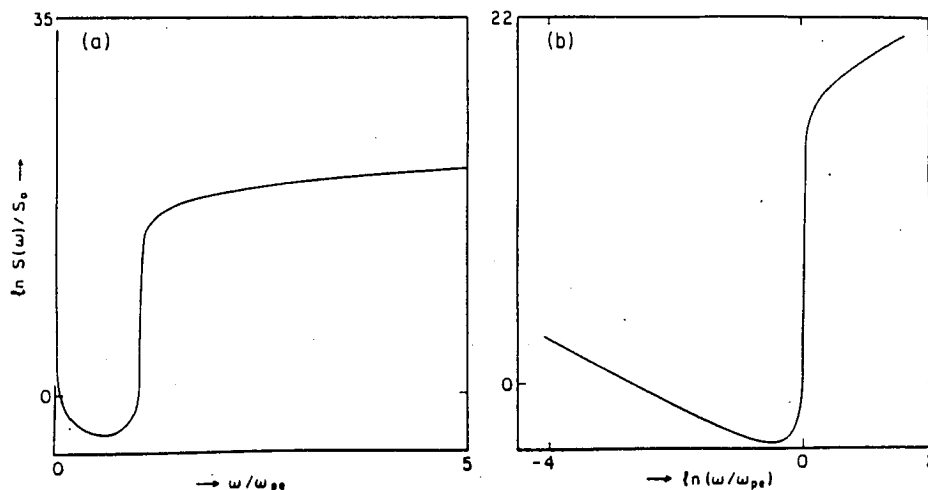Figure 1.3: $\ell n(S(\omega)/S_0)$ the plasma 10^8 sec after big bang. $T = 10^{6\circ}$ K; $n_e = 6.5 \times 10^9$/cc.

a) $\ell n(S(\omega)/S_0)$ plotted linearly in ω. Zero-frequency peak is at the top of the graph.

b) $\ell n(S(\omega)/S_0)$ plotted logarithmically in ω. Slope of low-frequency line is ~ -2. Rises to peak at $\omega = 0$.
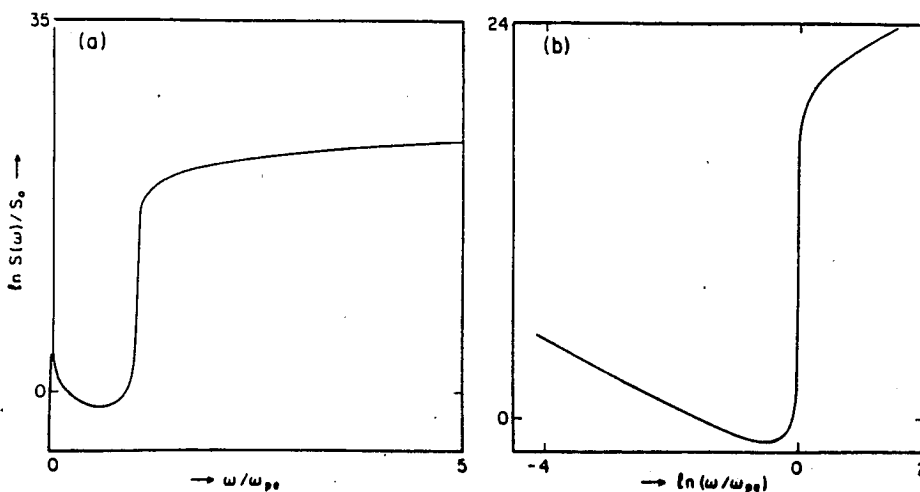

Figure 1.4: Corresponding to the plasma of 10^{12} sec after big bang. $T = 10^{4\circ}$ K; $n_e = 6.5 \times 10^3$/cc.

a) $\ell n S(\omega)/S_0$ plotted linearly in ω. Zero-frequency peak is at the top of the graph.

b) $\ell n S(\omega)/S_0$ plotted logarithmically in ω. Slope of low-frequency line is around -2. Continues to rise until peaking at $\omega = 0$.

Figure 1.5: The dispersion relations and magnetic field fluctuation strengths for the two direction-independent modes of the electron-positron plasma in a uniform magnetic field.

a) Dispersion relations of the two direction-independent modes of the electron-positron plasma in a uniform magnetic field. Roman numerals label modes in increasing value of frequency. The modes shown here are labeled II and V. Modes I, III, and IV, being dependent on propagation direction, are shown in Fig. 4.

b) $\frac{\langle B^2 \rangle_k}{8\pi}$ of the two direction-independent modes. Roman numerals label corresponding modes in Fig. 3(a).
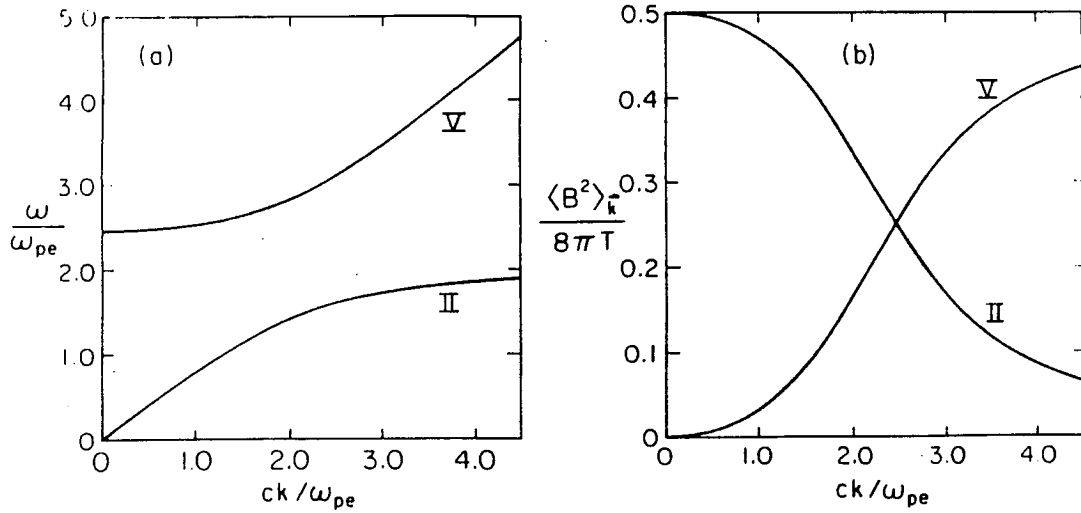
Figure 1.6: Dispersion relations and magnetic field fluctuation strengths for the three direction-dependent modes of the electron-positron plasma in a uniform magnetic field.

Roman numerals label modes in order of increasing frequency. θ indicates angle between imposed magnetic field and angle of propagation. Note that the lowest frequency branch (the shear Alfven branch) is not plotted in d1, since its frequency is identically zero when propagating perpendicularly to the magnetic field. However, as shown in d2, it retains a finite amount of energy.
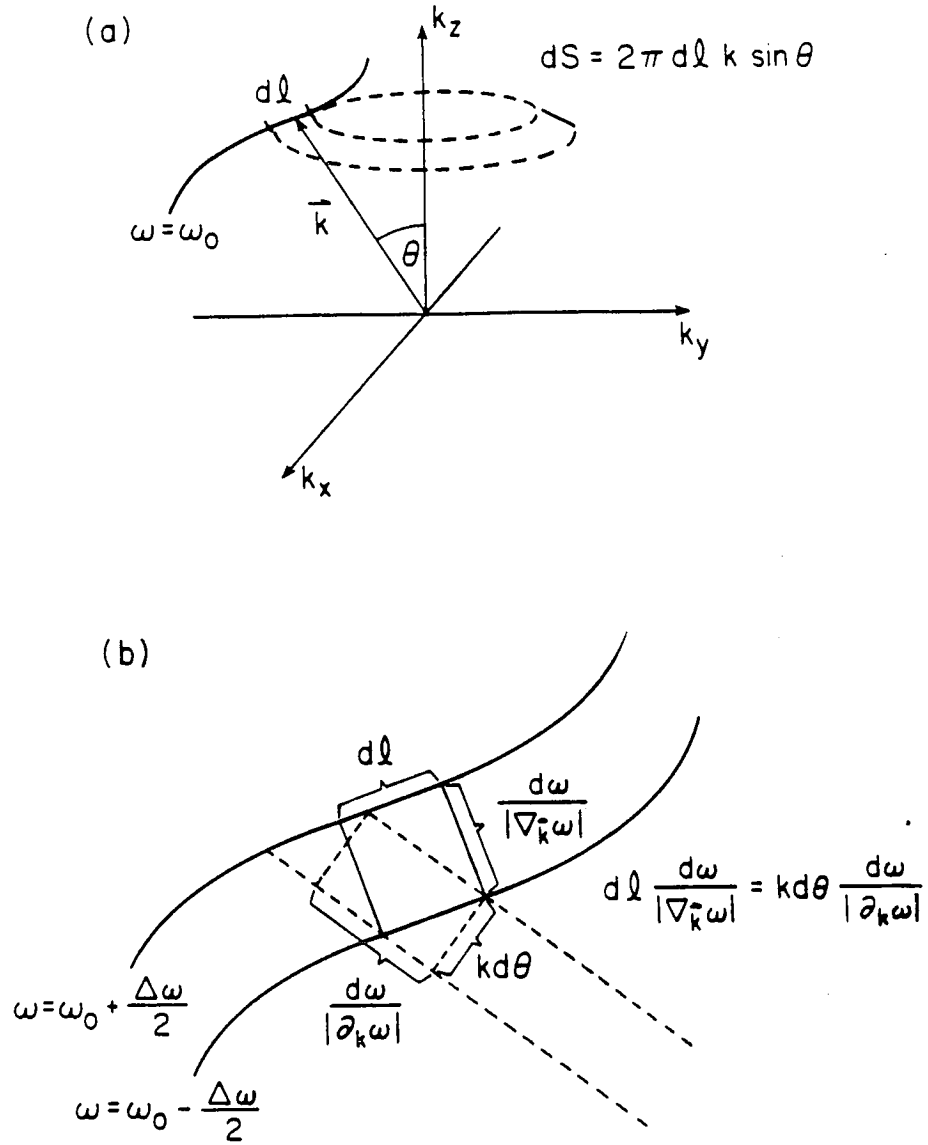
Figure 1.7: Elements of integration in d^3k.

a) The differential surface obtained from rotating a line element dl about the k_z axis is $dS = 2\pi \times dlk\sin\theta$.

b) The areas of the two rectangles are equal for infinitesimal $d\theta$. Therefore, $dl/|\nabla_k\omega| = kd\theta/|\partial_k\omega|$. So, the differential volume $dV = dS \times d\omega/|\nabla_k\omega| = 2\pi \times k^2d\omega\sin\theta d\theta/|\partial_k\omega|$.
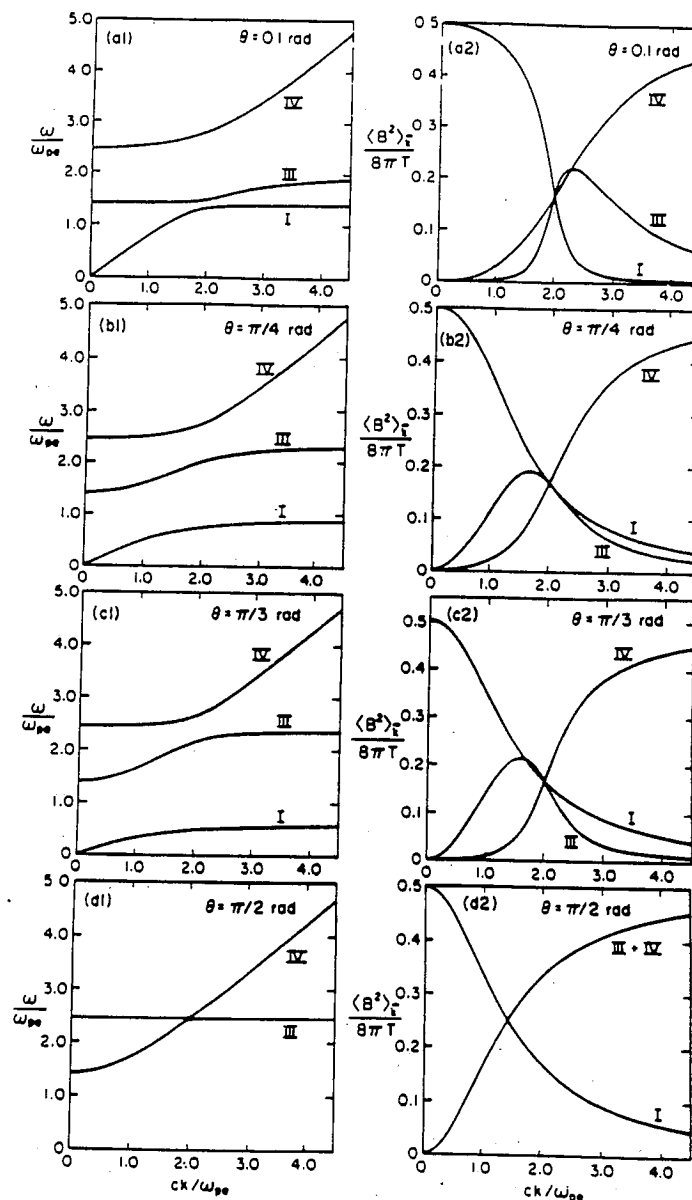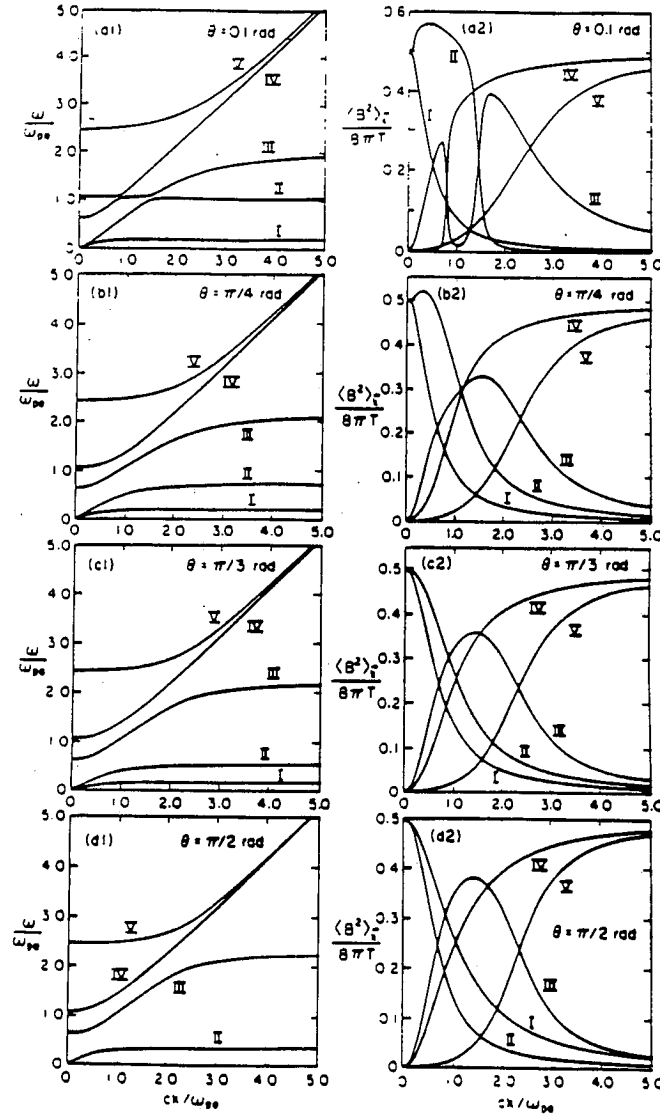
Figure 1.8: Dispersion relations and magnetic field fluctuation strengths for the modes of the electron-ion plasma in a uniform magnetic field.

Roman numerals label modes in order of increasing frequency. θ indicates angle between imposed magnetic field and angle of propagation. Note that the lowest frequency branch (the shear Alfven branch) is not plotted in d1, since its frequency is identically zero when propagating perpendicularly to the magnetic field. However, as shown in d2, it retains a finite amount of energy. Close to $\omega = 0$, the power spectra of modes I and II should be regarded as qualitatively, not quantitatively, correct because of limitations in our numerical analysis.
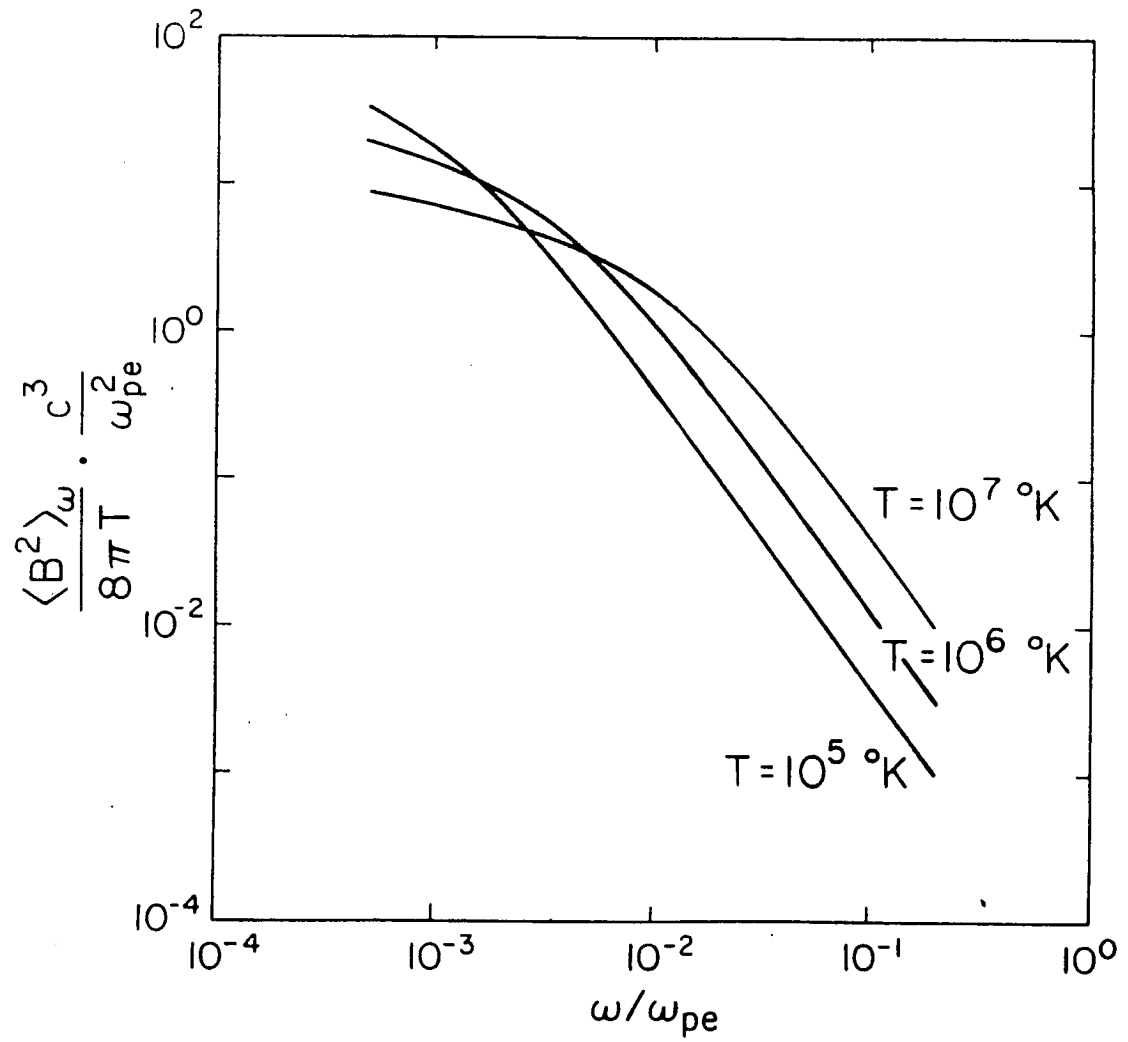
Figure 1.9: Kinetic theory results for magnetic field fluctuation frequency power spectra of thermal plasmas.

Shown are results for electron-ion plasmas at temperatures $T = 10^5 K, 10^6 K$, and $10^{7\circ} K$.
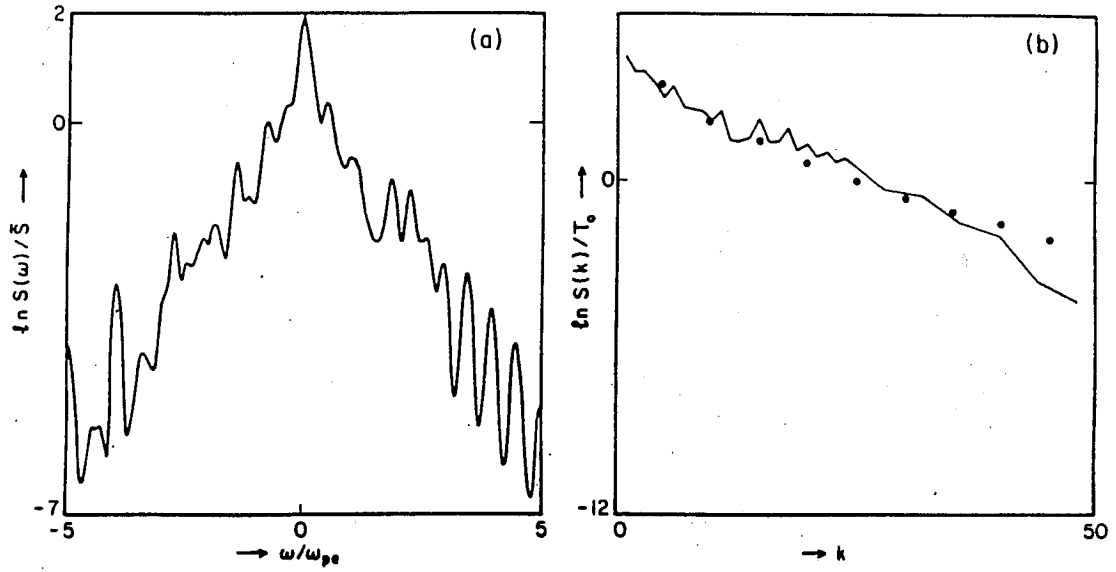
Figure 1.10: Spectral intensities $S(\omega) = \langle B^2 \rangle_\omega /8\pi$ and $S(k) = \langle B^2 \rangle_k /8\pi$ from a 1D simulation of an electron-positron plasma. $\gamma_{\text{therm}} = 34.7 (T = 2 \times 10^{11\circ}$ K)

a) $\ell n(S(\omega)/\overline{S})$. Note peak at $\omega = 0$, where $\overline{S}$ is the normalization

b) $\ell n(S(k)/T_0)$.Line is from simulation results. Dots represent theoretical values: $6.7 - \ell n \left(1 + c^2 \frac{\gamma}{\omega_p^2} k^2 e^{k^2 a^2} \right)$ where 6.7 is obtained from least squares fitting. $k = \frac{2\pi m}{L_x \Delta}$ with m being integer. The finite size effect of the code is taken into consideration.
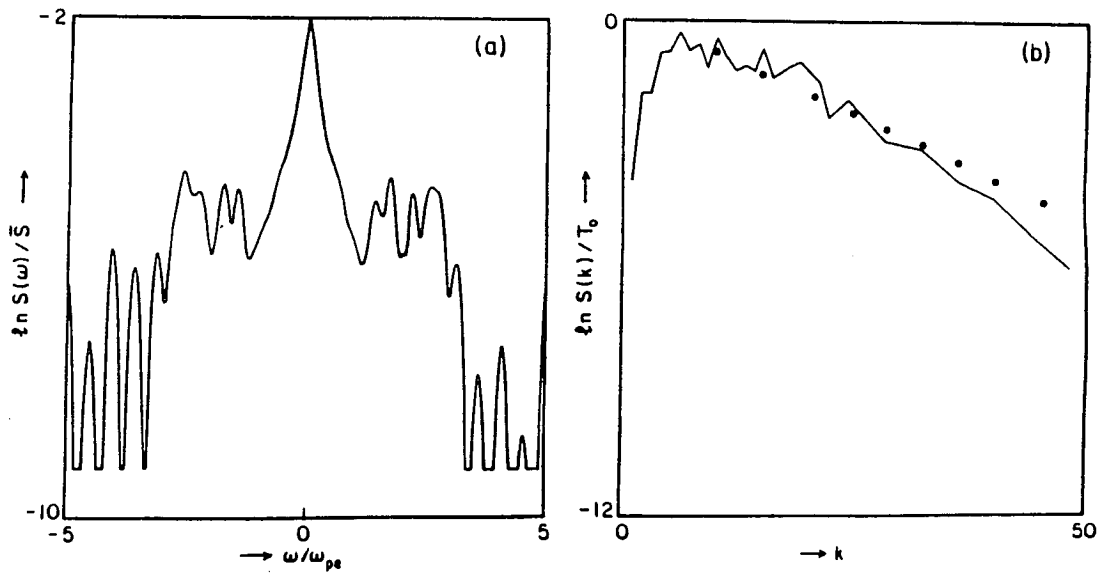
Figure 1.11: Spectral intensities $S(\omega)$ and $S(k) \langle B^2 \rangle_k /8\pi$ from a 1D $e^+ - e^-$ simulation. $\gamma_{\text{therm}} = 1.2(T = 1.3 \times 10^{9\circ}$ K)

a) $\ell n S(\omega)/\bar{S}$. Note zero-frequency peak.

b) $\ell n S(k)/T_0$. Solid line is from simulation results. Dots represent theoretical values $-0.21 - \ell n(1 + c^2 \frac{\gamma}{\omega_p^2} k^2 e^{k^2 a^2})$ where -0.21 is obtained from least squares fitting.
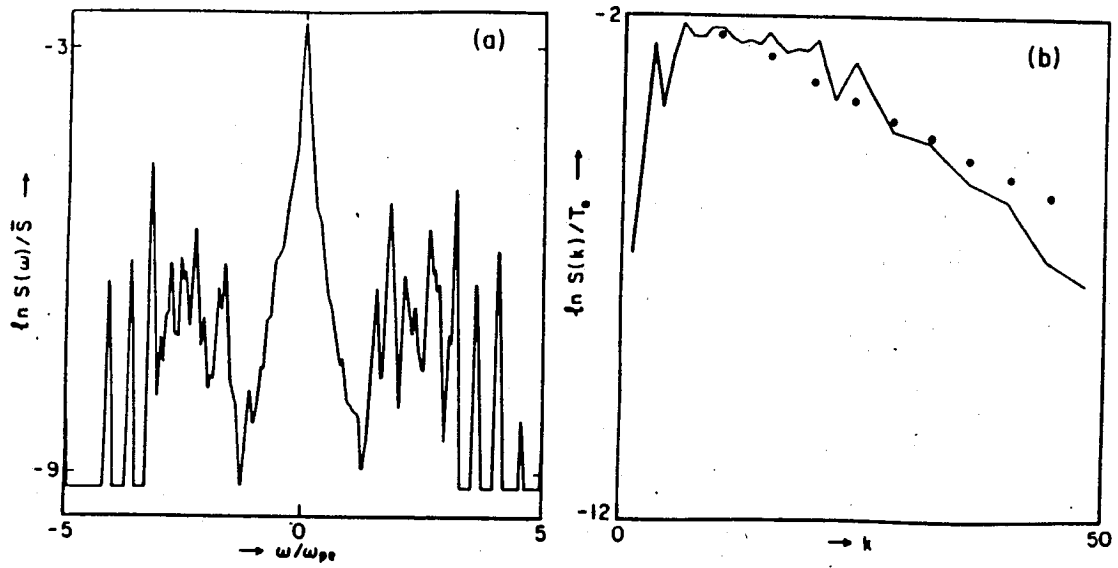
Figure 1.12: Spectral intensities $S(\omega)$ and $S(k) \langle B^2 \rangle_k /8\pi$ from a 1D $e^+ -$ e^- simulation. $\gamma_{\text{therm}} = 1.05(T = 3 \times 10^{8\circ}$ K). Simulation was run for 4096 timesteps.

a) $\ell n S(\omega)/\overline{S}$. Zero-frequency peak is still present in 2D.

b) $\ell n S(k)/S_0$. Line is from simulation results. Dots represent $-1.7 - \ell n(1 + c^2 \frac{\gamma}{\omega_p^2} k^2 e^{k^2 a^2})$ where -1.7 was obtained from least squares fitting.
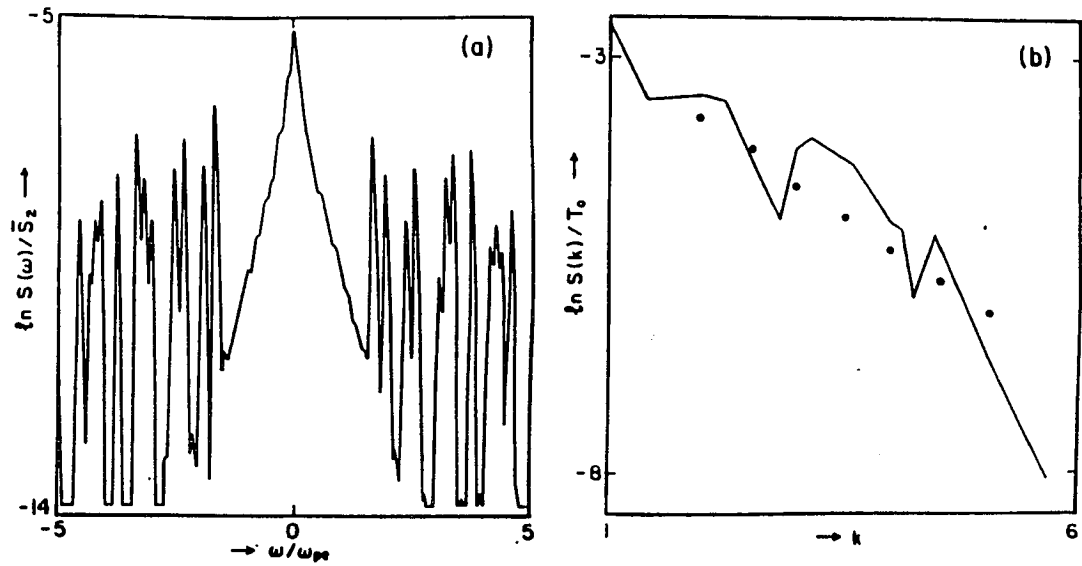
Figure 1.13: Spectral intensities $S(\omega)$ and $S(k)\langle B^2\rangle_{\mathbf{k}}/8\pi$ from a 2D $e^+ - e^-$ simulation. $\gamma_{\text{therm}} = 1.05(T = 3 \times 10^{8\circ}$ K$)$.

a) $\ell n S(\omega)/\overline{S}$. Zero-frequency peak is still present in 2D.

b) $\ell n S(k)/S_0$. Line is from simulation results. Dots represent $-2.6 - \ell n(1 + c^2 \frac{\gamma}{\omega_p^2} k^2 e^{k^2 a^2})$ where -2.6 was obtained from least squares fitting.
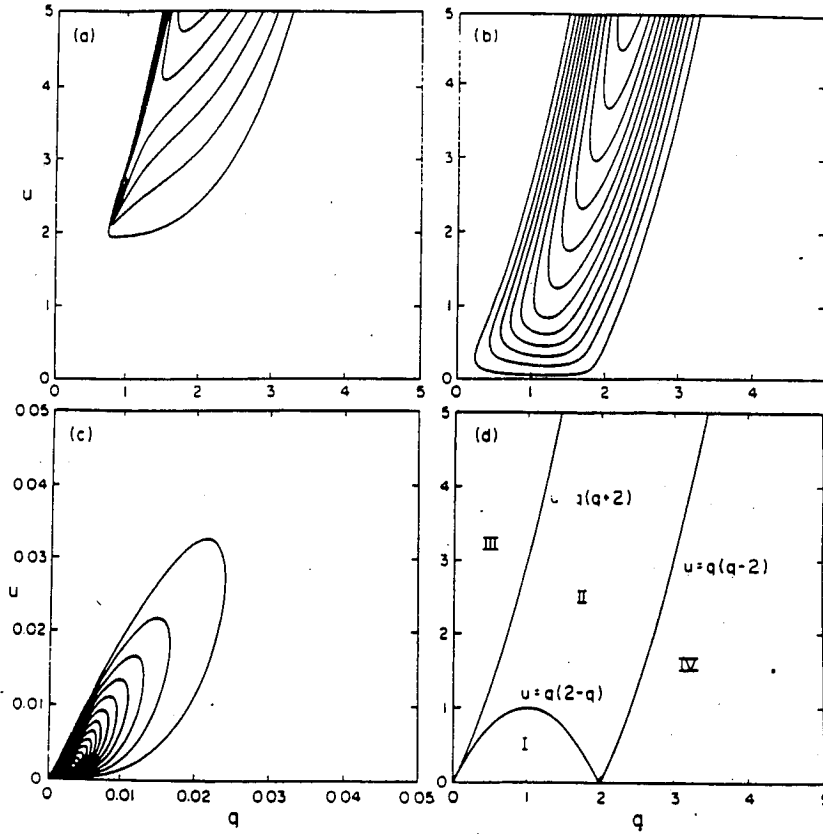
Figure 1.14: Fluctuation power spectra of various quantities in a degenerate plasma.

Plasmon energy divided by Fermi energy is 1.49.

a) Power spectrum of parallel current fluctuations $\langle j_{||}^2 \rangle_{k\omega} \times (\hbar/E_F^2) \times (k\hbar/p_F)^2/2\pi^2$. Contours run from 0. to about 0.03. Contours are highest at the top of the graph, and at the "island" near (q,u)=(0.75,2.3). The outside contour is close to zero.

b) Power spectrum of transverse current fluctuations $\langle j_{\perp}^2 \rangle_{k\omega} \times (\hbar/E_F^2) \times (k\hbar/p_F)^2/2\pi^2$. Contours run from 0 to 0.024. Contours are highest at the top of the graph. The outside contour is close to zero.

c) Power spectrum of magnetic field fluctuations $\frac{\langle B^2 \rangle_{k\omega}}{8\pi}k^2 \times (\hbar/2m_e c)^2/2\pi^2$. Contour interval is 1×10^{-7}. Contours diverge at the origin. The outside contour is close to zero.

d) Finite fluctuations of non-propagating electrostatic and electromagnetic modes can occur only in regions I and II for a fully degenerate plasma.
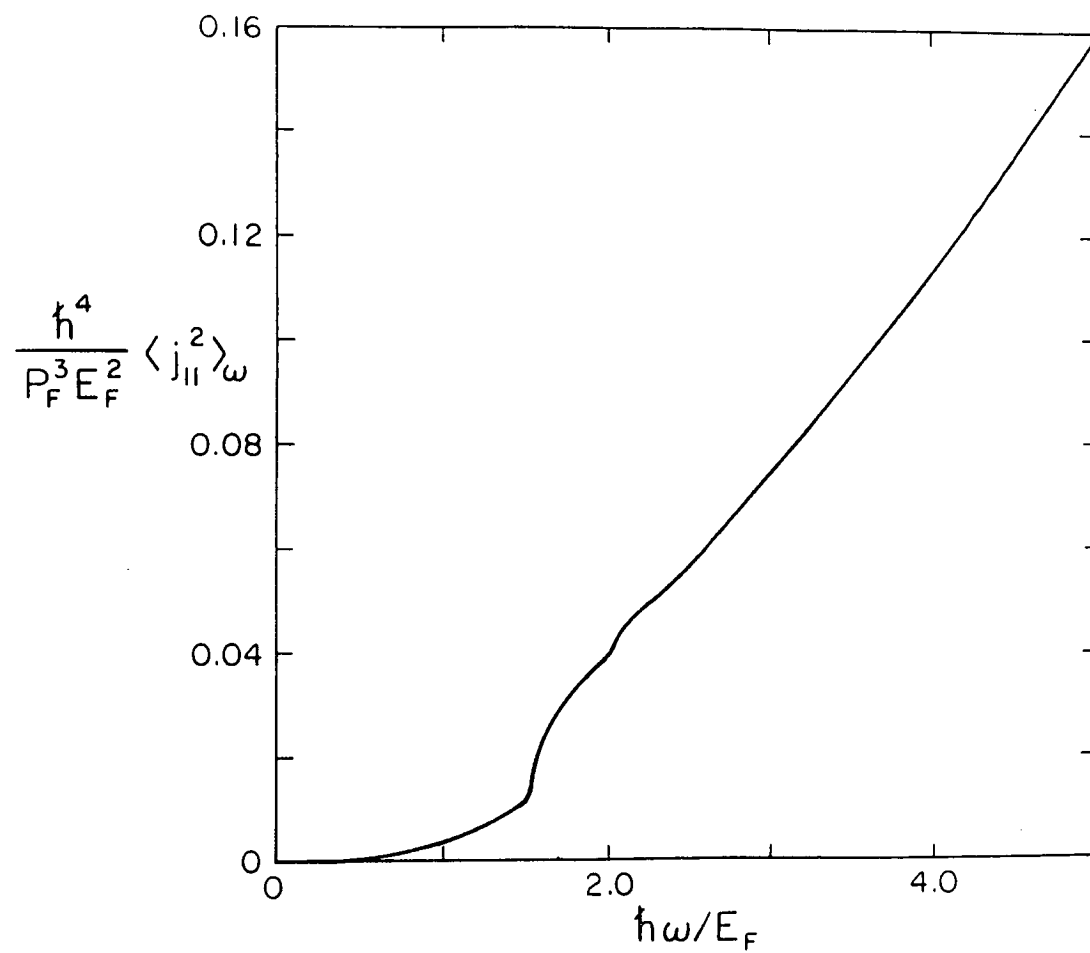
Figure 1.15: Frequency power spectrum of fluctuations in longitudinal current in degenerate electron plasma.

Plasmon energy divided by Fermi energy is 1.49.
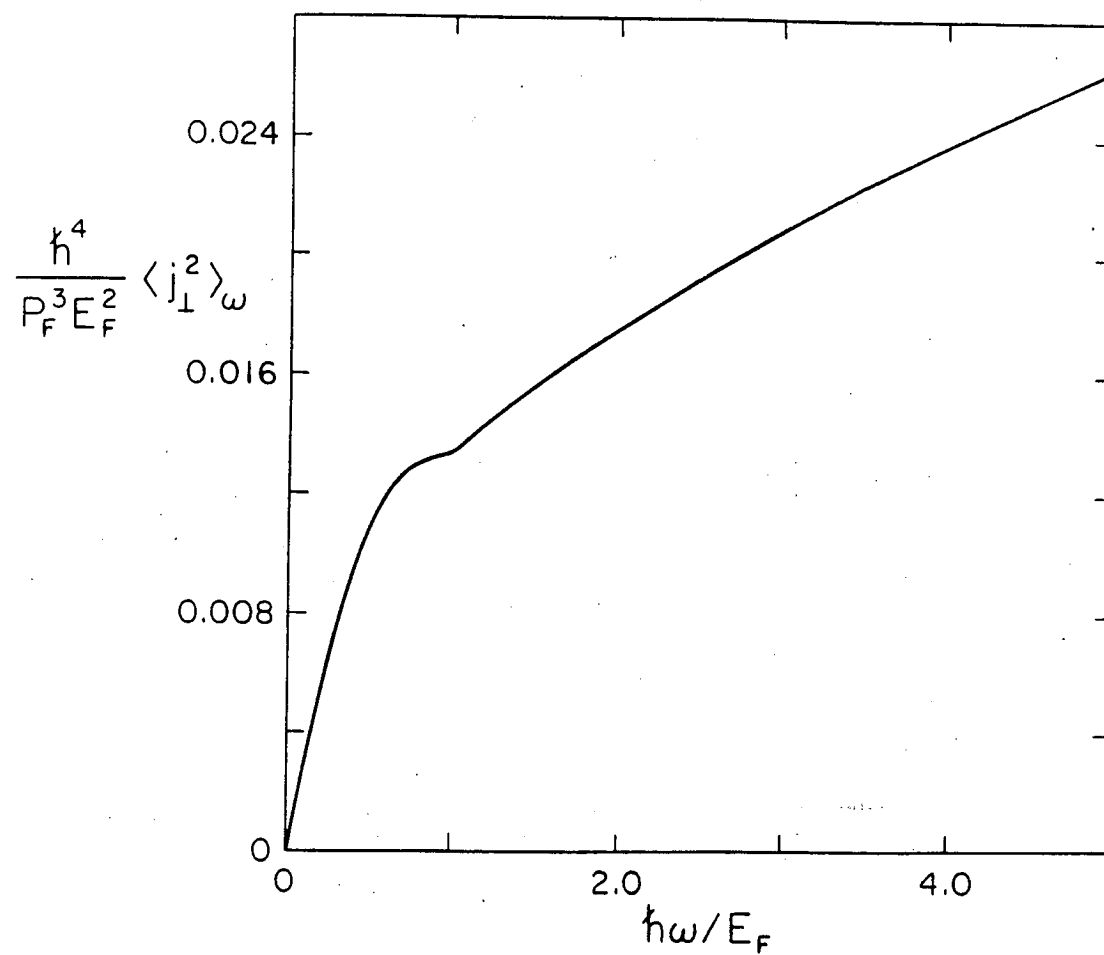
Figure 1.16: Frequency power spectrum of fluctuations in transverse current in degenerate electron plasma.
Plasmon energy divided by Fermi energy is 1.49.
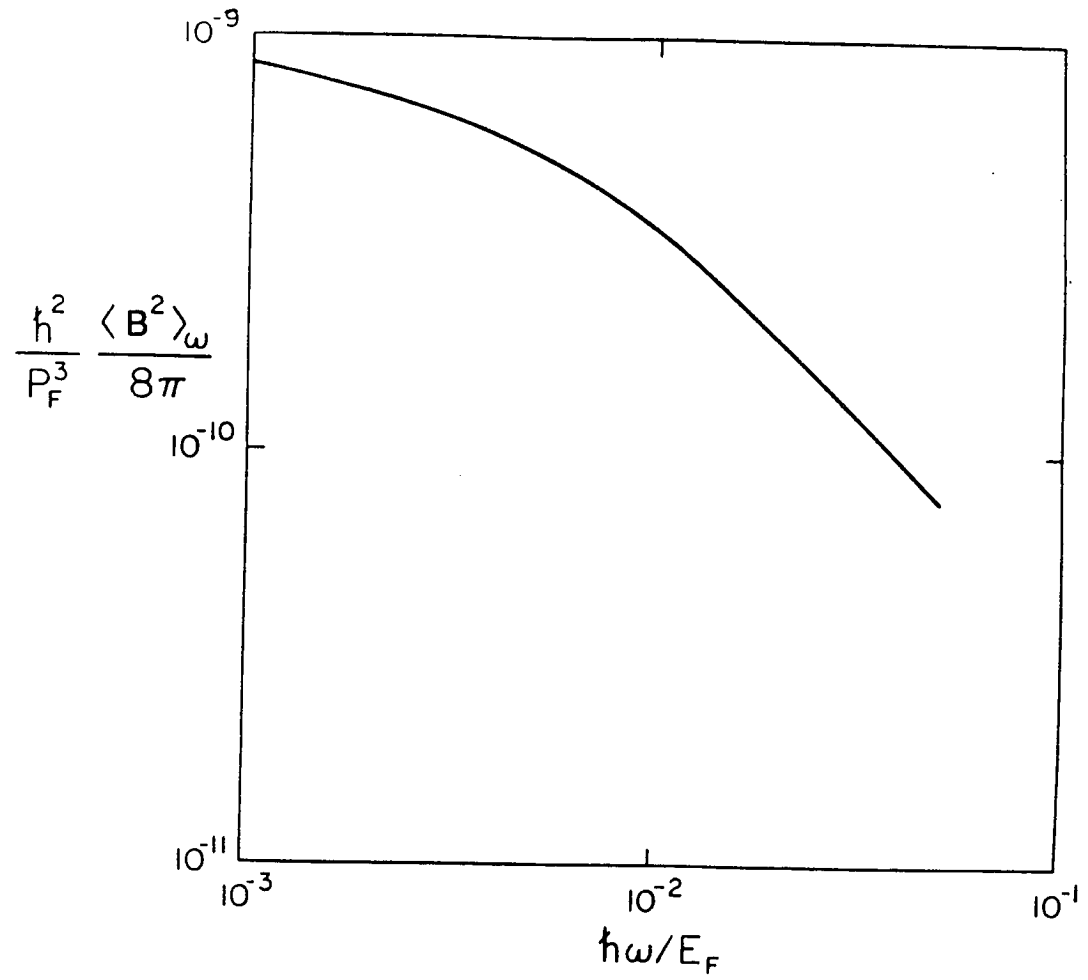
Figure 1.17: Frequency power spectrum of fluctuations in magnetic field in degenerate electron plasma.

Plasmon energy divided by Fermi energy is 1.49.

1.10   Fluctuation Spectra in Semiconductor Plasmas

Before we move on to examine some of the possible consequences of the phenomena we have discussed, we present some preliminary work we have done on fluctuation spectra in semiconductor plasmas. We will begin with magnetic fluctuation spectra and close with voltage fluctuation spectra.

We present the spectra arising from two different models of particle motion. Carrier density in semiconductors is much lower than in metals, so much so that in many cases we can neglect Fermion degeneracy. We therefore revert to classical equations of motion and thermal distributions in this section. We will first model the electrons as being affected by electromagnetic fields and hard collisions with other electrons. We will then model the electrons as being affected by electromagnetic fields and hard collisions with the lattice ions. The two models should give identical results in the limit of infinite collision time but, as will be seen, they give radically different results for finite collision time.

First: hard collisions between electrons. The semiconductor electrons are assumed to lie in a single conduction band, all with a similar effective mass m_e. The equations of motion for electrons and ions respectively are

$$m_e \frac{d\mathbf{v}_e}{dt} = -e\mathbf{E} - \eta m_e \mathbf{v}_e \tag{1.164}$$

$$m_i \frac{d\mathbf{v}_i}{dt} = e\mathbf{E} - \mathbf{F}_{lat} \tag{1.165}$$

where $\mathbf{F}_{lat}$ is a lattice spring force. Specifically, the lattice force acting on the ion n is given by

$$\mathbf{F}_{lat} = K_\perp(\mathbf{x}_{n+1} - 2\mathbf{x}_n + \mathbf{x}_{n-1})$$

where $K_\perp$ is the effective transverse spring constant of the lattice. In the

continuum, long-wavelength limit, the ion equation of motion is written

$$m_i \frac{d^2 \mathbf{x}_i}{dt^2} = e\mathbf{E} + K_\perp a \nabla^2 \mathbf{x}_i, \tag{1.166}$$

where a is a typical value of the lattice constant.

We Fourier transform these equations of motion and combine them with Maxwell's equations, and, again, the fluctuation dissipation theorem, to obtain the magnetic field fluctuation spectrum in $\mathbf{k} - \omega$ space. The result is

$$\frac{\langle B^2 \rangle_{\mathbf{k}\omega}}{8\pi} = T \times \tag{1.167}$$

$$\frac{\eta {\omega_{pe}}^2 c^2 k^2 A^2(k,\omega)}{(\omega(A(k,\omega)(B(k,\omega) - \omega_{pe}^2) - \omega_{pi}^2 \omega^2))^2 + \eta^2 (A(k,\omega)B(k,\omega) - \omega_{pi}^2 \omega^2)^2},$$

where

$$A(k,\omega) = \omega^2 + \frac{K_\perp}{m_i}(2\cos(ak) - 2),$$

$$B(k,\omega) = \omega^2 - c^2 k^2.$$

It should be pointed out that only one independent polarization of $\mathbf{B}$ is contained in this result. Also, since we are dealing with low frequencies here, we have taken the limit of $\hbar \to 0$.

When we integrate this expression to find the frequency spectrum, we find that, as for the classical gaseous plasmas of the preceding sections, we need to introduce a cutoff in k to keep the integral finite. We again choose k_{cut} to be ω_p/c. The frequency spectrum is shown in Fig. 1.18. The parameters chosen were $\eta = 0.1\omega_{pe}$, $a = 0.01c/\omega_{pe}$, $K_\perp = 0.01\omega_{pe}^2$, and $m_i/m_e = 0.001$. At frequencies above $\omega \approx 5 \times 10^{-2}\omega_p$, the spectrum falls off as $\omega^{-1.8}$. This fall-off is slower than that found for the gaseous plasmas. Presumably, then, the magnetic energy contained in the transverse acoustic mode causes the low frequency peak to spread out.
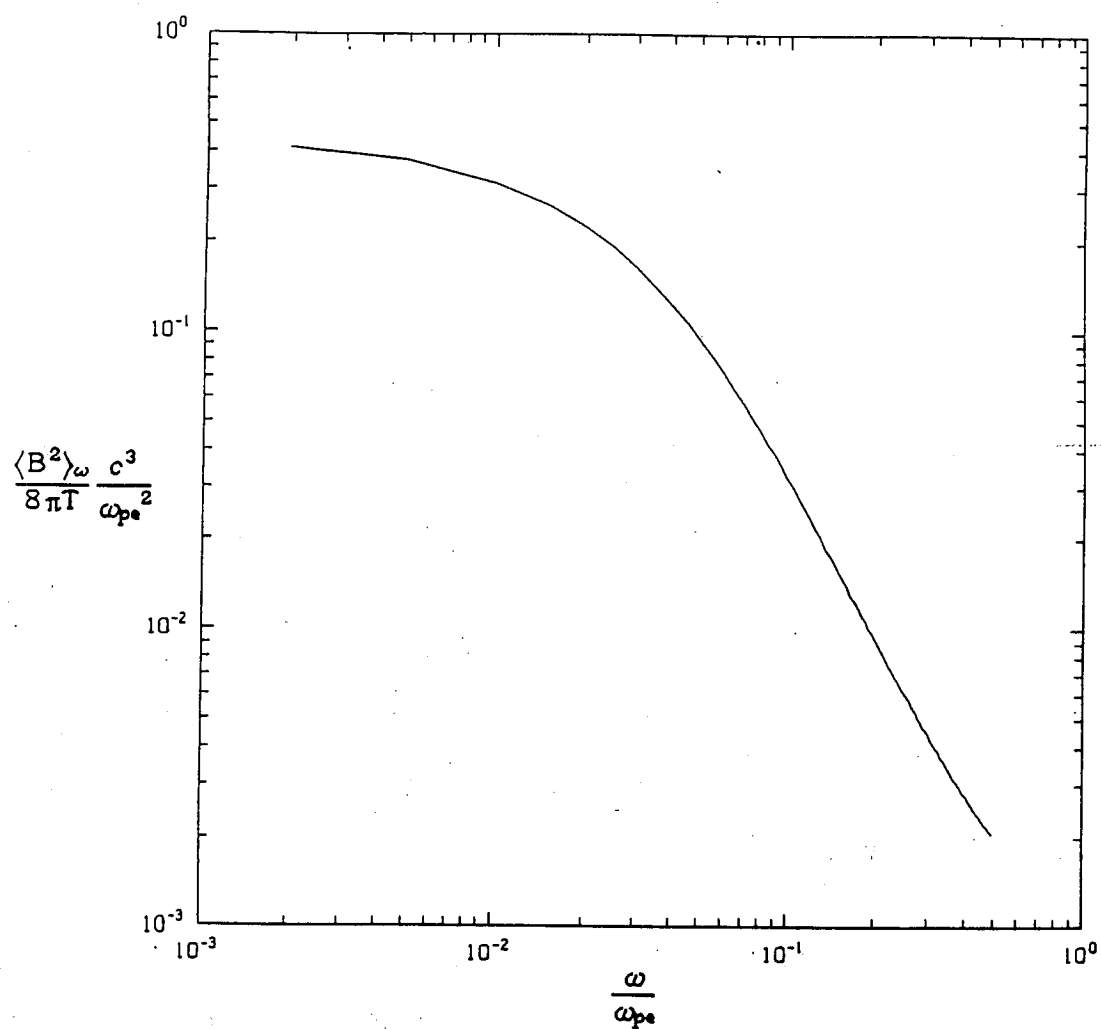
Figure 1.18: $\langle B^2 \rangle_\omega / 8\pi$ in semiconductor plasma. Dominant dissipation mechanism assumed to be collisions between electrons.

Parameters are: $\eta = 0.1\omega_{pe}$, $a = 0.01c/\omega_{pe}$, $K_\perp = 0.01\omega_{pe}^2$, and $m_i/m_e = 0.001$

Now suppose the major dissipating factor in the semiconductor is hard collision between electrons and ions. The equations of motion are now

$$m_e \frac{d\mathbf{v}_e}{dt} = -e\mathbf{E} - \eta m_e(\mathbf{v}_e - \mathbf{v}_i) \qquad (1.168)$$

$$m_i \frac{d\mathbf{v}_i}{dt} = e\mathbf{E} - \mathbf{F}_{lat} - \eta \frac{m_e}{m_i}(\mathbf{v}_i - \mathbf{v}_e). \qquad (1.169)$$

These equations of motion return a fluctuation spectrum of

$$\frac{\langle B^2 \rangle_{\mathbf{k}\omega}}{8\pi} = T \times \qquad (1.170)$$

$$\frac{\eta \omega_{pe}^2 c^2 k^2 (A(k,\omega) + (m_e/m_i)\omega^2)^2}{(\omega(A(k,\omega)(B(k,\omega) - \omega_{pe}^2) - \omega_{pi}^2\omega^2))^2 + \eta^2 B^2(k,\omega)(A(k,\omega) + (m_e/m_i)\omega^2)^2},$$

where $A(k,\omega)$ and $B(k,\omega)$ have the same meanings as above. The frequency spectrum $\langle B^2 \rangle_\omega/8\pi$, obtained by integrating this expression over d^3k, is shown in Fig. 1.19. Parameters are the same as given above. Above $\omega = 0.1\omega_{pe}$, the spectrum decays as $\omega^{(-1.9)}$, close to the decay found above. However, as clearly seen in Fig. 1.19b., the spectrum has an absolute maximum at $\omega \approx 0.001\omega_{pe}$, not at $\omega = 0$. This change in the spectrum's behavior is apparently due to more energy being deposited in the transverse acoustic mode. Clearly, the dominant mode of dissipation can strongly affect the magnetic field spectrum. It should be noted that, in semiconductors, the collision frequency is fairly high, $0.1 - 1.0 \times \omega_{pe}$ so the effects of dissipation here are likely to be higher than in gaseous plasmas.

Lastly, we study electrostatic voltage fluctuations. The electrons are assumed to move under the influence of electromagnetic fields, electron pressure, and hard collisions with ions. The equation of motion is, therefore

$$m_e \frac{dv_e}{dt} = -eE - \frac{\nabla p_e}{n_{0e}} - \eta m_e(v_e - v_i). \qquad (1.171)$$

In the long wavelength limit, the ion equation of motion is

$$m_i \frac{d^2\mathbf{x}_i}{dt^2} = e\mathbf{E} + K_\parallel a \nabla^2 \mathbf{x}_i, \qquad (1.172)$$

where $K_\parallel$ is the longitudinal spring constant. We again bring in Maxwell's equations, Fourier transform, and substitute the value of the longitudinal dielectric $\epsilon_\parallel(k,\omega)$ into the fluctuation-dissipation expression for voltage fluctuations. The resulting spectrum is

$$\langle V^2 \rangle_{\mathbf{k},\omega} = T\frac{8\pi}{k^2} \times \qquad (1.173)$$

$$\frac{\eta \omega_{pe}^2 (C(k,\omega) + (m_e/m_i)D(k,\omega))^2}{C(k,\omega)(D(k,\omega) - \omega_{pe}^2) - \omega_{pi}^2\omega_{pe}^2))^2 + \eta^2\omega^2((m_e/m_i)D(k,\omega) + C(k,\omega))^2},$$

where

$$C(k,\omega) = \omega^2 + \frac{K_\parallel}{m_i}(2\cos(ak) - 2),$$

$$D(k,\omega) = \omega^2 - c_s^2 k^2, \qquad (1.174)$$

c_s being the electron sound speed. This expression is integrated over d^3k to give the voltage frequency spectrum which is displayed in Fig. 1.20. The parameters chosen were: $\eta = 0.1\omega_{pe}$, $c_s = v_e$ (the electron thermal velocity), $a = 0.01 v_e/\omega_{pe}$, $K_\parallel/m_i = 10^{-4}\omega_{pe}$, and $m_e/m_i = 0.001$. Once again, an integration cutoff was necessary; it was chosen as the DeBye length v_e/ω_{pe}. The spectrum drops off sharply above $\omega \approx 0.022\omega_{pe}$. This happens because of the integration cutoff: at higher frequencies, integration does not pick up the contribution to the spectrum from the longitudinal acoustic mode. The very low values of the spectrum at frequencies below $0.004\omega_{pe}$ should be held suspect as this range was problematic for the numerical integrator used to obtain these results. At frequencies above $0.012\omega_{pe}$, the spectrum rises as an exponential

function of frequency: $\langle V^2 \rangle_\omega \sim e^{\alpha \omega}$ with $\alpha \approx 196/\omega_{pe}$. In a typical semiconductor, $\alpha \approx 10^{-11}$sec.

PIC simulations of a semiconductor plasma show clearly the existence of a peak in the magnetic field spectrum at $\omega = 0$. To simulate a semiconductor plasma, the 2D PIC code described in Sec. 1.6 was altered so that ions moved under the influence of nearest neighbor lattice forces, in addition to electromagnetic fields. Two types of simulations were performed: one type using the spring-type lattices forces mentioned above, and the other type using the exponentially decaying forces of the Toda lattice. In the spring force simulations, the dispersion relations of electromagnetic plasma waves compared very well with the predictions of linear theory. In the Toda force simulations, we were able to achieve soliton motion which compared very well with that predicted by Toda. The fluctuation spectra returned by the two types of simulations were very similar at thermal equilibrium. Shown in Fig. 1.21 is the frequency spectrum of the $(1,0)$ mode (i.e. $\mathbf{k} = (2\pi/L_x, 0)$, L_x being the length of the computational area in the x-direction) of the B_y oscillations. A peak at $\omega = 0$ is clearly seen. The two flanking peaks are electromagnetic plasma waves. All other modes $(k_x, 0)$ showed similar peaks at $omega = 0$. The relative magnitudes of the plasma wave peaks and $\omega = 0$ peaks were all similar that shown in Fig. 1.21.

1.11   Cosmological Implications

We have discovered in the previous sections that electromagnetic waves in the primordial plasma fall into two categories: one with large wavelengths ($k \lesssim \omega_{pe}c$) and nearly zero frequency ($\omega \ll \omega_{pe}$) and one with small wavelengths ($k \gg \omega_{pe}/c$) and frequency greater than ω_{pe}. Those modes with

$k \gtrsim \omega_p/c$ are not significantly modified by the presence of the plasma ('hard photon'), while those with $k \ll \omega_p/c$ are significantly modified ('soft or plastic photon') (Tajima, 1985). It is those 'plastic photons' or their magnetic fields that we are interested in, as they can have more 'magnetic' fields in nature and can leave possible structural imprints on the primordial plasma. The strength of magnetic fluctuations $\langle B^2 \rangle_\lambda /8\pi$, whose wavelengths are longer than λ, is given by $\langle B^2 \rangle_\lambda /8\pi = (T/2)(4\pi/3)\lambda^{-3}$. For $\lambda_p = 2\pi c/\omega_p$,

$$\sqrt{\langle B^2 \rangle_{\lambda_p}} = 1.4 \times 10^{-12}(n/10^4 \text{ cc})^{3/4}(T/10^4 \text{K})^{1/2} \text{ Gauss} . \tag{1.175}$$

We might be interested in global magnetic fields whose wavelengths at the beginning of the plasma epoch are 10^{14} cm or longer, which correspond to the length of the present galaxies. In this case $\sqrt{\langle B^2 \rangle_\lambda} = 4 \times 10^{-24}$ Gauss in the absence of dynamo actions and coalescence of magnetic structures. In Fig. 1.25 we plot the fluctuating magnetic field strength vs. the wavelength. (Note that the magnetic fields due to thermal fluctuations according to the present calculations are $\sim 10^{-3}$ G, $\sim 10^{-15}$ G, and $\sim 10^4$ G for the solar photosphere plasma, interstellar clouds, and the solar center, respectively, which are all physically negligible.) Note, however, that the cosmological plasma, comparatively speaking, has strong magnetic field fluctuations because of its high temperature.

According to the standard big bang theory (e.g., Misner *et al.*, 1970), the cosmic expansion in the plasma epoch is characterized by the scale factor $a = a(t) = a_0(t/t_0)^{1/2}$, where a_0 and t_0 are the scale factor and the time at present. On the other hand, after magnetic fields detach from the plasma and photons $\delta B \propto t^{-1}$ due to the flux conservation. We now express all physical quantities in terms of the scale factor a and the wavelength λ. The particle

density of background matter n is related to a as $n = n_0(a/a_0)^{-3}$, where $n_0 = 10^{-6}\,\mathrm{cm}^{-3}$ at $t = t_0$. The collisionless skin depth $\lambda_p = 3.3 \times 10^9 (a/a_0)^{3/2}\,\mathrm{cm}$ and the temperature of the Universe $T = T_0(a/a_0)^{-1}$, where $T_0 = 2.7K$. From these relationships we obtain

$$B_\lambda \equiv \sqrt{\langle B^2 \rangle_\lambda} = 9.4 \times 10^{-7} \left(\frac{a}{a_0}\right)^{-1/2} \left(\frac{\lambda}{1\,\mathrm{cm}}\right)^{-3/2} \mathrm{Gauss} , \quad (1.176)$$

and

$$B_{\lambda_p} = 10^{-21}(a/a_0)^{-11/4}\mathrm{Gauss} . \tag{1.177}$$

These results are shown in Fig. 1.25, where we see that the cosmic expansion dilutes the primordial magnetic fluctuations so much that the remnant field strength is quite small if we start with mere thermal fluctuations and do not incorporate any other physical processes such as the dynamo process and the coalescence process [30]. It is noted, however, that these fluctuations based on the thermal equilibria are the least we can expect and can act as seed fields for possible dynamo action. If this takes place, the plasma β would decrease in time. The field magnitudes could be higher if some additional turbulence or primordial fluctuations are present [31]. These are clearly important but beyond the scope of the present paper.

In Table 1.2 we summarize our results. Including the physical quantities we already discussed, we survey physical quantities of importance that characterize the radiation epoch (or the plasma epoch). The scaling of density and temperature have been noted above. The frequency of the maximum intensity of the black-body radiation is $\omega_{\max} = 2.81\,T/\hbar$. It scales with temperature: $\omega_{\max} \sim a^{-1}$. It follows that the plasma frequency scales as $\omega_{pe} \propto n^{1/2} \propto a^{-3/2}$. The electron collision frequency changes as $\eta_e \propto n\,T^{-3/2} \propto a^{-3/2}$. The plasma parameter (and the collisionality) is therefore $g = (n\lambda_{De}^3)^{-1} \cong \eta_e/\omega_{pe} \propto a^0$

(independent of a) and thus invariant during the epoch in which the numbers of constituent particles are conserved; e.g. during $t = 10^{-2} - 10^0 \sec$ $g \sim 10^{-3}$ (invariant) and it changes around $t = 10^0 \sec$ as positrons annihilate with electrons to $g \sim 10^{-7}$ and stays invariant till the recombination. On the other hand, the collision frequency between electrons and photons may be given from the Thompson cross-section or in relativistic cases from the Klein-Nishina cross-section to be $\nu_{\mathrm{TH}} \propto n\,T^{1/2} \propto a^{-7/2}$ and $\nu_{\mathrm{KN}} \propto n\,T^{-1} \propto a^{-2}$, respectively. The Reynolds number R_e is Lv/μ, where L, v, and μ are the typical sizes of the length, velocity, and viscosity. By taking v to be the thermal velocity, Lv/μ scales as $L\,a^{-1}$ and if we take L as the horizon size ct, $R_e \propto t^{1/2}$ in the radiation epoch.

The magnetic energy $\langle B^2 \rangle_\omega^{bb}\, d\omega$ contained in the black-body radiation around $\omega_{\max}$ is proportional to $\omega_{\max}^2$ so $\langle B^2 \rangle_\omega^{bb} \propto T^3 \propto a^{-3}$. On the other hand, the zero frequency magnetic fluctuation energy $\langle B^2 \rangle_{\omega \to 0} \propto T\,\omega_p^3/\eta \propto a^{-4}$. Thus the ratio of the energy in $\omega = 0$ to the black-body energy in $\omega = omega_{\mathbf{max}}$ is proportional to a^{-1}. If we assume here that the energy of nearly static magnetic field is given by $\langle B^2 \rangle^0 /8\pi = T(\omega_p/c)^3$ at each instant of time after ω integration, the plasma beta scales as $\beta = \dfrac{nT}{\langle B^2 \rangle^0 /8\pi} \propto n(c/\omega_p)^3 \propto a^{3/2}$. This is based on the instantaneous adjustment of the magnetic fields to the level of thermal energy of the Universe. It should be noted that nevertheless this result of $\beta \propto a^{3/2}$ differs from the earlier discussion of the magnetic field scaling when the magnetic flux conservation was invoked. Most likely, $\beta \propto a^{3/2}$ until a certain time t_d, when magnetic fields detach from plasma and thereon $\beta \propto a^0$ in the absence of dynamo action.

The significance of the presence of static (or nearly zero frequency) magnetic fields in the cosmological plasma may be appreciated in the following.

Two main scenarios [32] have been considered for primordial fluctuations, adiabatic fluctuations and isothermal fluctuations. The adiabatic (or isentropic) fluctuations are like those accompanied by ordinary sound waves and a cartoon illustration of this situation is displayed in Fig. 1.26(a). In such fluctuations the density of matter (electrons, positrons, and protons [and helium ions] for the case of the early radiation epoch) is accompanied by that of photons, as indicated in Fig. 1.26(a). Therefore, after electrons and positrons annihilate around $t = 1$ sec or after electrons and ions recombine around $t = 10^{13}$ sec, the imprint of matter fluctuations would remain in photon fluctuations as a fossil of the primordial plasma structure. Thus the background microwave spectra would show a certain fluctuation or anisotropy/inhomogeneity on top of the black-body spectra. This would be a contradiction to the latest observations by COBE *etc.* [33,34].

On the other hand, imagine that as we have shown, there exist static magnetic fields in the primordial plasma. Charged particles in the early radiation epoch ($t \lesssim 1$ sec) or in the late radiation epoch ($t \lesssim 10^{13}$ sec) readily respond to these magnetic fields. Charged particle matter is concentrated into regions of lower magnetic field strength and vacated from regions of higher magnetic field strength, in such a way as to keep the total pressure, that is, $p_{\text{therm}} + B^2/8\pi$, spatially constant. Now on top of this, photons are present. Photons do couple strongly with charged particles but not as strongly as static magnetic fields do with charged particles. Furthermore, photons are less strongly coupled with magnetic fields. This should leave a landscape of fluctuations in such a way that the sum of the magnetic and charged particle pressure is constant in space, while the photon pressure remains nearly constant in space, although it may slightly anticorrelate with the magnetic pressure (or slightly correlate with the charged particle pressure). Such fluctuations are

similar to the second category of isothermal fluctuations [37], (but they can be isentropic at the same time), as they are nearly frequencyless.

Although there may remain a certain residual photon fluctuation incurred by the isothermal matter fluctuations sustained by the zero frequency magnetic fields according to our findings, the level of photon fluctuations reflected in the bulk of microwave black-body radiation spectra is practically undetectably miniscule. The reason for this is two-fold. First, after positron annihilation ($t = 1$ sec) photons are overwhelmingly abundant over charged particles by some 10^8 and thus even the possible photon fluctuations incurred by the matter fluctuations is diluted by 10^8 in terms of the relative fluctuations strength. Second, the magnetic fluctuations are in the far low end of the frequency of the electromagnetic fluctuations (see Fig. 1.2). Thus when we inspect the present day microwave background frequency spectra, it would be difficult to detect the imprint of magnetic fluctuations on its main bulk.

Questions remain to be tackled to see if fluctuations (see the corresponding plasma β in Table 1.2) may be sufficient to cause the needed matter fluctuation of $10^{-3} - 10^{-4}$ [32] for galaxy formation. Of course, we have to wait for a conclusion until a thorough treatments of dynamo action and evolutionary calculations on coalescence of magnetic and plasma structures during the radiation epoch are carried out in order to have a more definite answer.

1.12 Other Applications

The present theory indicates that the amount of low frequency magnetic fluctuations in a plasma, Eq. (1.51), is proportional to the temperature T and density of the plasma to the three halves power $n^{3/2}$. Thus the higher the density and/or temperature, the greater these fluctuations are. More sig-

	$t = 10^{-2}$	$t = 1$	$t = 10^{13}$	$t = 3 \times 10^{17}\text{sec}$
T eV	10^7	10^6	0.4	$T_\gamma = 0.0003$
n cm^{-3}	5×10^{34}	4×10^{31}	10^3	10^{-6}
L_{hor} cm	10^8	10^{10}	10^{23}	10^{28}
B G	10^{16}	10^{13}	10^{-12}	
$\frac{\langle B^2 \rangle^0}{\langle B^2 \rangle^{bb}}$	0.1-1	10^{-2}	10^{-25}	
β	1	$10 - 10^2$	10^{15}	
R_e	10^{17}	10^{18}	10^{15}	

Table 1.2: Some characteristic parameters of the early Universe, with calculated values of zero-frequency magnetic fields.
Temperature T, electron density n, horizon size L_{hor}, typical magnetic field at zero-frequency B, ratio of zero-frequency energy to blackbody magnetic field energy, plasma β and maximum Reynolds number $R - e$ are tabulated. No attempt has been made to include dynamo effects in the calculation of the magnetic field strengths. The table is not completed since the Universe is not an equilibrium plasma at $t = 3 \times 10^{17}$ sec.

nificant examples may be found, therefore, in high n and/or T plasmas. Two examples are discussed here.

1.12.1   Electron Density Fluctuations in Gaseous Plasmas

In addition to calculating the magnetic field spectrum, we have elsewhere [33] calculated the longitudinal ion density fluctuation spectrum arising from ion acoustic waves in a fluid plasma. We find a fluctuation spectrum given by

$$\langle \delta n_i^2 \rangle_{\mathbf{k}\omega} = \frac{\hbar\omega}{e^{\hbar\omega/T} - 1} \cdot \frac{\eta\omega_{pi}^2}{2\pi e^2} \left(1 + \frac{k_D^2}{k^2}\right)^2 \frac{k^2}{[\omega^2(1 + \frac{k_D^2}{k^2}) - \omega_{pi}^2]^2 + \eta^2\omega^2(1 + \frac{k_D^2}{k^2})^2},$$

where k_D is the Debye wavenumber. This spectrum is plotted as a function of frequency at $k = 0.1 \times k_D$, for a hydrogen plasma of temperature $T = 100\text{eV}$ and density $n = 10^{16}\text{cm}^{-3}$ in Fig. 1.27(a). The spectrum peaks around the ion acoustic frequency of the given wavenumber. It should be noted that in an ion

plasma, mass density is nearly proportional to ion density, therefore the ion density spectrum automatically gives the mass density spectrum as well.

Zhang and DeSilva [34] have included more elaborate dissipation effects by way of the Braginskii transport equations (a set of two-fluid equations accounting for inter- and intra- species collisions, electron and ion thermal conductivity, electron and ion viscosity, and longitudinal electric fields). They have calculated and measured the low-frequency electron density fluctuation spectrum in an Ar plasma. Fig. 1.27(b) shows the result for $\langle \delta n_e^2 \rangle_{k\omega}$ as a function of frequency at $k = 415 \mathrm{cm}^{-1}$, based on their theoretical treatment. The spectrum shown has been generated using the transport coefficients for an Ar plasma that Zhang and DeSilva derived from their experimental studies. In addition to the ion acoustic peak, there is a strong peak at $\omega = 0$. Its existence was confirmed experimentally by Zhang and DeSilva. Their work shows that in a plasma where thermal conductivity and viscosity are important, fluctuations can be sustained in particle density as well as in magnetic field. In addition to Zhang and DeSilva's work, Stenzel's work on magnetic fluctuations [35] may have bearing on the present theory.

It may be of interest to measure particle transport in a plasma sustaining such magnetic fluctuations. Trace particles may be followed in an experiment. Some theoretical treatment in such a direction has been laid-out recently [36].

1.12.2   Anomalous Spin Relaxation in Condensed Matter.

Another example of high n "plasma" is electrons or other matter in a condensed state. When one tries to cool a metal below 10's of m°K by the standard nuclear adiabatic demagnetization cryostat technique, the spins

of metallic electrons are manipulated from external magnets. The standard Korringa theory [37] predicts that the spin equilibration time τ is inversely proportional to the temperature T of electrons. However, experiments [38] usually show an anomalous decrease in the product $T\tau$. A similar phenomenon was first observed in the spin equilibration time anomaly in liquid He^3 in the superfluid phase by Avenel et al. [39]. Although this anomaly is not well understood at present, it is typically explained by resorting to impurity scattering. We suggest that it may be possible to explain the phenomenon of anomalously rapid relaxation by spontaneous magnetic fluctuations in the condensed matter as discussed in Sec. 9, and the interactions between these fields and particle spins.

In addition to these three examples, the present methods may eventually be found useful to tackle tough problems that have resisted full resolution to date, such as the $1/f$ noise [40] and the fluctuations in a (stable) nonuniform plasma (e.g. a certain type of stellarator plasma).
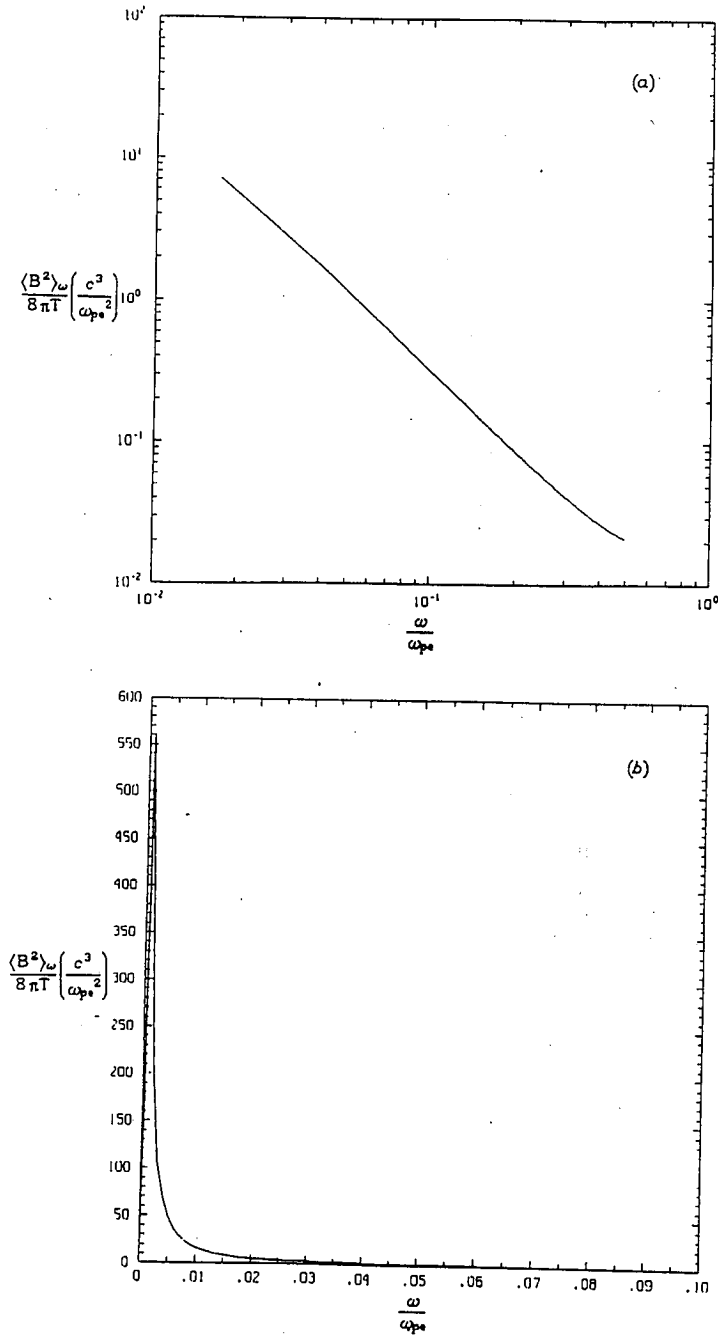
Figure 1.19: $\langle B^2 \rangle_\omega / 8\pi$ in semiconductor plasma. Dominant dissipation mechanism is assumed to be collisions of electrons with ions.
Parameters are: $\eta = 0.1\omega_{pe}$, $a = 0.01c/\omega_{pe}$, $K_\perp = 0.01\omega_{pe}^2$, and $m_i/m_e = 0.001$
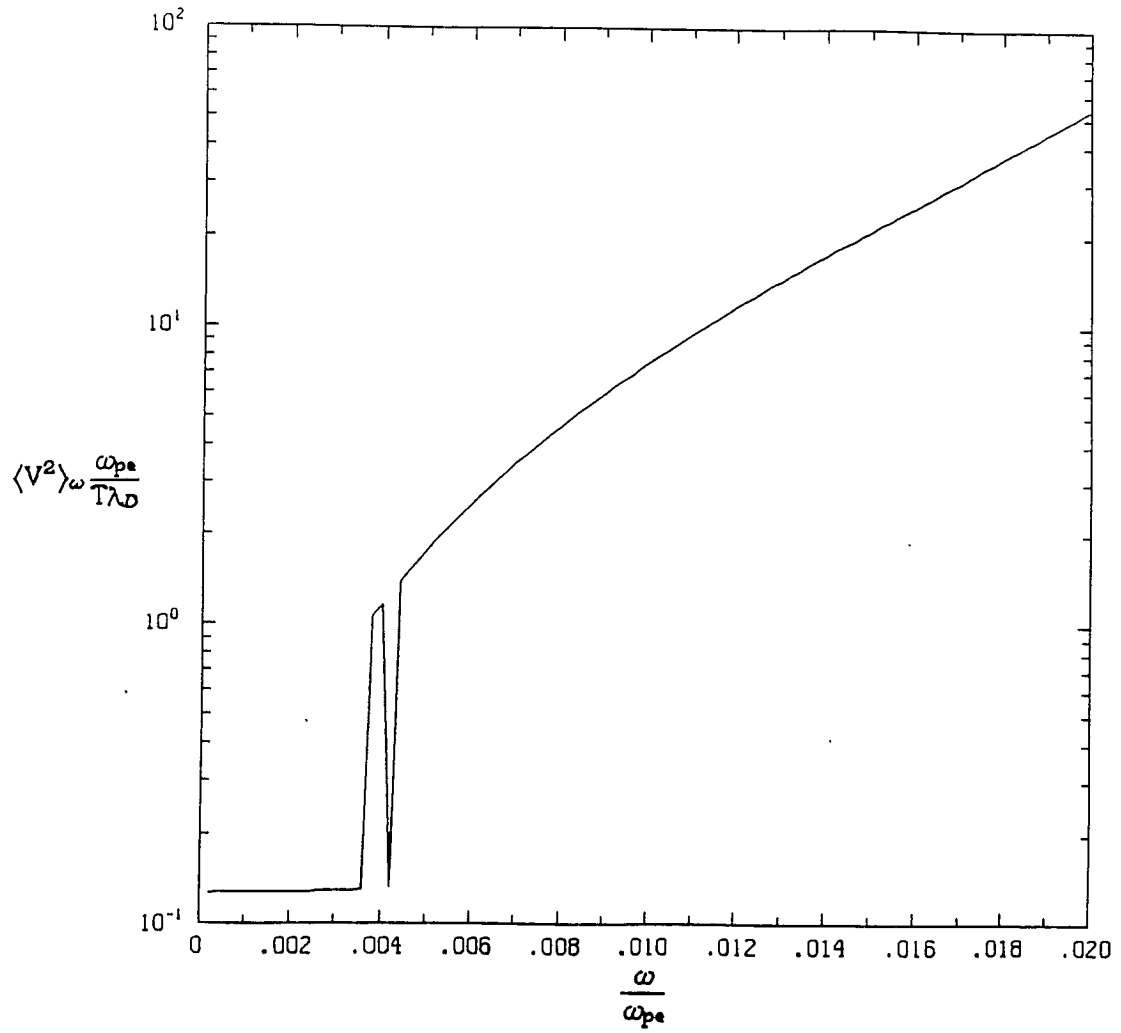
Figure 1.20: $\langle V^2 \rangle_\omega$ in semiconductor plasma.

Dominant dissipation mechanism is assumed to be collisions between electrons and ions. Parameters are: $\eta = 0.1\omega_{pe}$, $c_s = v_e$, $a = 0.01v_e/\omega_{pe}$, $K_\parallel/m_i = 10^{-4}\omega_{pe}$, and $m_e/m_i = 0.001$.
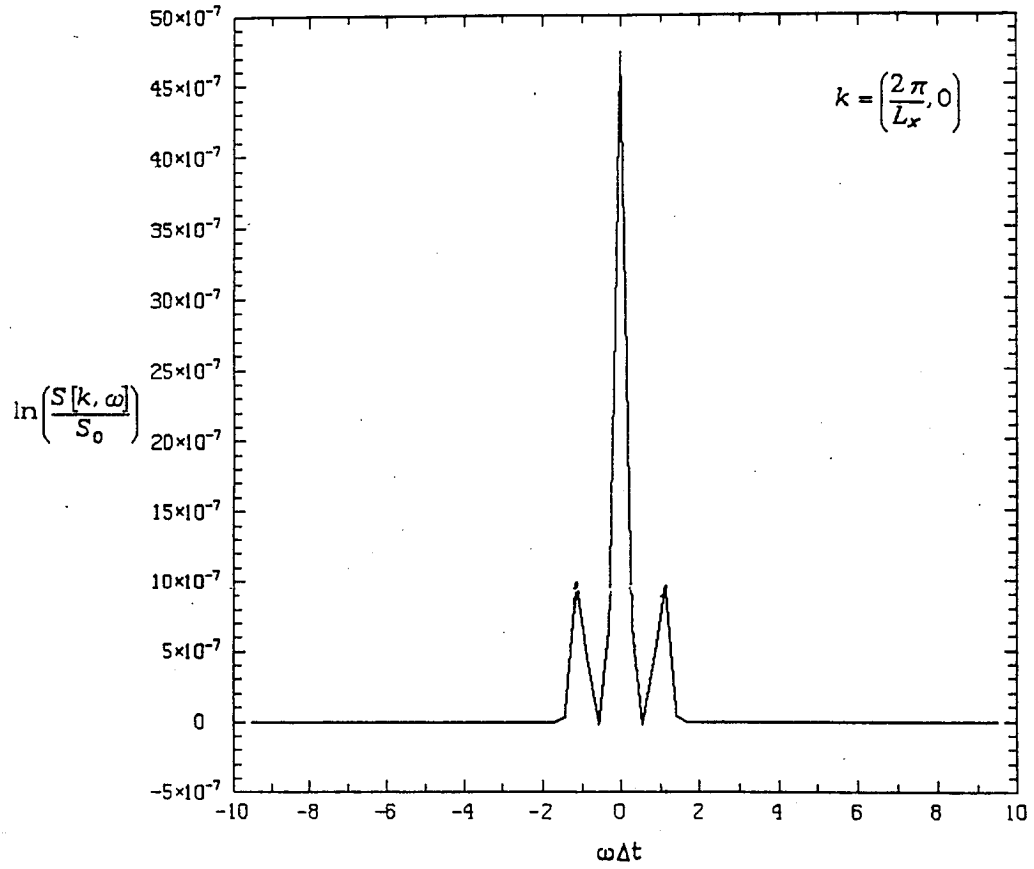
Figure 1.21: Frequency spectrum of (1,0) mode of B_y oscillations from PIC simulation of semiconductor plasma. $\omega = 0$ peak is clearly visible.
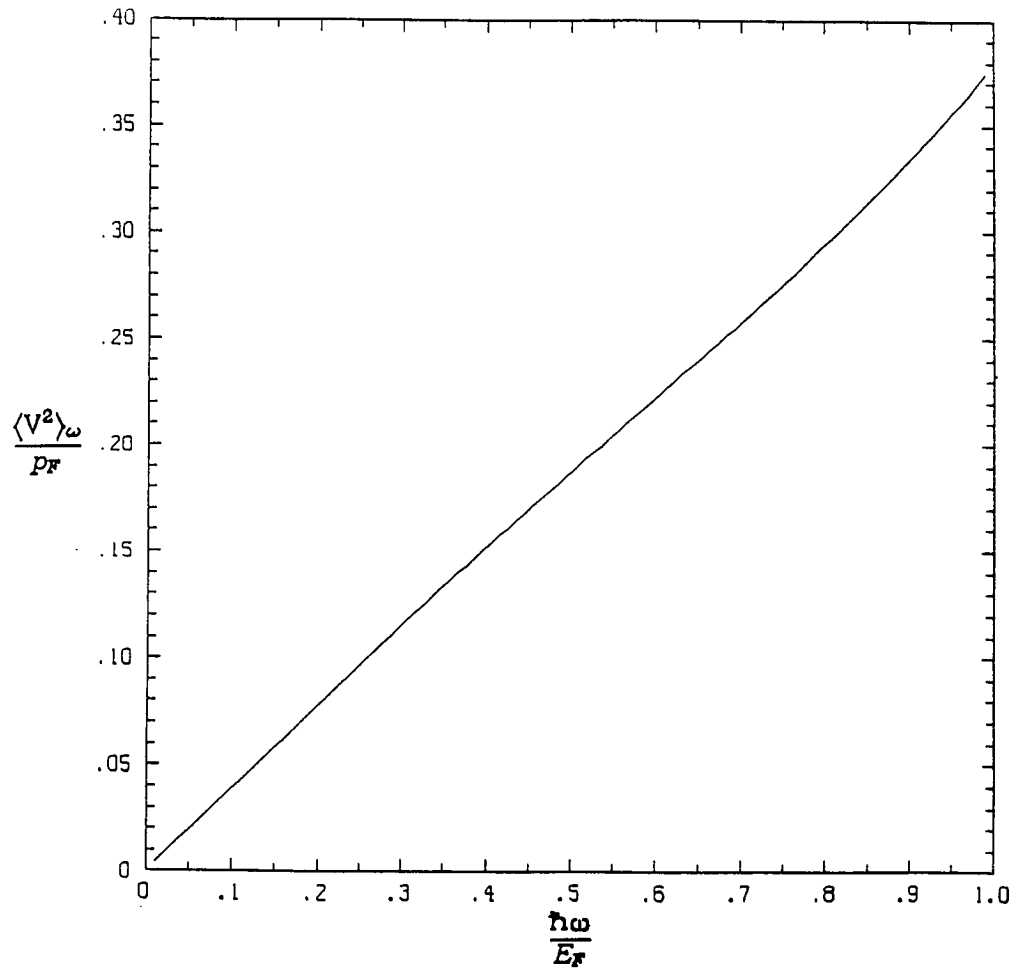
Figure 1.22: Voltage flucutation spectrum $\langle V \rangle - \omega$ for degenerate electron plasma. Plasmon to Fermi energy ratio is 1.52; drift velocity is $2.82 \times 10^{-6} v_F$.
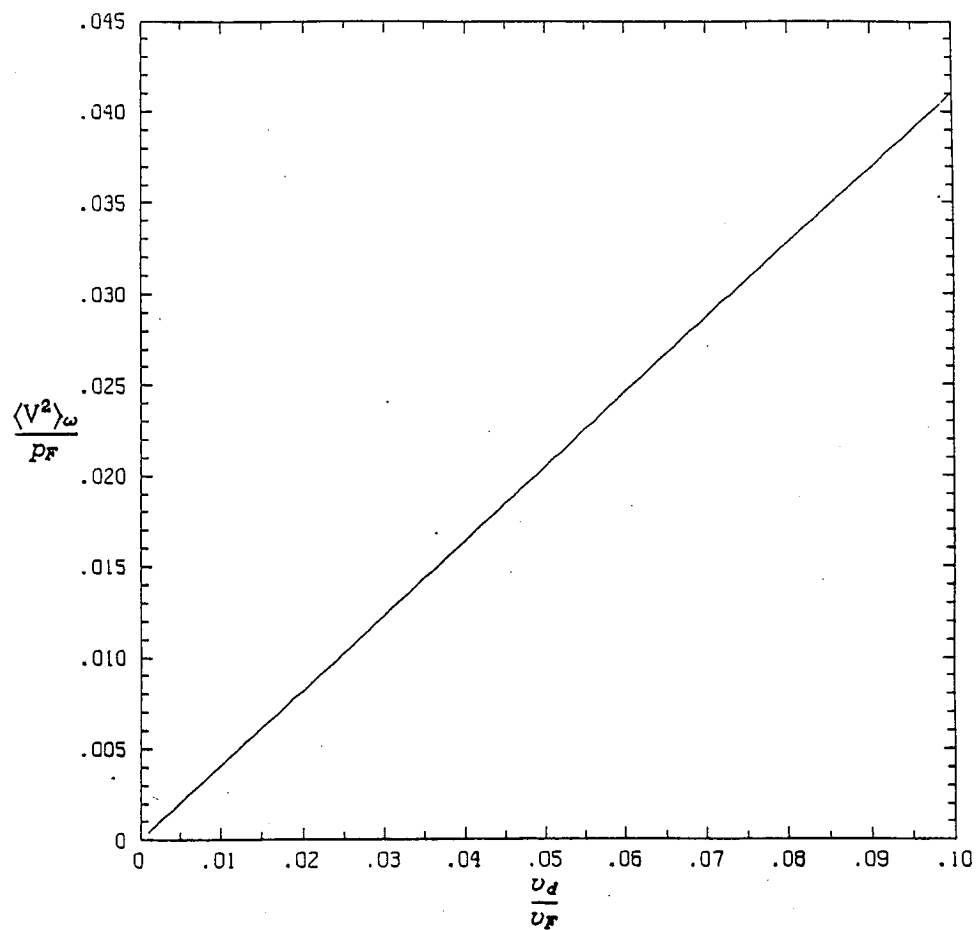
Figure 1.23: Low frequency white noise voltage spectrum magnitude *vs.* drift velocity. Plasmon to Fermi energy is 1.52.
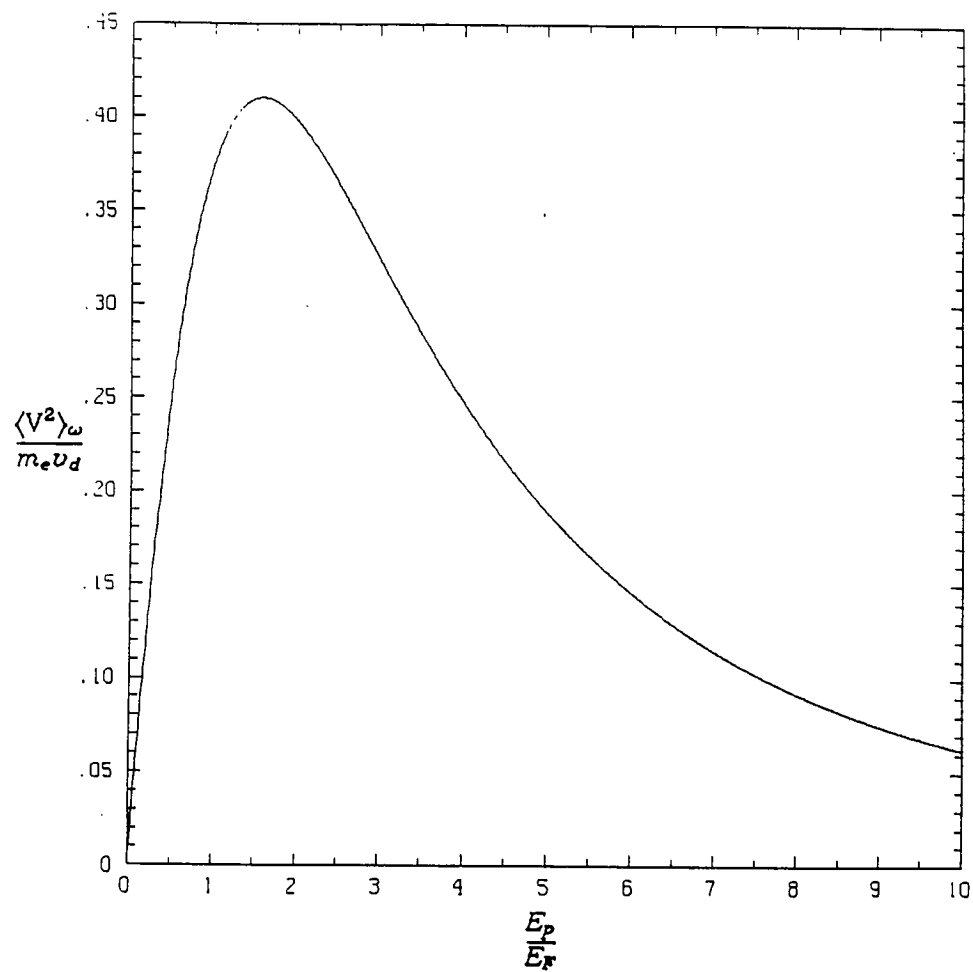
Figure 1.24: Constant of proportionality, α, between voltage white noise and drift velocity *vs.* plasmon to Fermi energy ratio r_E.
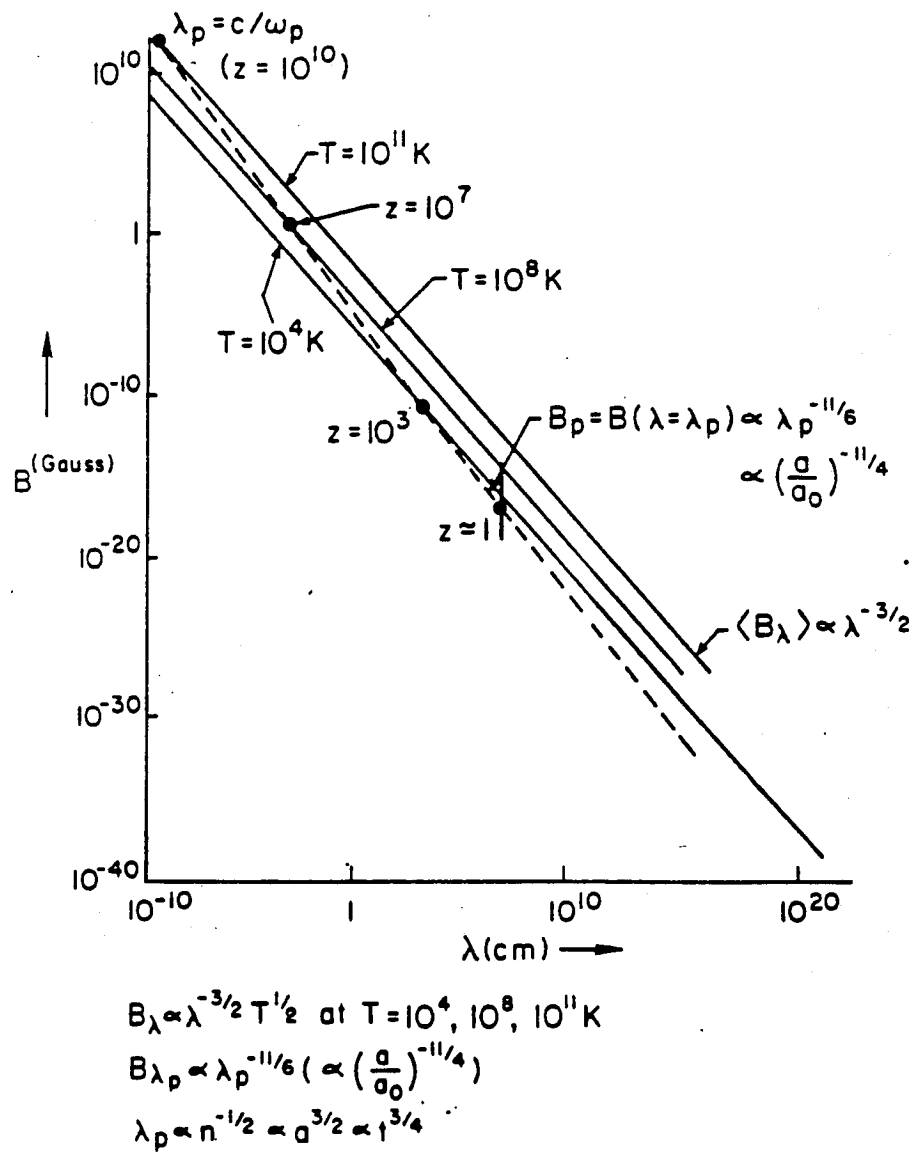
Figure 1.25: Magnetic fluctuations of spatial scale size (*i.e.* wavelength) λ. Three different epochs plotted: $T = 10^{11}, 10^8, 10^{4\circ} K$. Dotted line is from Eq. (1.66).
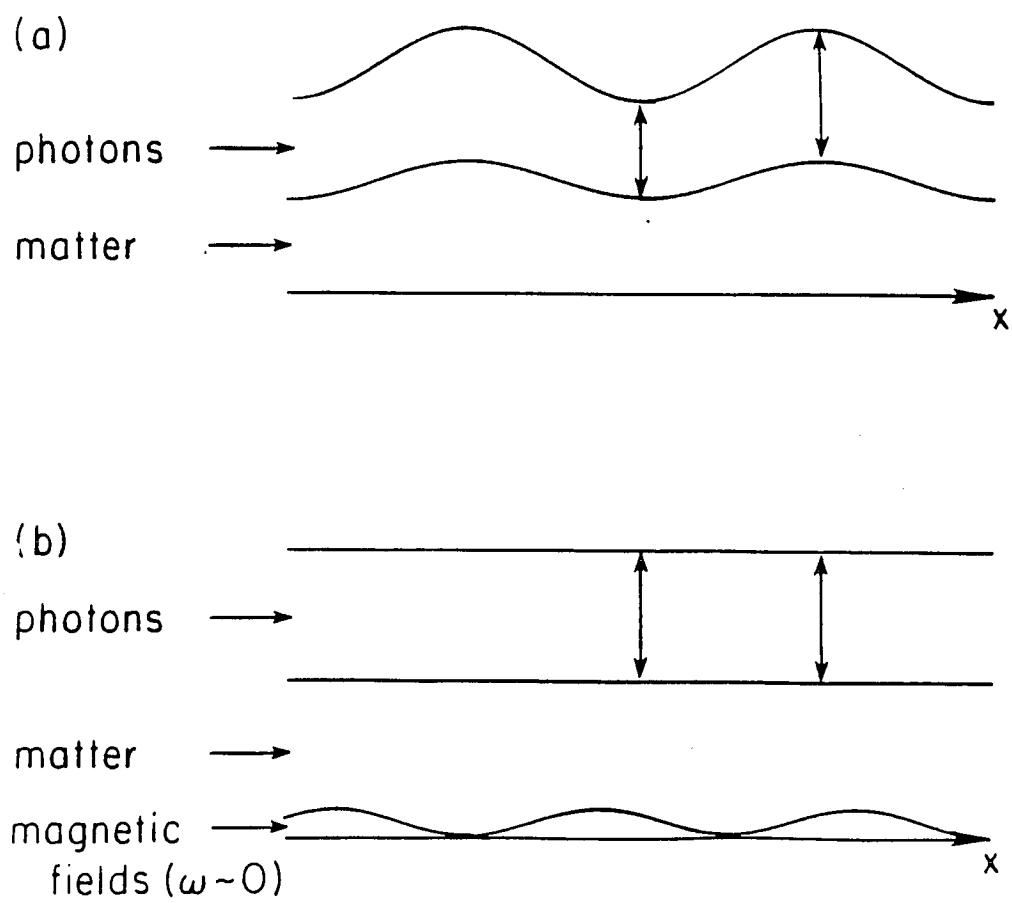
Figure 1.26: Cartoon illustration of zero-frequency magnetic fields and their influence on the plasma.
a) Adiabatically induced fluctuations without magnetic fields.
b) Fluctuations induced by inhomogeneous zero-frequency magnetic fields.
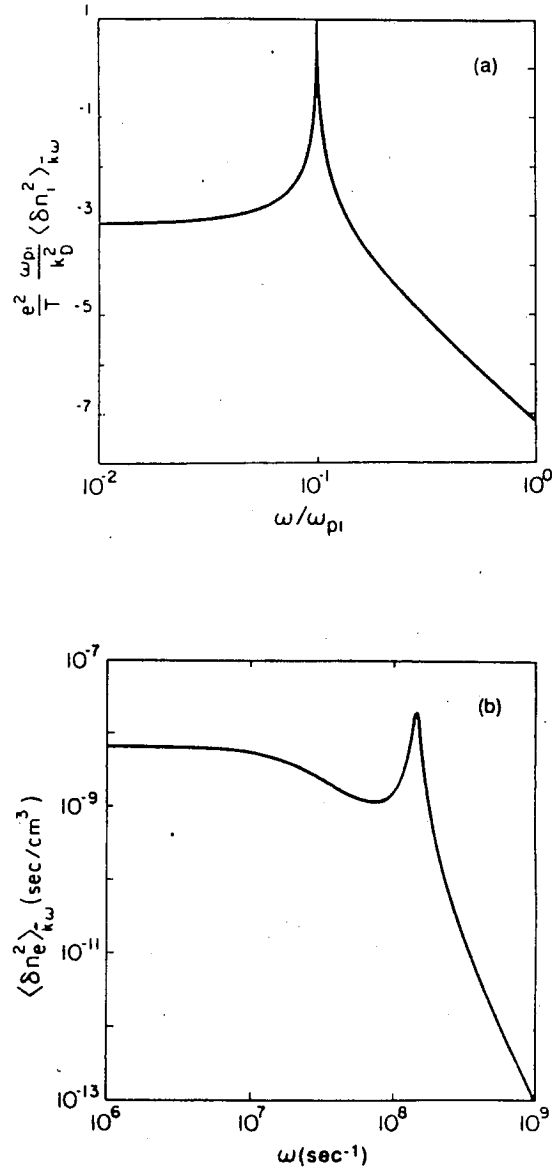
Figure 1.27: Density fluctuation power spectra in a gaseous plasmas.

a) Ion fluctuation power spectrum $\langle \delta n_i \rangle_{k\omega}$ as a function of frequency at $k = .1k_D$.

b) Electron density flucutation power spectrum after Zhang and DeSilva [23]. $\langle \delta n_e^2 \rangle_{k\omega}$ as a function of ω at $k = 415 \text{cm}^{-1}$.

Chapter 2

Numerical Simulations of the Rayleigh-Taylor Instability

2.1 The Rayleigh-Taylor Instability in Expanding Fluids

2.1.1 Introduction

Many physical fluid systems of interest undergo overall expansion or contraction. Examples include inertial confinement fusion targets [41,42,43], supernovae [44,45], the plasma of the early Universe [46], Z-pinch plasmas undergoing Felber oscillations [47], and, probably, D-T ice crystals in muon-catalyzed fusion reactors [48]. It is to be expected that such global motion will affect the character of many fluid processes such as the propagation of waves and the growth of instabilities.

In this paper, we concern ourselves with the effect of homogeneous expansion on the Rayleigh-Taylor (RT) instability. This topic has been addressed for several particular systems. A perusal of the literature will show that expansion has a slowing effect on the instability: the instability growth, relative to the (growing) size of the fluid system, is sub-exponential. This is to be expected since the quantities driving the instability, namely the gradients in pressure and in the magnetic field strength, are depleted by the expansion.

We present two new analytical studies of expanding fluid systems undergoing RT unstable motion. In both of these systems, we find sub-exponential relative growth of the instability. We also present a numerical algorithm for sim-

ulating expanding (and contracting) fluid systems. Simulation results obtained with this algorithm show a marked retardation of the growth of a Rayleigh-Taylor instability in an expanding fluid.

2.1.2 Analytical Studies of RT Instabilities in Expanding Fluids

2.1.3 Incompressible Flow

We look first at expansion in an R-T unstable, two-fluid, incompressible system. We take gravity to be in the y direction. The fluid interface lies in the x-z plane ($y = 0$). Zero-order motion in the z direction is given by

$$v_{z0} = \frac{\dot{a}(t)}{a(t)} z \ .$$

To satisfy incompressibility, v_{x0} and v_{y0} can be taken to be

$$v_{x0} = -\alpha \frac{\dot{a}(t)}{a(t)} x \quad ; \quad v_{y0} = (\alpha - 1) \frac{\dot{a}(t)}{a(t)} y$$

where α is a constant.

We assume that $\rho_0 = \rho_0(y)$. Solution of the zero-order momentum equation shows

$$p_0(x, y, z, t) = -\int_0^x \rho_0(y)(-\alpha x) \left(\partial_t \left(\frac{\dot{a}}{a} \right) - \alpha \left(\frac{\dot{a}}{a} \right)^2 \right) dx$$

$$- \int_0^y \left[\rho_0(y)(\alpha - 1)y \left(\partial_t \left(\frac{\dot{a}}{a} \right) + (\alpha - 1) \left(\frac{\dot{a}}{a} \right)^2 \right) + \rho_0(y)g \right] dy$$

$$- \int_0^z \rho_0(y) \left(\partial_t \left(\frac{\dot{a}}{a} \right) + \left(\frac{\dot{a}}{a} \right)^2 \right) dz + p_0(0, 0, 0, t) \ .$$

With this in mind, we perturb the fluid velocity field with $\delta \mathbf{v} = \delta v_x \hat{x} + \delta v_y \hat{y}$ and linearize the equations of motion:

$$\partial_t \delta \rho + (\alpha - 1) \frac{\dot{a}}{a} y \, \delta \rho - \alpha \frac{\dot{a}}{a} x \partial_x \, \delta \rho + \delta v_y \, \partial_y \rho_0 = 0 \quad (2.1)$$

$$\rho_0 \left(\partial_t\, \delta v_x - \alpha\, \frac{\dot a}{a}\, x\, \partial_x\, \delta v_x + (\alpha - 1)\, \frac{\dot a}{a}\, y\, \partial_y\, \delta v_x - \alpha\, \frac{\dot a}{a}\, \delta v_x \right)$$

$$+ \left(\alpha^2 \left(\frac{\dot a}{a} \right)^2 - \alpha\, \partial_t \left(\frac{\dot a}{a} \right) \right) x\, \delta\rho + \partial_x\, \delta p = 0 \quad (2.2)$$

$$\rho_0 \left(\partial_t\, \delta v_y - \alpha\, \frac{\dot a}{a}\, x\, \partial_x\, \delta v_y + (\alpha - 1)\, \frac{\dot a}{a}\, y\, \partial_y\, \delta v_y + (\alpha - 1)\, \frac{\dot a}{a}\, \delta v_y \right)$$

$$+ \left((\alpha - 1)^2 \left(\frac{\dot a}{a} \right)^2 + (\alpha - 1)\partial_t \left(\frac{\dot a}{a} \right) \right) y\, \delta\rho + \partial_y\, \delta p + g\delta\rho = 0 \quad (2.3)$$

$$\partial_x\, \delta v_x + \partial_y\, \delta v_y = 0 \quad (2.4)$$

where Eq.(2.1) is the mass conservation equation, Eq.(2.2) is the x momentum equation, Eq.(2.3) is the y momentum equation, and Eq. (2.4) is the equation of state.

To solve this system, we first eliminate δv_x from equation Eq.(2.2). This is accomplished by substituting from Eq.(2.4), then operating on the resulting equation with ∂_x, then substituting Eq.(2.4) again. The result is

$$\rho_0 \left(-\partial_t\, \partial_y\, \delta v_y + \alpha\, \frac{\dot a}{a}\, \partial_x \left(x\, \partial_y\, \delta v_0 \right) \right) - (\alpha - 1)\, \frac{\dot a}{a}\, y\, p_y^2\, \delta v_y + \alpha\, \frac{\dot a}{a}\, \partial_y\, \delta v_y$$

$$+ \partial_x \left(\delta\rho\, h(\alpha, x, a) \right) + \partial_x^2\, \delta p \quad (2.5)$$

where $h(\alpha, x, a) = \left(\alpha^2 \left(\frac{\dot a}{a} \right)^2 - \alpha\partial_t \left(\frac{\dot a}{a} \right) \right) x$.

Now we operate on Eq.(2.5) with ∂_y and on Eq.(2.3) with ∂_x^2. We then get two results for $\partial_x^2\, \partial_y\, \delta p$. Equating them gives

$$\partial_y \left\{ \rho_0 \left(-\partial_t\, \partial_y\, \delta v_y + \alpha\, \frac{\dot a}{a}\, \partial_x (x\, \partial_y\, \delta v_y) - (\alpha - 1)y\, \frac{\dot a}{a}\, \partial_y^2\, \delta v_y + \alpha\, \frac{\dot a}{a}\, \partial_y\, \delta v_y \right) \right\}$$

$$- \rho_0\, \partial_x^2 \left\{ \partial_t\, \delta v_y - \alpha\, \frac{\dot a}{a}\, x\, \partial_x\, \delta v_y + (\alpha - 1)\, \frac{\dot a}{a}\, y\, \partial_y\, \delta v_y + (\alpha - 1)\, \frac{\dot a}{a}\, \delta v_y \right\}$$

$$+ \partial_y\, \partial_x \left(\delta\rho\, h(\alpha, x, a) \right) - \partial_x^2 \left[(n(\alpha, y, a) + g)\, \delta p \right] = 0 \quad (2.6)$$

where $n(\alpha, y, a) = \left((\alpha - 1)^2 \left(\dfrac{\dot{a}}{a} \right)^2 + (\alpha - 1) \partial_t \left(\dfrac{\dot{a}}{a} \right) \right) y.$

Thus far we have assumed: incompressible flow, $v_{z0} = \dfrac{\dot{a}}{a} z$, $v_{x0} = -\alpha \dfrac{\dot{a}}{a} x$, $v_{y0} = (\alpha - 1) \dfrac{\dot{a}}{a} y$; pressure to stabilize against gravity and to produce the above zero-order flows; $\rho_0 = \rho_0(y)$; and $\delta v_z = 0$. We now specify the system further. We assume two fluids with a sharp interface at $y = 0$. Each fluid has a constant density:

$$\rho(y) = \begin{cases} \rho_{0+} & y > 0 \\ \rho_{0-} & y < 0 . \end{cases}$$

Eq.(2.6) is now greatly simplified. Away from the interface, $\partial_y \rho_0 = 0$. Also, $\delta \rho = 0$ except near the interface. This can be seen from the mass conservation equation

$$\partial_t \rho + \mathbf{v} \cdot \nabla \rho = 0 \longrightarrow \partial_t \, \delta \rho + \delta \mathbf{v} \cdot \nabla \rho_0 + \mathbf{v}_0 \cdot \nabla \delta \rho = 0 .$$

In an incompressible fluid, density perturbations can arise only from advection or from some insertion of density fluctuations as an initial condition. As long as $\delta \rho = 0$ everywhere initially, it will, in this system, remain zero everywhere except near the interface.

So, away from the interface, Eq.(2.6) becomes

$$-\partial_t \, \partial_y^2 \, \delta v_y + \alpha \dfrac{\dot{a}}{a} \partial_x (x \, \partial_y^2 \, \delta v_y) - (\alpha - 1) \dfrac{\dot{a}}{a} \partial_y^2 \, \delta v_y - (\alpha - 1) \dfrac{\dot{a}}{a} y \, \partial_y^3 \, \delta v_y + \alpha \dfrac{\dot{a}}{a} \partial_y^2 \, \delta v_y$$

$$-\partial_t \, \partial_x^2 \, \delta v_y + \alpha \dfrac{\dot{a}}{a} \partial_x^2 (x \, \partial_x \, \delta v_y) - (\alpha - 1) \dfrac{\dot{a}}{a} y \, \partial_x^2 \, \partial_y \, \delta v_y$$

$$+ (\alpha - 1) \dfrac{\dot{a}}{a} \partial_x^2 \delta v_y \ = 0 \qquad (2.7)$$

Inspection will show that it is solved by any δv_y such that

$$\partial_x^2 \, \delta v_y = -\partial_y^2 \, \delta v_y .$$

Now we go back to Eq.(2.7) and integrate it across the interface

$$\left[\rho_0\left(-\partial_t\,\partial_y\,\delta v_y + \alpha\,\frac{\dot a}{a}\,\partial_x(x\,\partial_y\,\delta v_y) + \alpha\,\frac{\dot a}{a}\,\partial_y\,\delta v_y\right)\right]_-^+ = \partial_x^2\int_{-\epsilon}^{+\epsilon}\delta\rho\,g\,dy\ . \quad (2.8)$$

What we would eventually like is a solution of the form $\delta v_y = \delta v_{y0}(t)f(x,y,t)$. If this can be obtained, the final equation for $\delta v_{y0}(t)$ will have no x dependent terms. So, we eliminate them here, if possible.

This is possible if $\delta v_y = e^{\pm ika^\alpha x}\delta v_{y0}(y,t)$, for then

$$-\partial_t\,\partial_y\,\delta v_y = \left(\pm ika^\alpha\frac{\dot a}{a}\,\alpha x e^{\pm ika^\alpha x}\partial_y\,\delta v_{y0} + e^{\pm ika^\alpha x}\partial_t\,\partial_y\,\delta v_{y0}\right)$$

and

$$\alpha\,\frac{\dot a}{a}\,\partial_x(x\,\partial_y\,\delta v_y) = \alpha\,\frac{\dot a}{a}\,\partial_y\,\delta v_{y0}\,e^{\pm ika^\alpha x} \pm ika^\alpha\,\frac{\dot a}{a}\,\alpha x\,e^{\pm ika^\alpha x}\,\partial_y\,\delta v_{y0}\ .$$

So Eq.(2.8) becomes

$$e^{\pm ika^\alpha x}\left[\rho_0\left(-\partial_t\,\partial_y\,\delta v_{y0} + 2\alpha\,\frac{\dot a}{a}\,\partial_y\,\delta v_{y0}\right)\right]_-^+ = \partial_x^2\int_{-\epsilon}^{\epsilon}\delta\rho\,g\,dy\ .$$

The density perturbation $\delta\rho$ must have the same x-dependence as the left hand side of the equation, so

$$\left[\rho_0\left(-\partial_t\,\partial_y\,\delta v_{y0} + 2\alpha\,\frac{\dot a}{a}\,\partial_y\,\delta v_{y0}\right)\right]_-^+ = -k^2\,a^{2\alpha}\int_{-\epsilon}^{\epsilon}\delta\rho_0\,g\,dy\ . \quad (2.9)$$

Now, remembering $\partial_x^2\,\delta v_y = -\partial_y^2\,\delta v_y$, we see

$$\delta v_{y0} = \delta v_{y0}(t)e^{\pm ka^\alpha y}\ .$$

If $\delta v_y = 0$ at $y = \pm\infty$,

$$\delta v_{y0} = \delta v_{y0}(t)e^{-|ka^\alpha y|}\ .$$

So Eq.(2.8) is now

$$-(\rho_{0+} + \rho_{0-})|k|\left(-\partial_t + 2\alpha\,\frac{\dot a}{a}\right)(|a^\alpha|\delta v_{y0}(t)) = -k^2\,a^{2\alpha}\int_{-\epsilon}^{\epsilon}\delta\rho_0\,g\,dy\ .$$

Lastly, we eliminate $\delta\rho$ by making use of the mass conservation equation Eq.(2.1). The x dependence of $\delta\rho$ causes the x dependent terms in the equation to cancel. We then integrate it over the interface:

$$\partial_t \int_{-\epsilon}^{\epsilon} \delta\rho_0 \, dy + (\alpha - 1)\frac{\dot{a}}{a} \int_{-\epsilon}^{\epsilon} y \, \partial_y \, \delta\rho_0 \, dy + \delta v_y(t)(\rho_{0+} - \rho_{0-}) = 0 \ .$$

Since the interface is at $y = 0$:

$$\int_{-\epsilon}^{\epsilon} y \, \partial_y \, \delta\rho_0 \, dy = \int_{-\epsilon}^{\epsilon} \partial_y (y \, \delta\rho_0) dy - \int_{-\epsilon}^{\epsilon} \delta\rho_0 \, dy = -\int_{-\epsilon}^{\epsilon} \delta\rho_0 \, dy \ .$$

We see

$$\left[\partial_t - (\alpha - 1)\frac{\dot{a}}{a}\right] \int_{-\epsilon}^{\epsilon} \delta\rho_0 \, dy = -\delta v_{y0}(t)(\rho_{0+} - \rho_{0-}) \ . \tag{2.10}$$

So, by way of Eqs.(2.10) and (2.1.3),

$$\left[\partial_t - (\alpha - 1)\frac{\dot{a}}{a}\right] \left[\frac{1}{a^{2\alpha}} \left(-\partial_t + 2\alpha \frac{\dot{a}}{a}\right) (|a^\alpha| \delta v_y)\right] =$$
$$-g|k| \frac{\rho_{0+} - \rho_{0-}}{\rho_{0+} + \rho_{0-}} \delta v_y \ , \tag{2.11}$$

or

$$\left[\partial_t - (\alpha - 1)\frac{\dot{a}}{a}\right] \left[\frac{1}{a^{2\alpha}} \left(\partial_t - 2\alpha \frac{\dot{a}}{a}\right) (|a^\alpha| \delta v_{y0}(t))\right] =$$
$$g|k| \frac{\rho_{0+} - \rho_{0-}}{\rho_{0+} + \rho_{0-}} \delta v_{y0}(t) \ . \tag{2.12}$$

This equation is exactly solvable for certain cases of α and a. For instance, if we assume no z direction expansion ($\alpha = 0$), and we assume y direction expansion proportional to time along with corresponding z direction contraction ($a = t_0/t$) then

$$(\partial_t - 1/t) (\partial_t \, \delta v_{y0}(t)) = g|k| \frac{\rho_{0+} - \rho_{0-}}{\rho_{0+} + \rho_{0-}} \delta v_{y0}(t) \ .$$

This equation is solved by

$$d\delta v_{y0}(t) = c_1 \tau I_1(\tau) + c_2 \tau K_1(\tau)$$

where $1/\tau = \sqrt{g|k| \dfrac{\rho_{0+} - \rho_{0-}}{\rho_{0+} + \rho_{0-}}} \, t$, and I_1 and K_1 are hyperbolic Bessel and Basset functions respectively.

The function $\tau I_1(\tau)$ represents the growing mode of the instability. Asymptotically, $I_1(\tau)$ approaches $e^\tau / \sqrt{2\pi\tau}$ so $\delta v_{y0}(t)$ approaches $c_1 \sqrt{\tau/2\pi} \, e^\tau$. The instability growth relative to the overall expansion is $\propto \delta v_{y0}/\tau \propto e^\tau/\sqrt{\tau}$. In absolute terms, we have super-exponential growth. Relative to the expansion, however, we have sub-exponential growth. The relative growths of the RT instability for a static fluid and for the expanding fluid we have studied here, are plotted in Fig. 2.1. It might be said that the expansion causes a "relative stabilization" of the fluid. A similar relative stabilization of the RT instability has also been found for incompressible, spherically expanding fluids [49].

2.1.4 Adiabatic Flow

Similar phenomena occur in compressible fluids with overall expansion. Bernstein and Book [45] derive eigenmodes and growth rates of Rayleigh-Taylor instabilities in a spherically expanding compressible system. Their system is RT stable. That is, all density gradients point in the same direction as the pressure gradients. We will study a system which is unstable to RT perturbations by generalizing the adiabatic equation of state to allow for a spatial dependence in temperature. First, we review some of the results of Book and Bernstein. They require self-similar expansion and an equation of state $p = \widehat{p}(\rho/\widehat{\rho})^\gamma$ where $\widehat{p}, \widehat{\rho}$, and γ are constants. These conditions fix the

density profile:

$$\rho_0 = \widehat{\rho}\left[1 - \frac{\widehat{\rho}(\gamma-1)}{2\widehat{p}\gamma\tau^2}\,r_0^2\right]^{1/(\gamma-1)},$$

and lead to an equation for the expansion rate

$$\ddot{f}\,f^{1+\nu(\gamma-1)} = \tau^{-2},$$

where ν is the dimensionality of the expansion and τ is an arbitrary constant, the choice of which will fix the zero-order expansion rate and fluid quantity profiles. The perturbation equation of motion is found to be:

$$f^{3\gamma-1}\ddot{\boldsymbol{\xi}} = \nabla\left\{\left[\frac{\gamma\widehat{p}\tau^2}{\widehat{\rho}} - \frac{(\gamma-1)r^2}{2}\right]\nabla\cdot\boldsymbol{\xi}\right\} - \mathbf{r}\cdot\nabla\boldsymbol{\xi} - \mathbf{r}\times(\nabla\times\boldsymbol{\xi}) \quad (2.13)$$

where $\boldsymbol{\xi}$ is the Lagrangian perturbation and all r's and ∇'s refer to the initial positions of each fluid element.

If we perturb the fluid in an incompressible, irrotational manner, then Eq.(2.13) is simplified to

$$f^{3\gamma-1}\ddot{\boldsymbol{\xi}} = -\mathbf{r}\cdot\nabla\boldsymbol{\xi}\ . \tag{2.14}$$

Solution of this equation leads to $\boldsymbol{\xi} = \nabla\mathcal{X}(\mathbf{r},t)$, where $\mathcal{X}(\mathbf{r},t)$ solves the equations

$$\mathcal{X} = \sum_{\ell m}\left[X_+(\ell)r^\ell + X_-(\ell)r^{-\ell-1}\right]Y_{\ell m}$$

and

$$f^{3\gamma-1}\ddot{X}_\pm = \left[3/2 \mp (\ell+1/2)\right]X_\pm\ .$$

Bernstein and Book then show that all possible modes (compressible and rotational included) grow no faster than the rate of overall expansion when $\gamma \neq 1$.

When $\gamma = 1$, only the incompressible, irrotational modes grow faster than overall expansion. In this case, χ_+/f and χ_-/f diverge as $t \to \infty$, but they diverge extremely slowly.

Of interest here is the behavior of R-T modes in a decidedly unstable system; *i.e.* where $\partial \rho / \partial r < 0$ and acceleration points inward, slowing the expansion. Such a system can be described by a more general equation of state:

$$p = \hat{p}(\mathbf{r}) \left(\frac{\rho}{\hat{\rho}} \right)^{\gamma}$$

where $\hat{\rho}$ is a constant and r is the initial position of a fluid element. In other words, $\hat{\rho}$ is the same for all fluid elements, whereas $\hat{p}$ can vary from element to element but $\hat{p}$ for a given element never changes. We now have the freedom to choose initial conditions such that we have a dense fluid surrounded by a thinner fluid, with higher pressure in the thinner fluid, thus slowing expansion of the system. The equation of expansion then becomes

$$\ddot{f} \, f^{1+\nu(\gamma-1)} = -\tau^{-2} \ . \tag{2.15}$$

The equation of motion of the perturbations is

$$f^{2+\nu(\gamma-1)} \ddot{\xi} = \nabla \left(\tau^2 \frac{\partial p_0}{\partial \rho_0} \nabla \cdot \xi \right) + \mathbf{r} \times (\nabla \times \xi) + \mathbf{r} \cdot \nabla \xi - \tau^2 \frac{p_0}{\rho_0} \nabla \cdot \xi \nabla \ell n \hat{p}$$

where again $\mathbf{r}$ and ∇ refer to the initial positions of each fluid element and p_0 are the original unperturbed pressure and density of each element.

We find $f(t)$ from Eq.(2.15). Reduction of order of this equation gives

$$\left(\frac{df}{dt} \right)^2 - \left(\frac{df}{dt} \right)^2_{t=0} = -\frac{2}{3-3\gamma} \left(f^{3-3\gamma}(t) - f^{3-3\gamma}(0) \right) \frac{1}{\tau^2} \quad , \text{ for } \quad \gamma \neq 1 \ .$$

If we choose $f(0) = 1$ and $df/dt \to 0$ as $t \to \infty$ ("minimal escape velocity," speaking figuratively) then

$$f = \left(\frac{3\gamma - 1}{[2(3\gamma - 3)]^{1/2}} \frac{t}{\tau} + 1 \right)^{\frac{2}{3\gamma - 1}} \quad , \text{ for } \quad \gamma \neq 1 \ .$$

If we look at incompressible irrotational modes again, we find

$$f^{3\gamma - 1} \ddot{X}_+ = (\ell - 1) X_+ / \tau^2$$

$$f^{3\gamma - 1} \ddot{X}_- = (\ell - 2) X_- / \tau^2 \ .$$

A change of variable $t' = \dfrac{3\gamma - 1}{[2(3\gamma - 3)]^{1/2}} \dfrac{t}{\tau} + 1$ gives

$$t'^2 \ddot{X}_+ = \frac{(\ell - 1)}{\alpha^2} X_+ \tag{2.16}$$

$$t'^2 \ddot{X}_- = \frac{(-\ell - 2)}{\alpha^2} X_- \tag{2.17}$$

where $\alpha = \dfrac{3\gamma - 1}{[2(3\gamma - 3)]^{1/2}}$. Eqs. (2.16) and (2.17) are solved by $X = t'^n$ where n solves the equations

$$n(n - 1) = \frac{\ell - 1}{\alpha^2} \quad \text{or} \quad n(n - 1) = \frac{-\ell - 2}{\alpha^2} \ .$$

Note that, for $\ell - 1/\alpha^2 \geq 0$, X_+ has one growing mode ($t'^n, n > 0$) and one decaying mode ($t'^n, n < 0$). So, we have unstable modes, but they grow as power laws of t'. The instability growth rate is sub-exponential, both relative to the overall expansion and in absolute terms.

Should $(\ell - 1)/\alpha^2 < 0$ or, as is always the case, $(-\ell - 2)/\alpha^2 < 0$, the solutions to the equations take the form t^{a+ib} and t^{a-ib}. It can be shown that $a = 1$ so the real solutions that can be constructed from these solutions are:

$$t \cos(b \ln(t)) \quad , \quad t \sin(b \ln(t)) \ .$$

We have analytically studied two different fluid systems undergoing overall expansion (with necessary contraction in the incompressible case). In

each case, the growth of the R-T instability is sub-exponential relative to the overall expansion. This qualitative conclusion is an initial test which we have applied to our algorithm for simulating expanding fluid and MHD systems. We review the algorithm and the simulation results in the next section.

2.1.5 Computational Results

2.1.5.1 Algorithm Our simulation model is a non-resistive, adiabatic, two-dimensional MHD-plasma. We simulate the plasma with a Lax-Wendroff-type algorithm used by Nakagawa, Steinolfson, and Wu [50], and first developed by Rubin and Burstein [51].

To facilitate studying the R-T instability in an expanding plasma, the algorithm is altered so that each grid point becomes a co-moving point, tracking a predetermined zero-order expansion of the plasma. The advantage of this approach is that, if we deal with an expanding system, it will prevent an expanding system from growing beyond the computational boundaries. Conversely, it will prevent a contracting system from shrinking to a size smaller than the grid spacing can handle.

To see how this alteration is made, we first look at how the MHD equations can be rewritten in terms of variables co-moving with a homogeneous expansion.

Our static coordinates are r_x, r_y, r_z, and t. They can be expressed in terms of the co-moving coordinates x, y, z, t':

$$r_x = a_x(t)x$$

$$r_y = a_y(t)y$$

$$r_z = a_z(t)z$$

$$t = t' \ .$$

The $a_i(t)$ are functions of time chosen beforehand, and are not unlike the elements of a time-dependent metric in general relativity. Since what we are doing here amounts to a simple change of variable, the $a_i(t)$ can be, in principle, anything we like. However, the most useful $a_i(t)$ will be functions that lead to spatial coordinates which track, or nearly track, the overall expansion of the system. So we determine the $a_i(t)$ beforehand by first solving the zero-order fluid or MHD equations of motion. If these equations lead to a homogeneous expansion of the fluid, $i.e.$ a fluid element at (r_x, r_y, r_z) at $t = 0$ moves to $(f_x(t)r_x, f_y(t)r_y, f_z(t)r_z)$ at t, then $a_i(t) = f_i(t)$. If the fluid equations return an expansion which is not quite homogeneous, then we can still make some use of the algorithm by choosing the $a_i(t)$ to be large enough for the computational boundaries to always contain the entire system.

The velocities $u, v,$ and w can be expressed in terms of velocities relative to the local motion of expansion:

$$u(r_x, r_y, r_z, t) = v_x(x, y, z, t') + \dot{a}_x(t')x$$

$$v(r_x, r_y, r_z, t) = v_y(x, y, z, t') + \dot{a}_y(t')y$$

$$w(r_x, r_y, r_z, t) = v_z(x, y, z, t') + \dot{a}_z(t')z \ .$$

So, for example, if (v_x, v_y, v_z) is equal to $(0, 0, 0)$ at some point (x, y, z), then, at that point, the fluid is moving exactly with the expanding coordinates.

The derivatives are rewritten

$$\partial_{r_x} = \frac{1}{a_x(t)} \frac{\partial}{\partial x}$$

$$\partial_{r_y} = \frac{1}{a_y(t)} \frac{\partial}{\partial y}$$

$$\partial_{r_z} = \frac{1}{a_z(t)} \frac{\partial}{\partial z}$$

$$\partial_t = \partial_t' - \frac{\dot{a}_x}{a_x} x \frac{\partial}{\partial x} - \frac{\dot{a}_y}{a_y} y \frac{\partial}{\partial y} - \frac{\dot{a}_z}{a_z} z \frac{\partial}{\partial z} \; .$$

The MHD equations then become

$$\frac{\partial \rho}{\partial t} + \nabla_r \cdot (\rho \mathbf{v}) + \sum_j \frac{\dot{a}_j}{a_j} \rho = 0 \qquad (2.18)$$

$$\frac{\partial(\rho v_i)}{\partial t} + \nabla_r \cdot (\rho \mathbf{v} v_i) + \frac{1}{a_i} \partial_i p + \frac{1}{4\pi} [(\nabla_r \times \mathbf{B}) \times \mathbf{B}]_i +$$

$$\sum_j \frac{\dot{a}_j}{a_j} \rho v_i + \frac{\dot{a}_i}{a_i} \rho v_i + \rho \ddot{a}_i x_i = 0 \qquad (2.19)$$

$$\frac{\partial B_i}{\partial t} + [\nabla_r \times (\mathbf{v} \times \mathbf{B})]_i + B_i \sum_{j \neq i} \frac{\dot{a}_j}{a_j} = 0 \qquad (2.20)$$

$$\frac{\partial}{\partial t} \left(\frac{p}{\gamma - 1} + \frac{\rho v^2}{2} + \frac{B^2}{8\pi} \right) + \nabla_r \cdot \left[\mathbf{v} \left(\frac{\gamma p}{\gamma - 1} + \frac{\rho v^2}{2} \right) + \frac{1}{4\pi} \mathbf{B} \times (\mathbf{v} \times \mathbf{B}) \right]$$

$$+ \sum_j v_j \, \ddot{a}_j \, x_j \, \rho + \sum_j \frac{\dot{a}_j}{a_j} v_j^2 \, \rho + \left(\frac{\gamma p}{\gamma - 1} + \frac{\rho v^2}{2} \right) \sum_j \frac{\dot{a}_j}{a_j}$$

$$+ \frac{B_y^2 + B_z^2}{4\pi} \frac{\dot{a}_x}{a_x} + \frac{B_z^2 + B_x^2}{4\pi} \frac{\dot{a}_y}{a_y} + \frac{B_x^2 + B_y^2}{4\pi} \frac{\dot{a}_z}{a_z} = 0 \qquad (2.21)$$

where $\nabla_r = \left(\dfrac{1}{a_x} \dfrac{\partial}{\partial x}, \dfrac{1}{a_y} \dfrac{\partial}{\partial y}, \dfrac{1}{a_z} \dfrac{\partial}{\partial z} \right)$, and all summations are explicit, *i.e.* repeated indices do *not* imply summation. Our simulation is two-dimensional, but z direction terms have been retained here for completeness.

Now we must alter the computational algorithm to account for the "source terms" and the time-dependent coefficients appearing in the new equa-

tions. We now represent the MHD equations by

$$\partial_t U + \frac{1}{a_x} \partial_x F + \frac{1}{a_y} \partial_y G + S = 0 \ .$$

We first find mid-point values for U^{n+1}: Here, we closely follow the standard Lax-Wendroff algorithm, but we introduce two changes. First, the spatial derivatives are modified by the expansion factors a_x and a_y. For instance,

$$\frac{d}{dx} F^n \longrightarrow \frac{1}{a_x^n \Delta x} \left(F_{i+1,j}^n - F_{i,j}^n \right) \ .$$

Second, we account for the expansion source terms:

$$U_{i+1/2,j}^{n+1} = U_{i,j}^{n+1} + \Delta t \frac{dF^n}{dx} + \Delta t \frac{dG^n}{dy} - \frac{1}{2} \left(S_{i+1,j}^n + S_{i,j}^n \right) \ .$$

Midpoint values are then calculated for F^{n+1}, G^{n+1}, and S^{n+1}:

$$F_{i+1/2,j}^{n+1} = F \left(U_{i+1/2,j}^{n+1} \right) \qquad \text{etc.}$$

Lastly, grid point values are calculated for U^{n+1}:

$$U_{i,j}^{n+1} = U_{i,j}^n - \frac{\Delta t}{2} \left\{ \left(\frac{\partial F}{\partial x} \right)_{i,j}^{n+1} + \left(\frac{\partial F}{\partial x} \right)_{i,j}^n \right\} - \frac{\Delta t}{2} \left\{ \left(\frac{\partial G}{\partial y} \right)_{i,j}^{n+1} + \left(\frac{\partial G}{\partial y} \right)_{i,j}^n \right\}$$

$$- \frac{1}{2} \left(S_{i,j}^n + \overline{S}_{i,j}^{n+1} \right)$$

where $\overline{S}_{i,j}^{n+1} = \frac{1}{4} \left(S_{i+1/2,j}^{n+1} + S_{j+1/2}^{n+1}, S_{i-1/2,j}^{n+1} + S_{i,j-1/2}^{n+1} \right)$.

2.1.5.2 Simulation Results

We model a non-resistive, adiabatic MHD plasma. The adiabatic constant is $\gamma = 5/3$. The plasma is contained in a box with reflective boundary conditions. Physically, it is twice as long in the y direction as in the x direction. One hundred twenty two grids are evenly spaced along the y direction; thirty are spaced along the x direction. A dense

plasma occupies the lower third of the box, a thin plasma the upper two thirds. The interface between them is a transition region with a width of about 10 grid spaces. A magnetic field $B(y)\hat{z}$ is imposed; it is relatively weak in the thick plasma and strong in the thin plasma.

In detail, the pressure, density, and magnetic field strength profiles are:

$$p = p_0 - p_1 \tanh\left(\frac{y - y_0}{\ell}\right)$$

$$\rho = \rho_0 - \rho_1 \tanh\left(\frac{y - y_0}{\ell}\right)$$

$$\mathbf{B} = \left(B_0^2 + B_0^2 \tanh\left(\frac{y - y_0}{\ell}\right)\right)^{1/2} \hat{z} .$$

y_0 is the center of the transition region. ℓ is on the order of half the width of the transition region. p_0 and p_1 are chosen so that the thick region pressure (p_{tk}) is seven times that of the thin region pressure (p_{tn}). The variation in ρ is exactly proportional to the variation in p. The total pressure $(p + B^2/8\pi)$, however, increases as we cross the transition region from the thick plasma into the thin plasma:

$$p_{tn} + \frac{2B_0^2}{8\pi} = 1.2 p_{tk} .$$

The plasma β in the thin region is 0.11. The overall $\beta(= 8\pi\, p_{tk}/2B_0^2)$ is 0.77.

The imbalance in the total pressure creates a force across the transition region directed toward the thick plasma. This system is R-T unstable.

To test the code, we first studied the growth of initial R-T perturbations in a plasma without expansion. Velocity perturbations took the form

$$\left. \begin{array}{l} u = v_0 \sin\left(\frac{2\pi x}{\lambda}\right)\left(\frac{y}{\ell_{tk}}\right) \\[2mm] v = -v_0 \cos\left(\frac{2\pi x}{\lambda}\right)\left(\frac{y}{\ell_{tk}}\right) \end{array} \right\} \text{ in the thick plasma} \qquad (2.22)$$

$$
\left.
\begin{aligned}
u &= v_0 \left(1 - 2\frac{y - \ell_{tk}}{\ell_{tr}} \right) \sin\left(\frac{2\pi x}{\lambda} \right) \\
v &= -v_0 \cos\left(\frac{2\pi x}{\lambda} \right)
\end{aligned}
\right\} \text{ in the transition region} \qquad (2.23)
$$

$$
\left.
\begin{aligned}
u &= v_0 \left(1 - \frac{y - \ell_{tk} + \ell_{tr})}{\ell_{tn}} \right) \sin\left(\frac{2\pi x}{\lambda} \right) \\
v &= -v_0 \left(1 - \frac{\ell_{tk} + \ell_{tr})}{\ell_{tn}} \right) \cos\left(\frac{2\pi x}{\lambda} \right)
\end{aligned}
\right\} \text{ in the thin plasma} \qquad (2.24)
$$

$$(2.25)$$

where ℓ_{tk} is the size of the thick plasma, ℓ_{tr} is the size of the transition region, and ℓ_{tn} is the size of the plasma. λ, the perturbation wavelength, was set to twice the length of the x direction wall of the simulation box; v_0 is about 0.1 of the sound speed in the thick plasma . The transition region was also given a sinusoidal bend of the same wavelength having an amplitude of about one grid space.

The R-T instability grows qualitatively as standard theory and experimental results have indicated. Namely, the sinusoidal perturbation of the interface grows and then becomes cycloid-like, sending "spikes" of dense plasma into the thin plasma [52].

We have also compared the early growth rate of the instability to a "ball park" obtained from the standard expression for the growth rate of an incompressible, two-fluid R-T instability in gravity, namely:

$$
n = \sqrt{gk\,\frac{\rho_2 - \rho_1}{\rho + 2 + \rho_1}} \; ,
$$

where k is the perturbation wavenumber, g is the gravitational acceleration, and ρ_2 and ρ_1 are the fluid densities above and below the interface, respectively. For g, we substitute a number approximately equal to the average acceleration

in the transition region:

$$g = \frac{(2B_0^2/8\pi + \Delta p)/\ell_{tr}}{\rho(y_{tr})}$$

where $\Delta p < 0$. Given that

$$k = \frac{2\pi}{\lambda} = \frac{2\pi}{2\ell_x} = \frac{2\pi}{\ell_y} \ ,$$

we find

$$n_{class} = 5.17 \frac{c_s}{\ell_y} \ ,$$

where c_s is the dense plasma sound speed and ℓ_y is the y direction box length. This is, indeed, within the "ball park" of the simulation results:

$$n = 3.05 \frac{c_s}{\ell_y} \ ,$$

or

$$n = 0.58 n_{class}.$$

The main result of interest from these simulations is the somewhat stabilizing effect of the expansion on the instability. Let the amplitude of the "bend" in the interface be denoted by $I(t)$. Then the amplitude relative to expansion is

$$s(t) = I(t)/a_y(t) \ .$$

If $a_y(t)$ is a constant, then our present problem reduces to the static case with some exponential growth rate

$$I(t) \propto e^{nt} \propto s(t) \ .$$

However, if $a_y(t)$ is a function of time, such as $\alpha t + 1$, the simulations shows that $s(t)$ is some sub-exponential function of time. The time evolutions of

the density contours of static and expanding plasmas is shown in Fig. 2.2. Note that, after equal times, the interface of the expanding plasma remains much more planar than that of the static plasma. The $s(t)$ for two different expansions, $a(t) = t+1$ and $a(t) = 4t+1$ (t being normalized to the time needed for a wave traveling at the thick plasma sound speed to traverse the y extent of the computational grid) along with the results of the static plasma are shown in Fig. 2.3. The plasma instability growth is slowed relative to the overall expansion of the plasma. In particular, the early-time growth of the instability is slowed by 7% when $a(t) = t + 1$ and by 14% when $a(t) = 4t + 1$. Also, the instability appears to saturate and enter a non-linear regime earlier with faster expansion. When $a(t) = 1$, fall-off from linear growth begins at about 0.17 of the classical growth time. This occurs at about 0.15 of the classical growth time when $a(t) = t + 1$ and at about 0.1 of the classical growth time when $a(t) = 4t + 1$.

We take a moment here to review the relationships between the two systems we studied in Sec. 2 and the system we have simulated. In each of the Sec. 2 systems, the instability growth rate, relative to the overall expansion, is sub-exponential. However there are significant differences in the makeup of the two systems: The incompressible instability under consideration is driven by a constant gravitational force while the expansion (and accompanying contraction) of the fluid is chosen to be constant. On the other hand, the compressible instability is driven by the same pressure gradient that cause the expansion to slow down; it is precisely this deceleration that destabilizes the system. The incompressible system has a slab geometry; the compressible system has a spherical geometry.

The system we have simulated stands "half-way between" the other

two in certain respects. It is a compressible fluid in a slab geometry. Its overall expansion rate in the y direction is chosen to be constant but, since the fluid is compressible, there is no need for any contraction. The instability driving force is created by a pressure imbalance at the interface of the heavy and light plasmas. This imbalance is not responsible for any change in the overall expansion rate but, as in the compressible case, it is depleted by the expansion. Despite the differences in these systems, fluid expansion slows RT growth in them all. This can be taken as a successfully passed, qualitative test of the simulation algorithm.

2.1.6 Conclusions

A large number of specific expanding fluid systems give rise to slowed, or even sub-exponential relative growth of Rayleigh-Taylor instabilities. We have presented analytical results for two new systems which exhibit this phenomenon: an incompressible two-fluid system and an adiabatic fluid system. The adiabatic system is a generalization of Book and Bernstein [45]. They studied an expanding adiabatic fluid with a pressure completely dependent on fluid density. This led to a spherical system with both density and pressure falling off with radius. The density and pressure gradients were necessarily in the same direction and the system was RT stable. We have introduced a spatial variation of temperature into the equation of state, making possible a rise in pressure together with a fall-off in density. This makes the system RT unstable.

Results from a new MHD fluid code written specifically for simulating fluids undergoing overall expansion (or contraction) confirm this result for a simple slab geometry system undergoing a simple linear expansion.

It should be noted that fluid expansion will not always lead to stabilization of instabilities. Modes developing along magnetic field lines, called Parker modes or ballooning instabilities, behave in a marked way in an expanding gas in their nonlinear stages [53]. Expansion could contribute to nonlinear destabilization through mass motion along the field lines.

The computational algorithm presented here may find application in the study of astrophysical phenomena, such as certain stages of supernova behavior. For instance, it might be used to study the effects of the interstellar medium or magnetic field swept up in the leading edge of the explosion. It might also be usefully applied to problems in inertial confinement fusion. For example, fluid expansion and contraction might significantly affect the results of such research as Emery *et. al.* [41] and Kull [42].

2.2 Particle Simulation Algorithms for Introducing Short-Range Forces into MHD and Fluid Flow

2.2.1 Adiabatic Fluid Algorithm

We have constructed a PIC code for the purpose of studying the effects of short-range, intermolecular forces on fluid and MHD flow. Here we present the algorithm we have used. We also present two other algorithms which will, hopefully, be helpful in overcoming time-scale problems.

The algorithm is based on an adiabatic MHD PIC code developed by Brunel *et. al.* [54]. In this algorithm, computational particles carry mass and momentum. Fluid quantities such as pressure, density, and fluid velocity are interpolated from the particles to a computational grid. In return, these quantities are used to construct fluid forces which are interpolated back to the particles and used to alter the particle velocities.

The algorithm works as follows:

(1) Fluid density is computed: $\rho^n(\mathbf{x}) = \sum_p S_{pv}(\mathbf{x}^n - \mathbf{x}_p^n)$ where S_{pv} is the interpolation function and the sum is over all particle positions within some predetermined distance from the cell at $\mathbf{x}$.

(2) Pressure accelerations are calculated, as well as magnetic accelerations, if we are studying MHD flow:

$$\mathbf{F}_{pr}^n = -\nabla p^n / \rho^n, \qquad \text{where } p = p_0(\rho/\rho_0)^\gamma$$

$$\mathbf{F}_B^n = ((\nabla \times \mathbf{B}^n) \times \mathbf{B})^n / 4\pi\rho^n$$

(3) Fluid accelerations are interpolated to particle positions: $\mathbf{F}_p^n = \sum_v S_{pv}(\mathbf{x}^n - \mathbf{x}_p^n)(\mathbf{F}_{pr}^n + \mathbf{F}_B^n)$ where the sum is over all grid cells within a predetermined distance of the particle p.

(4) Short-range accelerations are calculated for each particle:

$$\mathbf{F}_{sp}^n = \sum_q \mathbf{F}_s(\mathbf{x}_p^n - \mathbf{x}_q^n)$$

These accelerations are then interpolated to the grid cells and then back to the particles. (In our particular code, the accelerations were calculated by a PPPM method [55].)

(5) Particle velocities are advanced by a half time-step:

$$\mathbf{v}_p^n = \mathbf{v}_p^{n-1/2} + \frac{\Delta t}{2}(\mathbf{F}_p^n + \mathbf{F}_{sp}^n)$$

(6) New fluid velocities are computed by interpolation: $\mathbf{v}_f^n = \sum_p S_{pv}(\mathbf{x} - \mathbf{x_p})\mathbf{v}_p^n$.

(7) The magnetic field is advanced a half time-step using a Lax method:

$$\mathbf{B}^{n+1/2} = \langle \mathbf{B}^n \rangle + \frac{\Delta t}{2}(\nabla \times (\mathbf{v}_f^n \times \mathbf{B}^n))$$

where $\langle \mathbf{B}^n \rangle_{i,j} = (\mathbf{B}^n_{i+1,j} + \mathbf{B}^n_{i-1,j} + \mathbf{B}^n_{i,j+1} + \mathbf{B}^n_{i,j-1})/4$.

(8) Particle velocities are advanced another half time-step:

$$\mathbf{v}^{n+1/2}_p = \mathbf{v}^n_p + \frac{\Delta t}{2}(\mathbf{F}^n_p + \mathbf{F}^n_{sp}) + \nu(\mathbf{v}^n_f - \mathbf{v}^n_p)$$

where ν is an arbitrary constant ranging from 0 to 1. $\nu = 1$ prevents multi-streaming.

(9) Particle positions are pushed a half time-step:

$$\mathbf{x}^{n+1/2} = \mathbf{x}^n + \mathbf{v}^{n+1/2}\frac{\Delta t}{2}$$

(10) New fluid velocities are calculated by interpolation:

$$\mathbf{v}^{n+1/2}_f = \sum_p S_{pv}(\mathbf{x} - \mathbf{x}_p)(\mathbf{v}^{n+1/2}, \mathbf{x}^{n+1/2})$$

(11) The magnetic field is pushed a full time-step, completing the Lax scheme:

$$\mathbf{B}^{n+1} = \mathbf{B}^n + \Delta t(\nabla \times (\mathbf{v}^{n+1/2}_f \times \mathbf{B}^{n+1/2}))$$

(12) The algorithm cycle is completed with the final advance of the particle positions:

$$\mathbf{x}^{n+1} = \mathbf{x}^{n+1/2} + \mathbf{v}^{n+1/2}\frac{\Delta t}{2}$$

Initially, an attempt was made to add the short range accelerations directly to the particles in step (4). This approach had to be abandoned because of problems with spatial aliasing of short wavelength fluctuations in the fluid quantities. The interpolation scheme acts as a spatial low-pass filter on the short-range force effects.

In an effort to get past the limitation on timestep imposed by the sound speed of the adiabatic fluid, we attempted to implement an incompressible fluid algorithm. It proceeds thusly:

(1) Fluid density, velocity, short-range forces, and magnetic field are calculated at each grid point. This is done in the same way as in the previous algorithm.

(2) Acceleration from the magnetic field and short-range forces are calculated on the grid points:

$$\mathbf{A}_B^n = ((\nabla \times \mathbf{B}^n) \times \mathbf{B})^n / 4\pi\rho^n.$$

(3) Preliminary values of the updated fluid velocities are calculated:

$$\tilde{\mathbf{U}}_v^n = \mathbf{U}_v^{n-\theta} + \mathbf{A}_v^n \theta \Delta t$$

where $\mathbf{A}_v^n = \mathbf{A}_{Bv}^n + \mathbf{A}_{sv}^n$.

(4) The velocity field is now made incompressible. This is accomplished by first solving a Poisson-type equation for the velocity potential ϕ:

$$\nabla \cdot (\nabla\phi_c^n + \frac{(\nabla\rho^n)_v}{\rho_v^n}\phi_v^n) = \nabla \cdot \tilde{\mathbf{U}}_v^n$$

where the subscript c indicates a quantity defined at the centers of the grid cells, as opposed to quantities defined at the grid points, which are labeled by v. The velocity potential ϕ is of physical significance in that it is proportional to the pressure divided by the density:

$$\phi_c^n = \frac{p_c^{n+\theta}}{\rho_c}\theta\Delta t.$$

$\mathbf{U}_v^n$ is now calculated by

$$\mathbf{U}_v^n = \tilde{\mathbf{U}}_v^n - ((\nabla\phi_c^n + \frac{(\nabla\rho^n)_v}{\rho_v^n}\phi_v^n).$$

(5) The magnetic field is advanced to its preliminary values:

$$\mathbf{B}^* = \langle \mathbf{B}^n \rangle + \frac{\Delta t}{2}(\nabla \times (\mathbf{U}_v^n \times \mathbf{B}^n)),$$

where $\langle \mathbf{B}^n \rangle_{i,j} = (\mathbf{B}^n_{i+1,j} + \mathbf{B}^n_{i-1,j} + \mathbf{B}^n_{i,j+1} + \mathbf{B}^n_{i,j-1})/4$.

(6) The fluid velocities are advanced to the next timestep:

$$\mathbf{U}^{n+1-\theta}_v = [\mathbf{U}^n_v - (1-\theta)\mathbf{U}^{n-\theta}_v]/\theta.$$

(7) Updated particle velocities are interpolated from the grid cells:

$$\mathbf{U}^{n+1-\theta}_p = \mathbf{U}^{n-\theta}_p + \sum_v (\mathbf{U}^{n+1-\theta}_v - \mathbf{U}^{n-\theta}_v)S_{pv}$$

where S_{pv} is the function of interpolation from grid point v to particle p.

(8) The magnetic field is advanced to the next time step:

$$\mathbf{B}^{n+1} = \mathbf{B}^n + \Delta t(\nabla \times (\mathbf{U}^{n+1-\theta}_v \times \mathbf{B}^*)).$$

(9) The cycle is completed by pushing the particle positions a full timestep:

$$\mathbf{x}^{n+1}_p = \mathbf{x}^n_p + \sum_v \mathbf{U}^{n+1-\theta}_p.$$

In our particular code, θ was set equal to $1/2$. The Poisson equation in step (4) was solved by an SOR method [56].

An alternative algorithm for introducing short-range force effects has been considered, but not, as yet, used in a simulation code. Short-range forces would not be explicitly calculated. Rather, a surface tension fluid force would be calculated wherever the fluid density gradient exceeded some predetermined value ϵ. In the physical equations of motion of fluid or MHD flow, the surface tension force at a sharp interface is given by

$$\mathbf{F}_T = \sigma \kappa \hat{n} \delta(\mathbf{x} - \mathbf{x}_s), \qquad (2.26)$$

where σ is the surface tension coefficient, and κ is the local radius of curvature of the interface, defined along with the unit vector $\hat{n}$ so that the force always points into the fluid from which the interface appears concave.

To adapt this force to a fluid code mesh, we would make the change

$$\sigma\kappa\hat{n}\delta(\mathbf{x} - \mathbf{x}_s) = \begin{cases} -\sigma\hat{n} \cdot \nabla\hat{n} & \text{if } |\nabla\rho| \geq \epsilon \\ 0 & \text{if } |\nabla\rho| < \epsilon \end{cases}, \tag{2.27}$$

where $\hat{n} = \nabla\rho/|\nabla\rho|$ and ϵ is chosen beforehand. This method of handling surface tension was developed by Brackbill, Kothe, and Zemach [57].

The algorithm proceeds in a fashion similar to the incompressible algorithm outlined above, with two exceptions. First, as has been stated, short-range forces are not directly calculated. Second, surface tension is included in the calculation of the preliminary velocities $\dot{\mathbf{U}}^n$. This is accomplished by an implicit inner iteration scheme in which the continuity and momentum equations are coupled:

$$\mathbf{R}_{m+1}^{n+\theta} = -\nabla\dot{\mathbf{U}}^{*n}_{m} \cdot \mathbf{R}_{m+1}^{n+\theta}\theta\delta t + \mathbf{R}^n$$

$$\hat{\mathbf{R}}_{m+1}^{n+\theta} = \mathbf{Q}_m^{n+\theta} \cdot (\nabla\tilde{\mathbf{U}}^{*n}_{m} \cdot \hat{\mathbf{R}}_{m+1}^{n+\theta})\theta\delta t + \hat{\mathbf{R}}^n$$

$$\tilde{\mathbf{U}}_{m+1}^n = \{\mathbf{A}_{Bv}^n - \frac{\sigma\mathbf{R}_{m+1}^{n+\theta}}{[\rho]\langle\rho\rangle}\nabla \cdot \mathbf{R}_{m+1}^{n+\theta}\}\theta\delta t + \mathbf{U}^n$$

$$\tilde{\mathbf{U}}^{*n+\theta}_{m+1} = \omega(\mathbf{U}_m^{n+\theta} - \mathbf{U}_{m+1}^{n+\theta}) + \mathbf{U}_{m-1}^{n+\theta},$$

where

$$\mathbf{R} \equiv \nabla\rho,$$

$$\hat{\mathbf{R}} \equiv \frac{\nabla\rho}{|\nabla\rho|},$$

$$\hat{\mathbf{Q}} \equiv \hat{\mathbf{R}}\hat{\mathbf{R}} - \mathbf{I}, \tag{2.28}$$

and $[\rho]$ is the difference in density across the interface and $\langle\rho\rangle$ is the average of the density across the interface. Upon convergence, $\mathbf{U}^n = \tilde{\mathbf{U}}_{m+1}^n$.

2.2.2 Simulation of a Rayleigh-Taylor Instability

We implemented the first algorithm in a simulation of a two-fluid Rayleigh-Taylor unstable system. The simulation code is two-dimensional. All distances were normalized to the grid spacing Δ. All velocities were normalized to the sound speed $c_s = \gamma p_0 / \bar{\rho}$ where $\bar{\rho}$ is the average mass density and p_0 is an arbitrary physical pressure. Time was normalized to $\Delta t = \Delta / c_s$. All mass was normalized to the particle mass. The computational grid size was 64×64. The timestep was $\Delta t = 0.05$.

The initial density profile was

$$\rho(y) = \frac{\rho_1 + \rho_2}{2} + \frac{\rho_2 - \rho_1}{2} \tanh\left(\frac{y - y_{int}}{y_{size}}\right),$$

where ρ_1 was the density at the bottom of the computational area, ρ_2 was the density at the top of the area, y_{int} was the location of the center of the interface region, and y_{size} was the approximate thickness of the interface region. In our particular simulation, $y_{int} = 32$, placing the interface half-way between the top and bottom of the computational area, and $y_{size} = 4$. ρ_1 was three particles per cell and ρ_2 was 12.3 particles per cell. Particle positions were initialized by first placing the particles in a series of horizontal rows. The x-direction spacing between particles was kept constant. The y-direction spacing between rows was set inversely proportional to the local density. Then, in each row of particles, alternate particles were moved one half of the distance up to the next row of particles. This was done to keep the particles in the thin region outside of one another's range of interaction. The entire system was made subject to a gravitational acceleration of $g = -0.05\hat{y}$, and was stabilized by an inhomogeneous magnetic field in the z direction (*i.e.* perpendicular to the computational area). The timestep was $\Delta t = 0.05$. Boundary conditions were chosen to be periodic at the x boundaries and reflective at the y boundaries.

Outside of the interface region, the fluid velocities were perturbed according to

$$v_{fx} = \sin(kx) \times \begin{cases} -.1 \times \dfrac{\cosh(ky)}{\sinh(ky_{int})}, & y < y_{int} - y_{size}/2 \\ p(y), & y_{int} - y_{size}/2 < y < y_{int} + y_{size}/2 \\ .1 \times \dfrac{\cosh(k(y_{max} - y))}{\sinh(k(y_{max} - y_{int}))}, & y > y_{int} + y_{size}/2. \end{cases} \quad (2.29)$$

and

$$v_{fy} = \cos(kx) \times \begin{cases} -.1 \times \dfrac{\sinh(ky)}{\sinh(ky_{int})}, & y < y_{int} - y_{size}/2 \\ q(y), & y_{int} - y_{size}/2 < y < y_{int} + y_{size}/2 \\ .1 \times \dfrac{\sinh(k(y_{max} - y))}{\sinh(k(y_{max} - y_{int}))}, & y > y_{int} + y_{size}/2. \end{cases} \quad , (2.30)$$

where $p(y)$ and $q(y)$ are second and third order polynomials respectively. These polynomials were chosen so that 1) the fluid flow would be initially incompressible in the interface region, as it was in the rest of the computational area, 2) v_y and $\partial_y v_y$ would be continuous at $y = y_{int} - y_{size}/2$ and at $y = y_{int} + y_{size}/2$, and 3) v_x would be continuous at $y = y_{int} - y_{size}/2$ and at $y = y_{int} + y_{size}/2$. The above velocities were assigned as fluid velocities to the computational grid points. Particle velocities were then initialized by interpolation from the grid.

For an initial test of the code, the short-range force on a particle 1 from a particle 2 was chosen to be particularly simple, namely

$$\mathbf{F}_{sr}(\mathbf{x}_1 - \mathbf{x}_2) = \begin{cases} sin(\pi|\mathbf{x}_1 - \mathbf{x}_2|/r_{eq})\dfrac{(\mathbf{x}_1 - \mathbf{x}_2)}{|\mathbf{x}_1 - \mathbf{x}_2|} & |\mathbf{x}_1 - \mathbf{x}_2| < 2r_{eq} \\ 0 & |\mathbf{x}_1 - \mathbf{x}_2| > 2r_{eq} \end{cases} \quad . (2.31)$$

The value of r_{eq} was chosen as $\sqrt{\rho_2}$. With this choice of a short range force, particle oscillation periods would be on the order of $1.9 \times \Delta/c_s$, so they would not be too short for the time step to handle.

The short-range forces could be expected to effect the system in a manner reminiscent of surface tension, namely, reducing the growth-rate of

the instability [58]. However, a 110 timestep simulation gave only ambiguous confirmation of this expectation. A simulation was first run with the short-range force "turned off." The growth rate of the instability was calculated from the square root of the kinetic energy, which is plotted as a function of time in Fig. 2.4. The kinetic energy followed a $\cosh(\gamma t)$ type of curve at early times. At the time that its growth became clearly exponential, it had reached a value of about 21.75. The growth rate was 0.033 in simulation units. This is in the ballpark with the classical value of 0.054. (It should be noted that attempts to measure the growth by the "bend" in the interface did not reveal a clear regime of exponential growth.)

A simulation with the short range force described above was also performed for 110 timesteps. When the kinetic energy began to grow in a clearly exponential manner, its value was about 16.44, about 24% less than the value of the kinetic energy without short-range forces. (See Fig. 2.5.) However, when exponential growth actually did begin, the growth rate was 0.074, over twice as high as the growth rate without short-range forces. By the end of the runs, the values of the two kinetic energies were comparable.

It might be thought that the added kinetic energy growth in the short-range force simulation came from particles moving toward more stable local equilibria with one another. It is true that the initial particle arrangement was not a true equilibrium. In a true equilibrium, the dense region particles would be arranged in a hexagonal configuration with nearest-neighbor particles separated approximately by the equilibrium distance of the short-range force [59]. In contrast, the initial arrangement of dense region particles was square packed, with nearest neighbors separated by $1/\sqrt{2}$ of the equilibrium distance. Of course, the particles pushing against one another would create a type of

equilibrium, at least temporarily. The truly problematic particles would be the ones near the interface. In order to keep the interface density gradient small enough for the computational grid to handle, the interface particles had to separated by distances greater than the equilibrium distance but less than the cut-off distance of the short-range force. This means that the particles near the interface were strongly attracted to one another.

However, it would appear that this non-equilibrium arrangement is not the source of the added growth of kinetic energy. The square root of the kinetic energy plus the change in the short-range potential energy is plotted as a function of time in Fig. 2.6. If the added kinetic energy growth came from particles moving toward local equilibria, the short-range potential energy would become more negative. Therefore, the kinetic energy added to the potential energy would grow more slowly than the kinetic energy in and of itself. However, this is not what happened. The kinetic energy plus the change in the potential energy grew much faster than the kinetic energy alone. In fact, this quantity had its own range of exponential growth; its growth rate was 0.65. In late times, this quantity drops off markedly, beginning at $t = 2.2$. However, this does not explain the enhanced growth at early times.

The algorithm described here amounts to a "marriage" of a fluid algorithm and a molecular dynamics algorithm. It has been managed to some degree, but is not without its expected problems. First and foremost is that, in a fluid code, short-range forces can be expected to act similarly to surface tensions. However, surface tensions have their most dramatic effects at short wavelengths [58]. It is precisely in such situations that the fluid algorithm fails. This problem can be overcome to some degree by increasing grid resolution (and particle number) at the expense of computing time. Finding a more elegant

solution to the problem must be deferred to further research. The code does seem to perform well at long wavelengths, however. A second problem is related to timescale. It may be desirable to introduce short-range forces with oscillation periods much shorter than the timescale of the overall fluid motion. To avoid overly long computer runs, this problem will have to be dealt with by altering the algorithm, probably by introducing some type of implicit time stepping scheme.

Of the algorithms presented in Section 1, we have had success in implementing only the one described here. Writing a code based on the third (continuous surface tension) algorithm has not been attempted. The second (incompressible) algorithm failed in modeling a Rayleigh-Taylor instability. A code based on the incompressible algorithm lost a substantial part of its kinetic energy in a 500 timestep run. This problem arose even with short-range forces "switched off." Several minor variations on the pushing of fluid and particle quantities were made to the code, none of which returned significant improvement. Another incompressible algorithm has been developed, based on the Eulerian algorithm of Aydemir and Barnes [60]. It has exhibited similar difficulties. The element common to both codes was the SOR routine used to isolate the compressible part of the fluid velocity. Perhaps this routine is introducing artificial viscosity into the fluid flow and needs to be replaced.
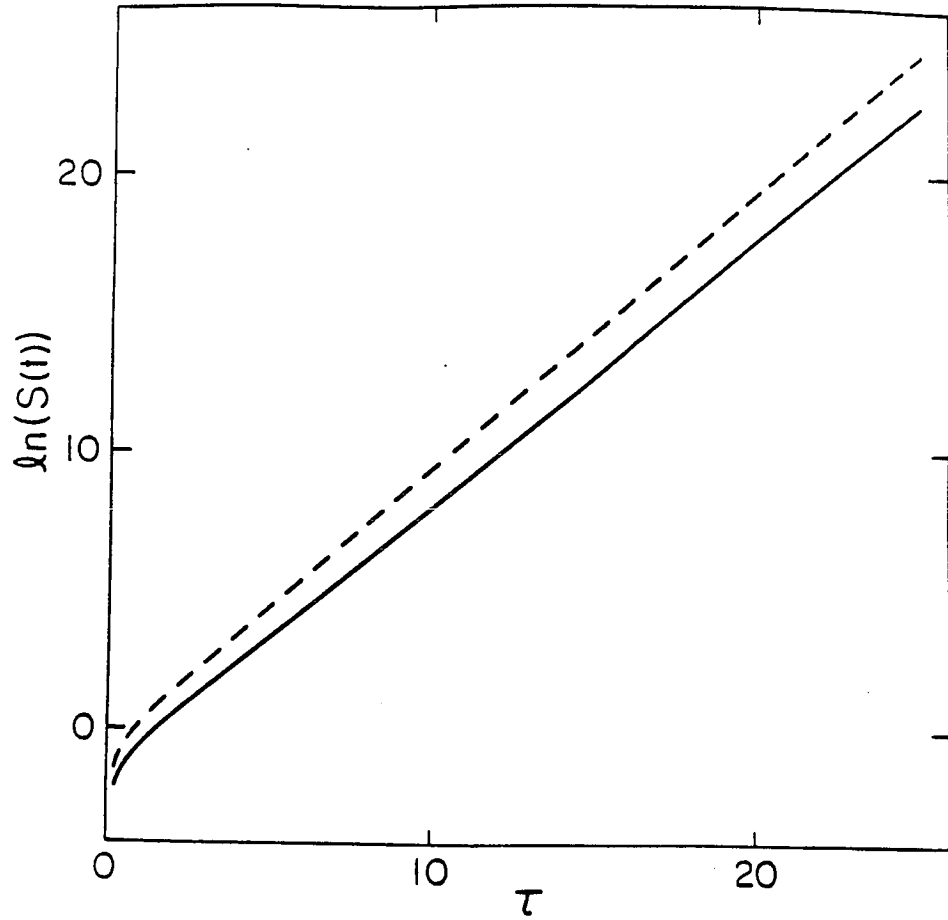
Figure 2.1: Growth of the two-fluid RT instability for a static fluid (dashed curve) and expanding fluid.

$s(t)$ is the growth of the instability relative to the instantaneous size of the fluid system. τ is time in terms of the instability growth time in the static fluid: $(gk(\rho_+ - \rho_-)/(\rho_+ + \rho_-)^{1/2}$.
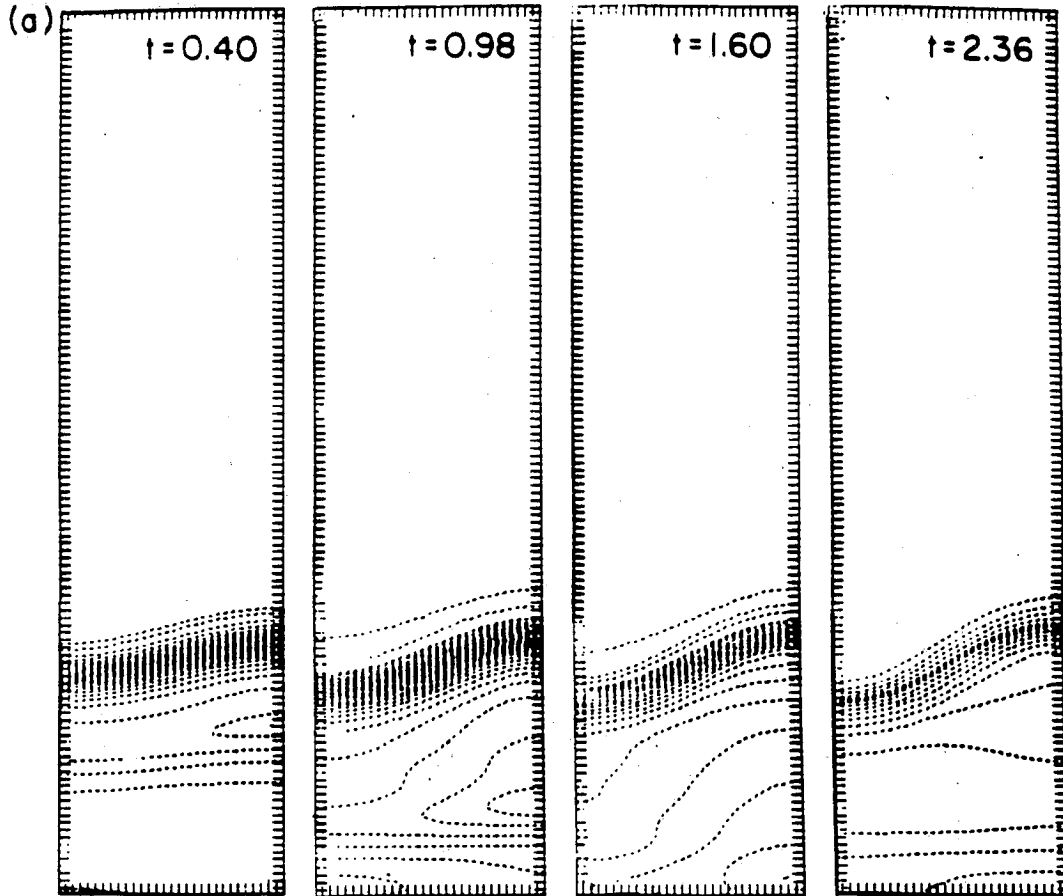
Figure 2.2: Time evolution of density contours of unstable fluids.
a) Density contours of the expanding MHD plasma undergoing RT unstable motion. Time is in terms of the classically calculated static RT growth time $|\nabla p_{tot}/\rho(y_{tr})|k(\rho_{tk} - \rho_{tn})/(\rho_{tk} + \rho_{tn})$ evaluated at $t = 0$. Expansion is in the y-direction only. The expansion factor is $a_y(t) = 4.t/t_{cs} + 1$, where t_{cs} is the t length of the box in the y direction (at $t = 0$) divided by the thick region soundspeed (at $t = 0$). Initial thin region density (at the top of the box) was 1/7 that of the thick region. Proportions remain the same through the simulation, but absolute density is cut in each frame by a factor of $1/a_y(t)$.

(b) t=0.40   t=0.98   t=1.60   t=2.36
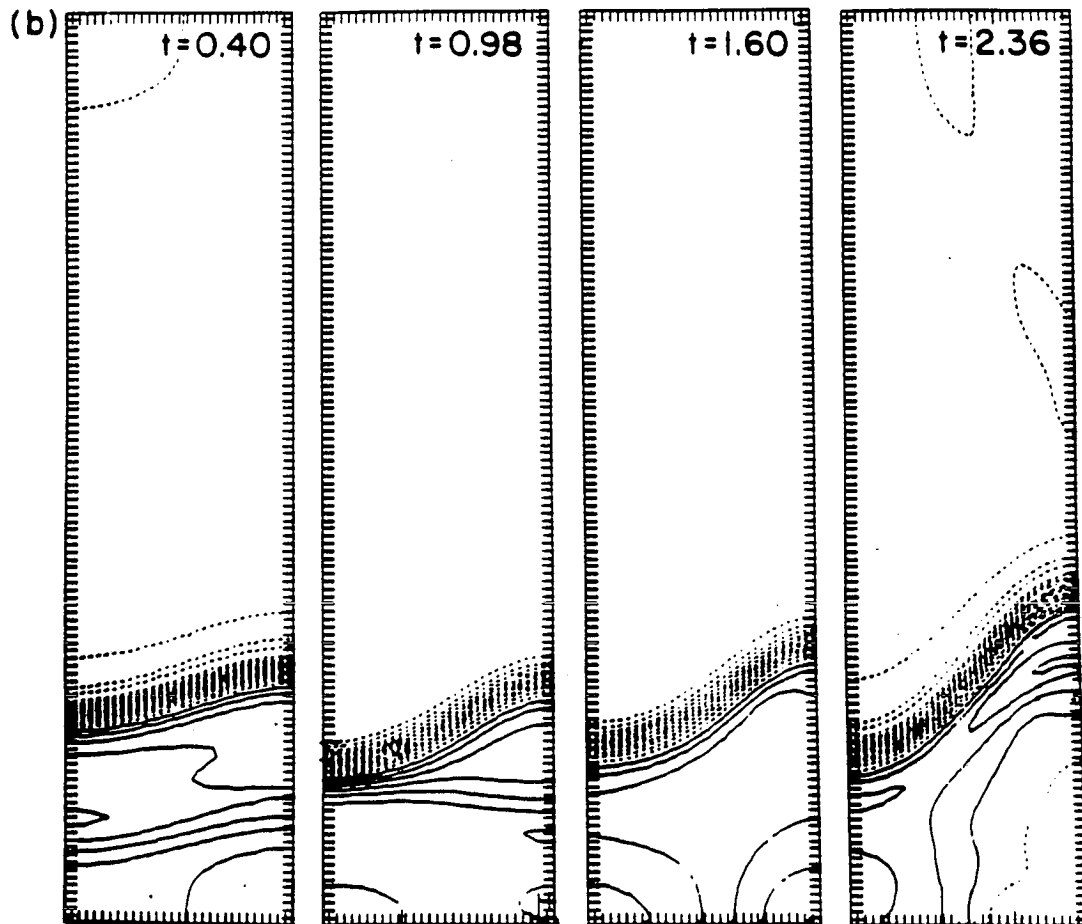
b) Density contours of the static MHD plasma undergoing RT unstable motion.
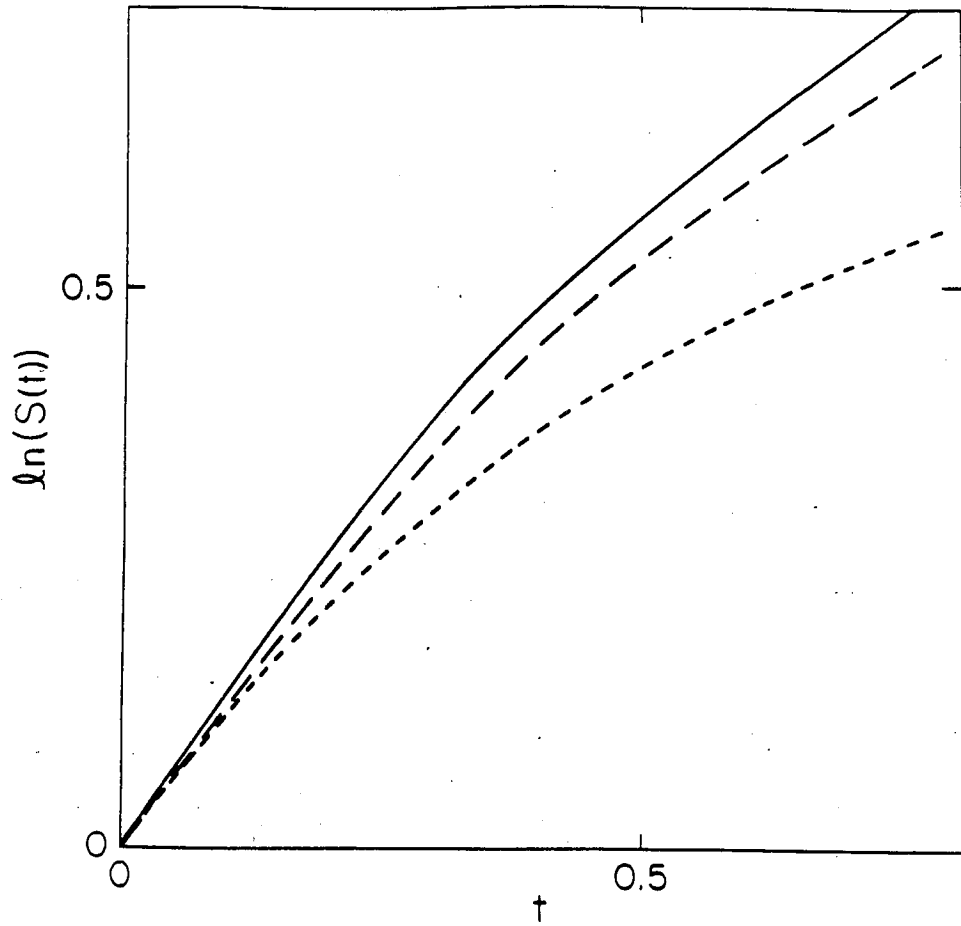Note much larger relative perturbation growth for static plasma.

Figure 2.3: Relative growth of RT instabilities from simulations of static plasma (solid curve), expanding plasma with $a_y(t) = t/t_{cs} + 1$ (long dashes), and expanding plasma with $a_y(t) = 4t/t_{cs} + 1$ (short dashes).

Time is in terms of classically calculated RT growth time for satatic plasma.

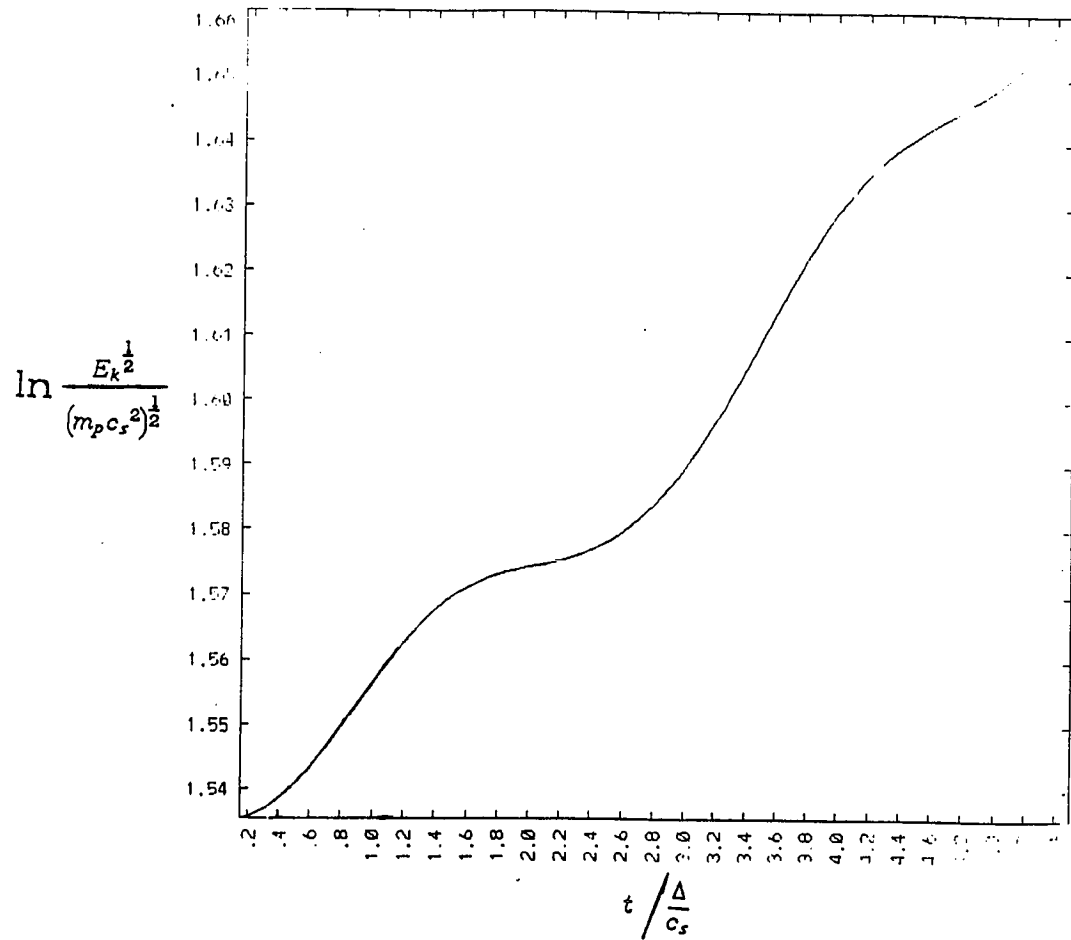$$\ln \frac{E_k^{\frac{1}{2}}}{\left(m_p c_s{}^2\right)^{\frac{1}{2}}}$$

Figure 2.4: Growth of square root of kinetic energy in simulation of Rayleigh-Taylor instability. No short-range force effects included.
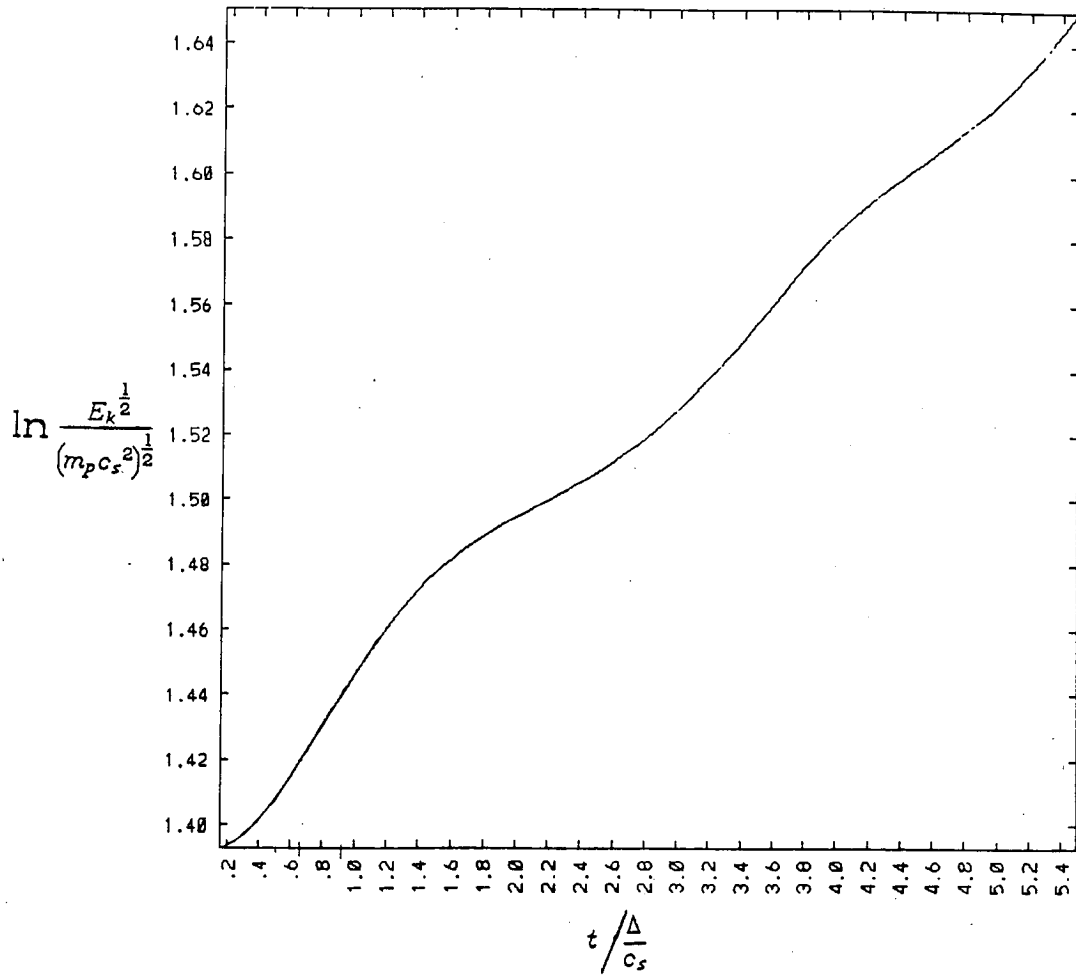
Figure 2.5: Growth of square root of kinetic energy in simulation of Rayleigh-Taylor instability. Short-range forces have been added to equations of particle motion.
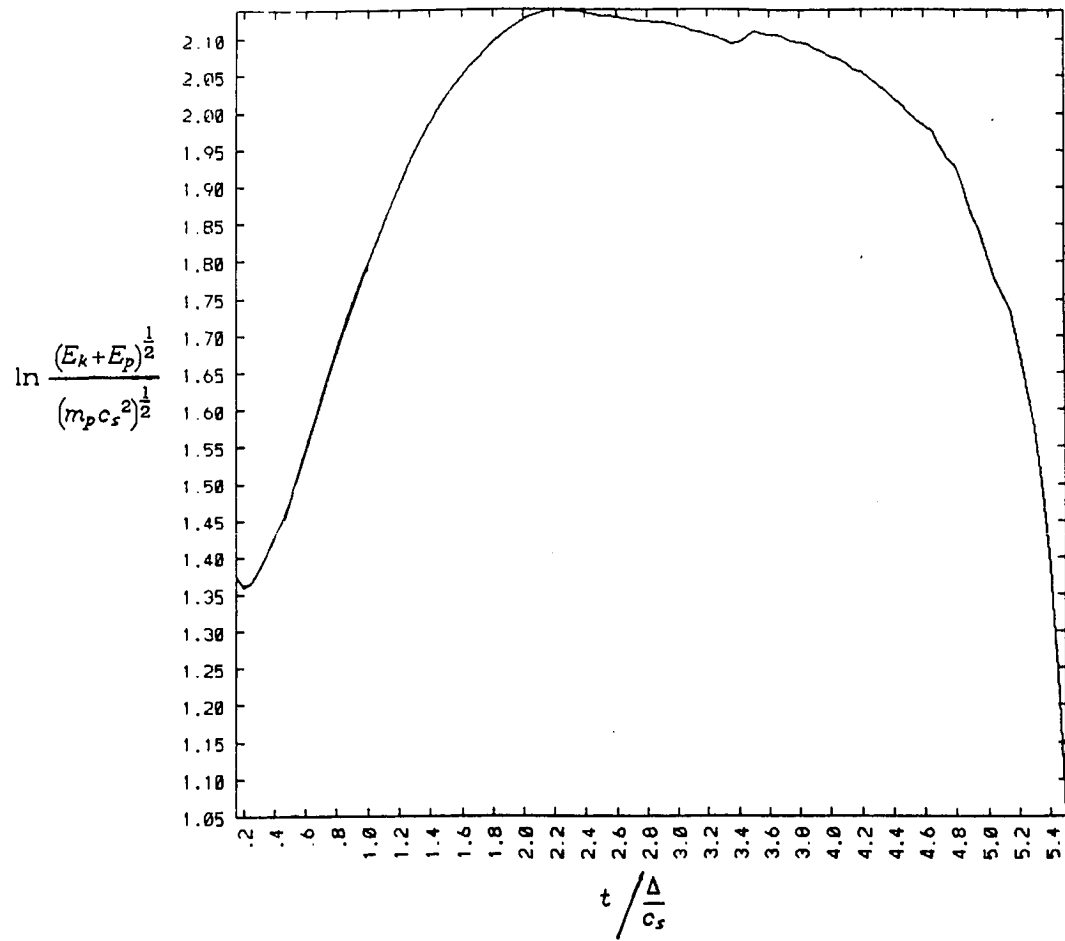
$$\ln \frac{(E_k + E_p)^{\frac{1}{2}}}{(m_p c_s{}^2)^{\frac{1}{2}}}$$

$$t \Big/ \frac{\Delta}{c_s}$$

Figure 2.6: Square root of kinetic energy plus short-range force potential energy.

Appendix A

Evaluating the Integral of Eq.(1.46)

The integral we need to evaluate is

$$\frac{2\hbar\omega}{e^{\hbar\omega/T} - 1}\eta\omega_p^2 c^2 \int_0^{k_{cut}} \frac{dk}{(2\pi)^3} 4\pi \frac{k^4}{Ac^4 k^4 + Bc^2 k^2 + C},\qquad (A.1)$$

where

$$A = \omega^2 + \eta^2,$$

$$B = 2\omega^2(\omega_p^2 - \omega^2 - \eta^2),$$

$$C = ((\omega^2 - \omega_p^2)^2 + \eta^2\omega^2)\omega^2.$$

Normalizing all frequencies by ω_{pe} gives

$$\frac{2\hbar\omega'}{e^{(\hbar\omega_{pe}/T)\omega'} - 1} \cdot \frac{\omega_p'^2 \eta'}{2\pi^2} \left(\frac{\omega_{pe}}{c}\right)^3 \int_0^{x_{cut}} dx \frac{x^4}{A'x^4 + B'x^2 + C'},\qquad (A.2)$$

where all primed quantities have been made dimensionless by division by the appropriate power of ω_{pe} (e.g. $\eta' = \eta/\omega_{pe}$), and $x = ck/\omega_{pe}$.

The first step to handling this integral is to rewrite it like

$$\frac{1}{A} \int_0^{x_c} dx - \frac{1}{A} \int_0^{x_c} dx \frac{Bx^2/A + C/A}{x^4 + Bx^2/A + C/A}.$$

The first integral gives

$$\frac{x_c}{A} = \frac{x_c}{\omega'^2 + \eta'^2}.$$

To evaluate the remaining integral, we find the (often complex) roots of the integrand's denominator:

$$x^2 = \frac{-B \pm \sqrt{B^2 - 4AC}}{2A} = r_\pm.$$

For the case $r_+ \neq r_-$,

$$-\frac{1}{A} \int_0^{x_c} dx \frac{Bx^2/A + C/A}{x^4 + Bx^2/A + C/A} = -\frac{1}{A^2} \int_0^{x_c} dx \frac{Bx^2 + C}{(x^2 - r_+)(x^2 - r_-)}$$

$$= -\frac{1}{A^2} \int_0^{x_c} dx \left\{ \frac{Bx^2 + C}{(r_+ - r_-)(x^2 - r_+)} + \frac{Bx^2 + C}{(r_- - r_+)(x^2 - r_-)} \right\}. \quad (A.3)$$

The full integral becomes

$$\frac{x_c}{A} - \frac{1}{A^2}(C + Br_+) \frac{1}{\sqrt{-r_+}} \cdot \frac{1}{(r_+ - r_-)} \tan^{-1} \frac{x_c}{\sqrt{-r_+}}$$

$$-\frac{1}{A^2}(C + Br_-) \frac{1}{\sqrt{-r_-}} \cdot \frac{1}{(r_- - r_+)} \tan^{-1} \frac{x_c}{\sqrt{-r_-}}. \quad (A.4)$$

It also shows the Lorentzian behavior of $\langle B^2 \rangle_\omega / 8\pi$ near $\omega = 0$. Notice that when ω becomes small, B and C both vanish. Remembering that $A = \omega'^2 + \eta'^2$, and multiplying by the leading factor we left behind in Eq. (A.2), we find

$$\frac{\langle B^2 \rangle_\omega}{8\pi} = \frac{2\hbar\omega'}{e^{(\hbar\omega_{pe}/T)\omega'} - 1} \cdot \frac{\omega_p'^2}{2\pi^2} \left(\frac{\omega_{pe}}{c} \right)^3 \frac{\eta'}{\omega'^2 + \eta'^2} x_c. \quad (A.5)$$

Notice that if $\eta \to 0$, this expression does *not* vanish. Rather, it becomes a Dirac δ-function.

For the exceptional case, $r_+ = r_- = r$, we write the integral as

$$\frac{x_c}{A} - \frac{1}{A^2} \int_0^{x_c} dx \frac{Bx^2 + C}{(x^2 - r)^2}.$$

The integrals left to do are

$$-\frac{C}{A^2} \int_0^{x_c} dx = \frac{C}{2A^2 r} \cdot \frac{x_c}{x_c^2 - r} + \frac{C}{4A^2 r\sqrt{r}} \ln \left(\frac{\sqrt{r} - x_c}{\sqrt{r} + x_c} \right), \quad (A.6)$$

$$-\frac{B}{A^2} \int_0^{x_c} dx = \frac{B}{2A^2} \cdot \frac{x_c}{x_c^2 - r} + \frac{B}{4A^2\sqrt{r}} \ln \left(\frac{\sqrt{r} - x_c}{\sqrt{r} + x_c} \right). \quad (A.7)$$

When $r_+ = r_-$, it is true that $B^2 = 4AC$ and $r = -B/2A$. The full integral is, then,

$$\frac{x_c}{A} + \left(\frac{B}{4A^2}\right)\frac{x_c}{x_c^2 - r} - \frac{3B}{8A^2\sqrt{r}}\ln\left(\frac{\sqrt{r} - x_c}{\sqrt{r} + x_c}\right). \tag{A.8}$$

Appendix B

Evaluating the Integral of Eq. (1.124)

Here we need to do an integral of the form

$$\int_0^{x_c} dx \, \frac{x^5}{x^6 + px^4 + qx^2 + r}. \tag{B.1}$$

We first make a change of variable:

$$u = x^2; \, dx = du/(2u^{1/2}),$$

which leads to

$$\int_0^{u_c} \frac{du}{2} \, \frac{u^2}{u^3 + pu^2 + qu + r}. \tag{B.2}$$

We can find the (usually complex) roots a, b, and c of the integrand's denominator. Since the only negative term in the denominator is vanishingly small in our region of interest, the roots will all be distinct. So we rewrite the integral as

$$\int_0^{u_c} \frac{du}{2} \, \frac{u^2}{(u - a)(u - b)(u - c)}. \tag{B.3}$$

The integrand can be rewritten

$$\frac{a^2}{(a - b)(a - c)(u - a)} + \frac{b^2}{(b - c)(b - a)(u - b)} + nonumber \tag{B.4}$$

$$\frac{c^2}{(c - a)(c - b)(u - c)}. \tag{B.5}$$

Each of these terms integrates to give a natural logarithm. The integral is given by

$$\frac{1}{2} \left\{ \frac{a^2}{(a-b)(a-c)} \ln |u - a| \Big|_0^{x_c^2} + (a \to b \to c \to a) + \right.$$

$$\left. (a \to b \to c \to a) \right\}. \qquad (B.6)$$

References

1. H. Nyquist, Phys. Rev. **32**, 110 (1928).

2. R. Kubo, J. Phys. Soc. Jpn. **12**, 570 (1957).

3. A.G. Sitenko, *Electromagnetic Fluctuations in Plasma* (Academic Press, New York, 1967).

4. N. Rostoker and M. Rosenbluth, Phys. Fluids **3**, 1 (1960).

5. N. Rostoker, R. Aamodt, and O. Eldridge, Ann. of Phys. **31**, 243 (1965).

6. R. Kubo, *Statistical Physics, vol. 2* (Springer-Verlag, Berlin, 1983).

7. J. Geary, T. Tajima, J.-N. Leboeuf, E. Zaidman, and J.H. Han, Comput. Phys. Commun. **42**, 313 (1986).

8. S. Weinberg, *Gravitation and Cosmology* (John Wiley and Sons, New York, 1972).

9. T. Tajima, Laser Part. Beams **3**, 351 (1985).

10. T. Tajima and T. Taniuti, Phys. Rev. A **42**, 3587 (1990).

11. S.I. Braginskii in *Reviews of Plasma Physics*, edited by M.A. Leontovich (Consultants Bureau, New York, 1964).

12. L. Spitzer, *Physics of Fully Ionized Gases* (John Wiley and Sons, New York, 1962).

13. T. Stix, *The Theory of Plasma Waves* (McGraw-Hill Book Company, Inc., New York, 1962).

14. C. Chu, M.-S. Chu, and T. Ohkawa, Phys. Rev. Lett. **41**, 653 (1978).

15. Y.Z. Agim and S.C. Prager, Phys. Fluids B **2**, 1138 (1990).

16. D. E. Baldwin and G. Rowling, Phys. Fluids **9**, 2444 (1966).

17. L.D. Landau, Phys. Z. Sowjet Union **10**, 154 (1936).

18. T. Tajima, *Computational Plasma Physics* (Addison-Wesley, Redwood City, CA, 1989).

19. N. Bohr, Dissertation, Copenhagen, 1911.

20. H.J. van Leeuwen, Dissertation, Leiden, 1919; Journal de Physique, **2**, 361 (1921).

21. J.H. van Vleck, *The Theory of Electric and Magnetic Susceptibilities* (Oxford University Press, London, 1965).

22. D. Pines and P. Nozieres, *The Theory of Quantum Liquids, vol. 1* (W.A. Benjamin, Inc., New York, 1966).

23. S. Gasiorowicz, *Quantum Physics* (John Wiley and Sons, New York, 1974).

24. J.W. Eberhard and P.M. Horn, Phys. Rev. B. **18**, 6681 (1978).

25. D.A. Bell, *Noise and the Solid State*, John Wiley and Sons, New York, (1985).

26. W.R. Bennett, *Electrical Noise* (McGraw-Hill, New York, 1960).

27. Bennett (1960) and Eberhard and Horn (1978).

28. G.V. Raynor, Reports on Progress in Physics **15**, 173 (1952).

29. C. Kittel, *Introduction to Solid-State Physics* (John Wiley and Sons, 1976).

30. A. Bhattacharjee, F. Brunel, and T. Tajima, Phys. Fluids **26**, 3332 (1983).

31. E.R. Harrison, Phys. Rev. D **1**, 2726 (1970); *ibid.*, Phys. Rev. Lett. **30**, 18 (1973); H. Kurki-Suonio, Phys. Rev. D **34**, 1719 (1986).

32. M. Rees in *The Very Early Universe*, edited by G.W. Gibbons, S.W. Hawking, and S.T.C. Siklos (Cambridge University Press, Cambridge, 1983) p. 29.

33. T. Tajima, S. Cable, K. Shibata, and R.M. Kulsrud, Ap. J., to be published (May, 1992).

34. Y.Q. Zhang and A.W. DeSilva, Phys. Rev. A. **44**, 3841 (1991).

35. R.L. Stenzel, Phys. Fluids B **1**, 1369 (1989).

36. I. Doxas, W. Horton, H.L. Berk, Phys. Fluids A **2**, 1906 (1990); A. Rechester, M.N. Rosenbluth, and R.B. White, Phys. Rev. Lett. **42**, 1247 (1979).

37. J. Korringa and A.N. Gerritsen, Physica **19**, 457 (1953).

38. Y. Takano, private communication (1991).

39. O. Avenel, P.M. Berglund, E. Varoquaux (1977), private communication from O.V. Lounasmaa; cited in D.E. Edwards, J.D. Feder, W.J. Gully, G.G. Ihas, J. Landau, and K.A. Muething, in *Physics at Ultralow Temperatures*, edited by T. Sugawara, S. Nakajima, T. Ohtsuka, and T. Usui (Phys. Soc. Japan, Tokyo, 1978) p. 280.

40. see, for example, M.B. Weissman, Rev. Mod. Phys. **60**, 537 (1988).

41. M. Emery, J.P. Dahlburg, J.H. Gardner, Phys. Fluids **31**, 1007 (1988).

42. H.J. Kull, Phys. Fluids **B1**, 170(1989).

43. D. Book and I. Bernstein, Phys. Fluids **22**, 79 (1979).

44. R.A. Chevalier, Ap. J. **207**, 872 (1976).

45. I. Bernstein and D. Book, Ap. J. **225**, 633 (1978).

46. K. Holcomb and T. Tajima, Phys. Rev. D **40**, 3809 (1989).

47. F.S. Felber, Phys. Fluids **25**, 643 (1982).

48. T. Tajima, S. Eliezer, R. Kulsrud, *AIP Conf. Proc. 181*, "Muon Catalyzed Fusion," eds. Jones S.E. *et. al.*, p. 423.

49. K.O. Mikaelin, Phys. Rev. Lett. **65**, 992 (1990).

50. Y. Nakagawa, R.S. Steinolfson, S.T. Wu, Solar Physics **47**, 193 (1976).

51. E.L. Rubin, S.Z. Burstein, J. Comp. Phys. **2**, 178 (1967).

52. G. Tryggvason, J. Comp. Phys. **75**, 253 (1988); B.S. Daly, Phys. Fluids **12**, 1340 (1969).

53. K. Shibata, T. Tajima, and R. Matsumoto, Phys. Fluids B2, 1989 (1990).

54. F. Brunel, J.N. Leboeuf, T. Tajima, and J.M. Dawson, J. Comput. Phys. **43**, 268 (1981).

55. R.W. Hockney and J.W. Eastwood, *Computer Simulation Using Particles* (McGraw-Hill, New York, 1981).

56. W.H. Press, B.P. Flannery, S.A. Teukolsky, and W.T. Vetterling, *Numerical Recipes* (Cambridge University Press, 1986).

57. J.U. Brackbill, D.B. Kothe, and C. Zemach

58. S. Chandrasekhar, *Hydrodynamic and Hydromagnetic Stability* (Oxford, 1961).

59. D. Greenspan, unpublished preprint.

60. A.Y. Aydemir and D.C. Barnes, J. Comput. Phys. **53**, 100 (1984).

VITA

Samuel Benjamin Cable was born in Asheville, N.C. on July 23, 1963, the son of the proud parents Clyde Joseph Cable and Ann Shaw Cable. Upon graduating from Clyde A. Erwin High School, he went north to the big city and entered The Massachusetts Institute of Technology in the fall of 1981. His four years there were relatively uneventful, conspicuously lacking in many of the elements of a typical undergraduate experience: no crisis of identity, no major doubts about traditional values, no sleep. He completed his senior thesis under the kindly guidance of Prof. Philip Morrison and graduated with a B.S. in physics in June of 1985. The following fall he entered The University of Texas at Austin as a graduate student in physics. He has been employed as a research assistant to Prof. Toshiki Tajima since June of 1987.

Permanent address: Route 4, 4 Holly Hill Drive
                          Asheville, North Carolina
                          28806

This dissertation was typeset[1] with LATEX by Suzy Crumley and the author.

---

[1] LATEX document preparation system was developed by Leslie Lamport as a special version of Donald Knuth's TEX program for computer typesetting. TEX is a trademark of the American Mathematical Society. The LATEX macro package for The University of Texas at Austin dissertation format was written by Khe-Sing The.